Phase Diagram Determination and Relative Dielectric Constant Measurements of the Butyronitrile-Chloroethane System

by

Robin Beth Michnick

B. S. School of Engineering at Columbia University (1987)
New York, New York

Submitted to the
Department of Materials Science and Engineering
in partial fulfillment of the requirements
for the degree of

DOCTOR OF PHILOSOPHY

at the Massachusetts Institute of Technology
Cambridge, Massachusetts

January, 1995

Signature of Author _____
Dept. of Mat. Sci. and Eng., January 1995

Certified by _____
Donald R. Sadoway, Prof. of Materials Chemistry, Thesis Supervisor

Accepted by _____
Prof. C. V. Thompson, Chairman, Dept. Grad. Comm.

PHASE DIAGRAM DETERMINATION AND RELATIVE DIELECTRIC CONSTANT MEASUREMENTS OF THE BUTYRONITRILE-CHLOROETHANE SYSTEM

by

Robin Beth Michnick

Submitted to the Department of Materials Science and Engineering on January 13, 1995 in partial fulfillment of the requirements for the Degree of Doctor of Philosophy in Metallurgy.

A systematic study of the physical chemistry of butyronitrile-chloroethane solutions was conducted with the intention of assessing their utility as electrolytic solvents for subambient electrochemistry. Both the solid-liquid phase diagram and the relative dielectric constants as a function of temperature and solution composition were measured.

The solid-liquid phase diagram was determined by differential thermal analysis. Apparatus was designed with a low temperature limit near the normal boiling point of liquid nitrogen. This is approximately 20° colder than commercially available equipment. The subambient boiling point of the chloroethane required the development of new protocols to ensure compositional control of the solutions. The butyronitrile-chloroethane phase diagram is a simple eutectic, the eutectic point being -185°C and 48 mole percent butyronitrile. The thermodynamics of the liquid phase were tested against a number of solution models and were found to be best represented by the Associated Solution Model.

The electrical conductivity and relative dielectric constant of butyronitrile, chloroethane, and their solutions were determined by electrochemical impedance spectroscopy (EIS) over the temperature range spanning -35°C to -105°C. The electrical conductivity exhibited Arrhenius behavior due to reduced ion mobility at lower temperatures. The relative dielectric constant varied linearly with inverse temperature, a behavior consistent with the greater alignment of the electric dipoles at reduced levels of thermal energy. The temperature dependence of the relative dielectric constant was fit to the Kirkwood model for dielectric media in order to determine the correlation factor of the molecules.

On the basis of the quasi-chemical solution model and the compositional variation of the correlation factor, the following was inferred to be the molecular configuration of the liquid: an associated solution composed of uncomplexed butyronitrile and chloroethane, dimolecular self-associates of butyronitrile, and dimolecular complexes composed of one butyronitrile and one chloroethane.

Thesis Supervisor: Donald R. Sadoway
Professor of Materials Chemistry

List of Figures

List of Tables

Symbols: Meanings and MKS Units

listed in the order that they appear in the document

Introduction

E	electrochemical potential [V]
E°	standard electrochemical potential [V]
R	gas constant [8.314 J/mole-K]
T	temperature [K]
F	faraday constant [9.64846×10^4 C/equivalent]
a_i	activity of species *i*

Phase Diagram

x_i	mole fraction of component *i*
ΔH_f	heat of fusion [J or J/mole]
T_m	melting temperature [K]
G^i	Gibbs free energy [J or J/mole]; *i* - ideal; *xs* - excess
b_j	excess enthalpy constant, *f*(T,P), [J or J/mole]
v_i	molar volume of *i* [m^3/mole]
δ_i	solubility parameter of *i* $[J/m^3]^{1/2}$
φ_i	volume fraction of *i*
ΔH_v	heat of vaporization [J or J/mole]
τ_i	polar component of solubility parameter of *i* $[J/m^3]^{1/2}$
λ_i	non-polar component of solubility parameter of *i* $[J/m^3]^{1/2}$
ψ_i	binary interaction energy [J or j/mole]
z	z-fraction

$$z_1 = \frac{x_1}{x_1 + rx_2} \qquad z_2 = \frac{rx_2}{x_1 + rx_2}$$

Δs^m	configurational entropy
n_i	number moles of *i*
n_{i1}	number moles of uncomplexed *i*
x_{i1}	mole fraction uncomplexed *i*
γ_i	activity coefficient of *i*
μ_i	chemical potential of *i* [J/mole]
μ_i°	standard chemical potential of *i* [J/mole]
x_{i1}°	mole fraction of *i* that is uncomplexed in a pure solution
K	dissociation constant
E	dissociation energy [J or J/mole]
r	distance between dipoles [m]
ε_o	permittivity of free space [8.854×10^{-12} F/m]
p_i°	partial pressure of *i* of the pure component [Pa]

Relative Dielectric Constant

ε or ε_r relative dielectric constant
C capacitance [F]
Q charge [coulombs]
P polarization charge [coulombs]
V volume [m]
α_i polarizability [i = o(rientation), a(tomic), or e(lectronic)]
μ_g dipole moment measured in the gas phase [C-m]
μ dipole moment in the liquid [C-m]
ε_o permittivity of free space [8.854×10^{-12} F/m]
n refractive index
a cavity radius [m]
ε_∞ dielectric constant at infinite frequency [actually related to atomic and electronic contributions to dielectric properties only]
g correlation factor
N_i number of dipoles/volume
N Avogadro's number [6.02×10^{23} atoms/mole]
G cell constant [m]
Z_i impedance of i
R resistance
ω angular frequency
ρ resistivity [Ω-m]
κ conductivity [S/m]
γ angle between dipole pair
W potential of average force and torque [J or J/mole]
z number of nearest neighbors
$\bar{\mu}_i$ effective dipole moment [C-m]

Abbreviations

BN butyronitrile molecule
CE chloroethane molecule
BNCE butyronitrile-chloroethane complex, no structure implied
BN_2 butyronitrile self-associate, no structure implied

Acknowledgments

There are may individuals who helped guide this work. I would first like to thank my thesis advisor, Professor Donald R. Sadoway. He guided my research efforts, the writing of this document, and broadened my abilities to pursue independent scientific research. The members of my thesis committee, Professors Rose, Cima, and Ceder, also contributed a great deal to my education at MIT and to the form of this document. Professor Ceder was especially helpful in the thermodynamic modeling of my measurements. Dr. Kevin Rhoads contributed so much in my understanding of the electrical experiments and their interpretation. His help and the help of Mr. Andrew Washabaugh in the design of the electrochemical cell were critical in the completion of the experimental measurements. Thank you all for your many contributions.

I would also like to thank Mr. Guenter Arndt who helped in the design and patiently constructed and reconstructed the experimental apparatus, repaired broken vacuum pumps almost overnight, and boosted my morale when the apparatus failed. Dr. Heather Shapiro and Mr. Masao Kurosaki were especially helpful through their construction of a reliable cryostat and their insights in scientific experimentation at subambient temperatures. Dr. Kwangbum Kim, Ms. Naomi Fried, and Ms. Susan Schiefelbein offered suggestions and insights that guided both the experimental and interpretative aspects of this research. The questions of Mr. David Pratt and Dr. Toru Okabe helped me focus the goals of this research.

Several groups contributed to the financial support for this research. The Materials Processing Center provided tuition support at the start of my studies at MIT. The Office of Naval Research and American Research and Development, Inc. contributed to the funding of this research.

Lastly, but most importantly, I would like to thank my parents, Judith and Bruce Michnick, and my siblings, Tamar, Sondra, and Michael, for their support and encouragement. It's been a long haul -- I couldn't have done it without you. Thanks so much.

All that I can convince him in, is this,/ The work is done; bright Sol is in his robe. The Alchemist II, iii.

1 Introduction

The new family of oxide superconductors brought on a surge of interest in what had become a near dormant field of research. Although there is little theoretical agreement about the origin of superconductivity in these materials, the oxygen content has been identified as a key element. In the $Ba_2YCu_3O_{(7-x)}$ perovskite when $0<x<0.2$, the transition temperature is approximately -181°C (92K). When $0.3<x<0.4$, the transition temperature drops sharply to -213°C (60K). As x approaches 0.7, the transition temperature slowly drops to -243°C (30K). Below x=0.7 the material has the characteristics of a semiconductor with no superconducting transition at all [Cava]. Clearly, there is a direct correlation between oxygen content and the superconducting transition temperature.

The oxygen content of the $Ba_2YCu_3O_{(7-x)}$ has been controlled by high temperature and/or high pressure anneals. An alternative method to equilibration with a gaseous atmosphere to oxidize the material is electrochemical processing.

By exploiting solid oxide electrolytes, potentiometric oxygen sensors were developed that detect oxygen concentrations in the environment. The Nernst equation allows the determination of the sample's chemical potential which in turn is related to the composition.

$$E = E^\circ + \frac{RT}{2F}\ell n\frac{a'}{a''} \qquad \text{eq.1.1}$$

where E° is the standard electrochemical potential
R is the gas constant [8.314 J/mole-K]
T is the temperature [K]
F is Faraday's constant [9.64846×10^4 C/equivalent]
a', a" are the activities of the species.

If a voltage is applied, as demonstrated in figure 1.1, a specific ratio of activities is established. For example if a" is known to be 1, then by selection of the appropriate voltage, a desired a' can be achieved [Gauthier].

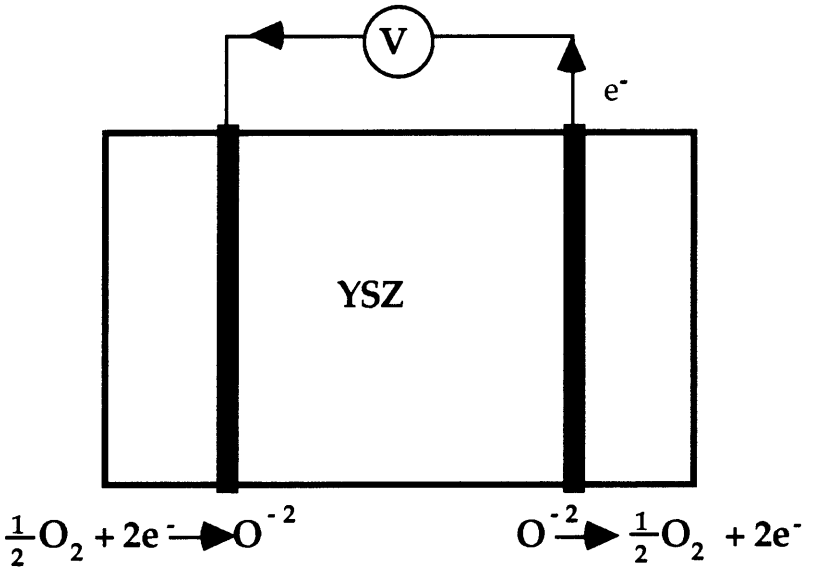

Figure 1.1 *Oxygen Pump.* By applying a potential across the solid oxygen ion electrolyte, yttria stabilized zirconia (YSZ), oxygen can be driven from one side to the other.

Because of the dependence on the oxygen content of the superconducting transition temperature, one posits that in a suitable system, it would be possible to alter the oxygen content of a $Ba_2YCu_3O_{(7-x)}$ electrode electrochemically thus offering in situ control of the material's transition temperature. Yugami *el al.* have reported electrochemical control of the bulk oxygen content in $Ba_2YCu_3O_{(7-x)}$ at elevated temperatures using a yttria stabilized zirconia (YSZ) solid electrolyte [Yugami]. In this system the oxygen deficiency was selected electrochemically at 500°C according to the following reaction:

$$\delta V^{\bullet\bullet}_{Ba_2YCu_3O_{7-x}} + \frac{1}{2}\delta O_2(g) \rightarrow \delta O_{Ba_2YCu_3O_{7-x}} + 2\delta h^{\bullet} \qquad \text{eq. 1.2}$$

The transition temperature was varied as predicted above with the results reproduced in figure 1.2. This is a clear demonstration of the control of the superconducting transition temperature of $Ba_2YCu_3O_{(7-x)}$ by electrochemical intervention.

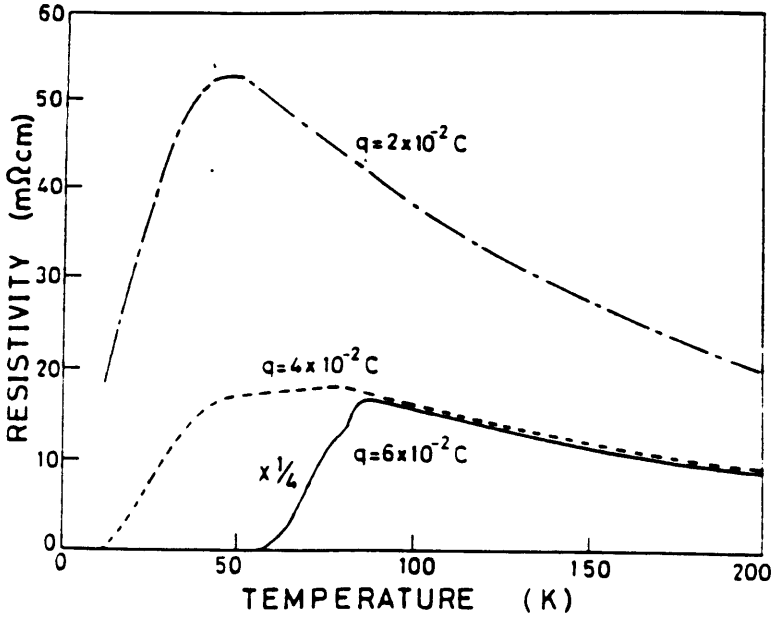

Figure 1.2. *Electrochemically Modulated* $Ba_2YCu_3O_{(7-x)}$. The superconducting transition temperature was raised electrochemically at 500°C by the addition of oxygen. Yttria stabilized zirconia was used as the oxygen electrolyte.

The electrochemical variation of the transition temperature was restricted to the stage of processing of the material because of the kinetic limitations of YSZ. Similar control of the oxygen content was done by O'Sullivan and Chang in their study of oxygen transport in these materials [O'Sullivan]. At room temperature, electrochemically controlled oxygen depletion had been studied by Schwartz,

Cahen *et al.* with a propylene carbonate electrolyte [Schwartz]. Electrochemical control of the oxygen content has been demonstrated.

This research was motivated initially by the desire to discover an electrolyte that is operative at -181 ℃ (92K), well below the operational limit of known electrolytes. The hope was that with such an electrolyte one could design cells in which the same electrochemical control of the $Ba_2YCu_3O_{(7-x)}$ transition temperature could be exerted. Because of kinetic limitations, only surface oxygen control would be possible. In such a system at -181 ℃ (92K) it would be possible to test if compositional control of the material's surface is feasible at temperatures where the material may be superconducting. One consequence would be the ability to alter, by varying the applied potential, the electrical properties of surface features, such as grain boundaries.

To examine this proposition, it is necessary to develop the appropriate electrochemical system. This requires an electrolyte that at the operating temperature is chemically inert with respect to $Ba_2YCu_3O_{(7-x)}$, ionically conductive, and contains a source of electrochemically reactive oxygen. Such an electrolyte would for the purposes of this study have to be operative at the normal transition temperature, i.e. -181 ℃ (92K).

An electrolyte is an electrically conductive medium where the charge carrier is an ion. It may be a molten salt, in which all of the species are ions, or an ion forming solute dissolved in a liquid or solid solvent. As there are no known molten salts or solid electrolytes that meet the temperature, chemical, and electrical requirements, the solvent sought in this work needs to be a liquid below -181 ℃ (92K) and still be able to dissolve and ionize the solute. Low temperature liquids, however, are typically molecular with low dielectric constants and thus low ionizing power; solvents with higher dielectric constants are solid at the required temperatures as seen in Table 1.1.

Table 1.1 Low Temperature Liquids as Candidate Solvents			
Solvent	T_{mp}(K)	T_{bp}(K)	Dielectric Constant
Methane	91 [Weast]	109 [Weast]	1.70 at 100K [Maryott]
Oxygen	55 [Weast]	90 [Weast]	1.51 at 80K [Maryott]
Ozone	81 [Weast]	161 [Weast]	4.75 at 90K [Pazumovski]
Chloroethane	134 [Timmermans, 1914]	286 [Timmermans, 1914]	13 to 20 from 168K to 238K [this study]
Butyronitrile	161 [Timmermans, 1936]	391 [Timmermans, 1936]	31 to 45 from 168 to 238K [this study]
Propylene Carbonate	275 [Texaco]	515 [Texaco]	65 at 298K [Texaco]

McDevitt *et al.* overcame the limitations of low temperature liquids by studying binary solvent systems. The solutions have a lower melting point then either of its constituents. When one or both of the components have moderate or high relative dielectric constants, the solution at low temperatures would tend to have a greater ability to ionize a solute than a single component liquid at the same temperature. At -185°C (88K) in a 1:1 mixture of butyronitrile and chloroethane, the redox couples of tetracyanoquinodimethane and bis(pentamethyoxydopentadienyl)iron were studied [McDevitt]. Thus demonstrating the feasibility of studying electrochemical reactions below -173°C (100K).

Many electrochemical studies have since been conducted [Breiter, Curtin, Green, Peck] in electrolytes where a butyronitrile-chloroethane solution was used as the solvent. Little, however, is known about this solvent system. Knowledge of the properties of this system as a function of the butyronitrile-chloroethane

compositional ratio and as a function of temperature will allow a more systematic selection of the optimum solvent composition for the desired experiment. By studying the physical chemistry, the arrangements of the molecules in the different phases may also be determined. This information enhances the selection of the appropriate solution as well. Also, knowledge of the liquid structure aids in the interpretation of the electrolyte behavior. The electrical conductivity, for instance, of an electrolyte is as much a function of the medium through which the ions travel as the number of traveling ions. This thesis addresses these issues in the exploration of the physical chemistry of butyronitrile, chloroethane, and their solutions.

By differential thermal analysis (**DTA**), the phase diagram of butyronitrile and chloroethane was measured. This technique provides an improved picture of the liquid, solid, and mixed phase regions of the phase diagram. An in house measurement system was developed to allow for measurements very near the liquid nitrogen boiling point, approximately 20°C colder than commercially available equipment. The more accurate portrait of the phase diagram will aid in selecting the appropriate solution of butyronitrile and chloroethane for a particular application. The thermodynamic interpretation of the phase diagram suggests certain molecular arrangements in the liquid phase.

Electrochemical impedance spectroscopy (**EIS**) measurements were conducted to determine the relative dielectric constant of this system. These measurements were made as a function of both temperature and composition of the solvent mixtures. From these measurements it was possible to speculate on the solvent structure of the mixtures. In particular, deviations from non-additive behavior at a given temperature as a function of composition indicated inter- and intra- molecular interactions.

To ascertain if a material's properties can indeed be controlled during use, requires the development of an appropriate test system . The particular goal of altering the surface properties of $Ba_2YCu_3O_{(7-x)}$ through control of the oxygen chemical potential requires an electrolyte with very particular characteristics. The first step in designing this electrolyte is the selection of the solvent or solvents. The research contained herein addresses some of the properties of butyronitrile, chloroethane, and their solutions as candidate solvents to test the feasibility of controlling the chemical potential of oxygen in $Ba_2YCu_3O_{(7-x)}$ at temperatures where the material may be in the superconducting state.

2 Phase Diagram

Electrochemical reactions occur at the interface between an ionically conductive medium and another conducting medium usually one which conducts electronically. Whether the medium through which the ions travel is a solid or a liquid is irrelevant to a first approximation. For organic solvents with subambient melting points, it is unlikely that an ionic current of reasonable magnitude exists when the solvent is in the solid state. For butyronitrile and chloroethane, the solvents studied in this work, the melting points are at temperatures exceeding the superconducting transition temperature of $Ba_2YCu_3O_{7-x}$ (-181 ℃, 92K) and so would be ineffectual as solvents for cryogenic electrolytes. However, liquid solutions of butyronitrile and chloroethane do meet this criterion. The temperature-composition phase diagram of butyronitrile-chloroethane indicates the compositions which are liquid at -181 ℃ (92K). It also shows regions where the solid and liquid phases are in equilibrium. As long as liquid is present, even as a microphase, electrochemical reactions can be studied [Grosser, Huang]. Solutions of butyronitrile and chloroethane within a two phase region would then also be suitable solvents for an electrolyte to study electrochemical reactions on superconducting electrodes.

2.1 Theory

In addition to aiding in the selection of an appropriate solvent solution, a phase diagram is ideally an equilibrium diagram allowing the determination of thermodynamic constants. Though the phase diagram for butyronitrile-

chloroethane is non-ideal, as the solution becomes more dilute in the second component the thermodynamic behavior should become more ideal. Under these conditions, Raoult's Law ($p = p^{\circ}x$) is valid for the solvent, and the van't Hoff equation, given below, may be used to determine the enthalpy of fusion [Wunderlich]

$$x_i = \frac{\Delta H_f}{R}\left[\frac{1}{T} - \frac{1}{T_m}\right] \qquad \text{eq. 2.1.1}$$

where x_i = mole fraction solute, impurity, etc.
ΔH_f = heat of fusion
T_m = melting point of pure solvent [K]
T = melting point of dilute solution [K]
R = gas constant.

This equation assumes that the enthalpy and entropy of fusion are independent of temperature, a reasonable assumption for small temperature changes. It further assumes that the activity coefficients of the solid and liquid are unity. A more general expression (eq. 2.1.2) may be used to compute the theoretical phase diagram with the same enthalpic, entropic, and activity coefficient assumptions.

$$\ell n\left[\frac{x_s}{x_i}\right] = \frac{\Delta H_f}{R}\left[\frac{1}{T} - \frac{1}{T_m}\right] \qquad \text{eq. 2.1.2}$$

where the terms have the same meaning as above.

2.2 Experimental Methods

There are a variety of methods for determining phase diagrams. Those most often used are dynamic methods which are variations on cooling and/or warming a sample while simultaneously measuring the sample's thermal environment and a system property, such as its electrical conductivity or

viscosity. The selected property typically varies linearly with temperature. When a phase change occurs, there is a deviation from the original linear behavior, oftentimes indicated as a change in slope of the property with temperature. The temperature at which this change occurs is deemed the transition temperature. This procedure is repeated at different sample compositions to develop the standard composition-temperature phase diagram. For organic compounds visual inspection, warming and noting the temperature at which melting begins and ends is a common technique. This method is unsatisfactory for a subambient system because icing and fogging hampers visibility.

An alternate method is to measure the change in viscosity as a function of temperature as was done by Ching *et al.* [Ching] for the butyronitrile-chloroethane system. In this technique melting or freezing is detected by the large viscosity difference between the solid and liquid. Supercooling is not indicated by this technique, so appropriate measures to compensate or eliminate supercooling cannot be taken. Butyronitrile, as measured in this laboratory, has a strong tendency to supercool even when mixed with alumina powder as a nucleating agent. Furthermore, the distinction between the liquidus and solidus is not made by this technique. As a result, the lowest temperature a particular composition still has liquid in equilibrium with the solid, as would be indicated by the solidus, is not known.

A last family of techniques involves measuring the actual temperature of the sample while it is cooling and warming often comparing it with a reference sample. Breaks in the curves occur during phase changes either as a thermal arrest, for pure samples, or a slope change, for solutions. These techniques fall under the heading of thermal analysis and are described in more detail below.

2.2.1 Thermal Methods

2.2.1.1 Thermometry

Thermal analysis techniques fall into two broad categories: thermometry and differential thermal analysis. In thermometry the deviations of the temperature from an applied linear cooling and warming rate (i.e. cooling and warming curves) are measured. Differential thermal analysis compares an unknown sample to a reference [Wunderlich]. Cooling and warming curves, recorded typically as a function of time, involve linearly varying the sample temperature with an external source. When an exothermic or endothermic event occurs, such as freezing or melting, the temperature of the sample is no longer controlled solely by the external source. The resulting deviation from the applied temperature profile, in the form of either a thermal arrest or a slope change, indicates the onset of the phase change (figure 2.2.1). Aside from the difficulties in constructing an apparatus that would vary temperature linearly to -196°C (77K), slope changes can often be obscure. Differential thermal analysis (**DTA**) overcomes this difficulty by having a reference material.

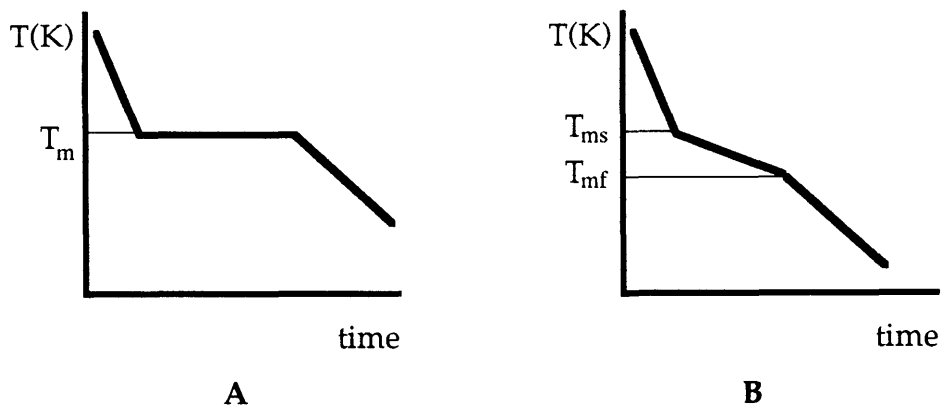

Figure 2.2.1. *Cooling curves.* **A.** For a pure material, the melting point (T_m) is indicated by a thermal arrest. **B.** For a solution, melting occurs over a range of temperatures starting at T_{ms} and finishing at T_{mf}, and is indicated by a slope change.

2.2.1.2 Differential Analysis

In DTA (figure 2.2.2), a sample and reference are cooled or warmed simultaneously. The temperature of the sample is compared to the temperature of the reference. Any non-uniformities in the cooling or warming rate should effect both the sample and reference equally thereby maintaining a zero temperature difference between them. Only when the sample undergoes a phase change, where heat is absorbed or liberated, is a non-zero temperature difference detected between the sample and the reference.

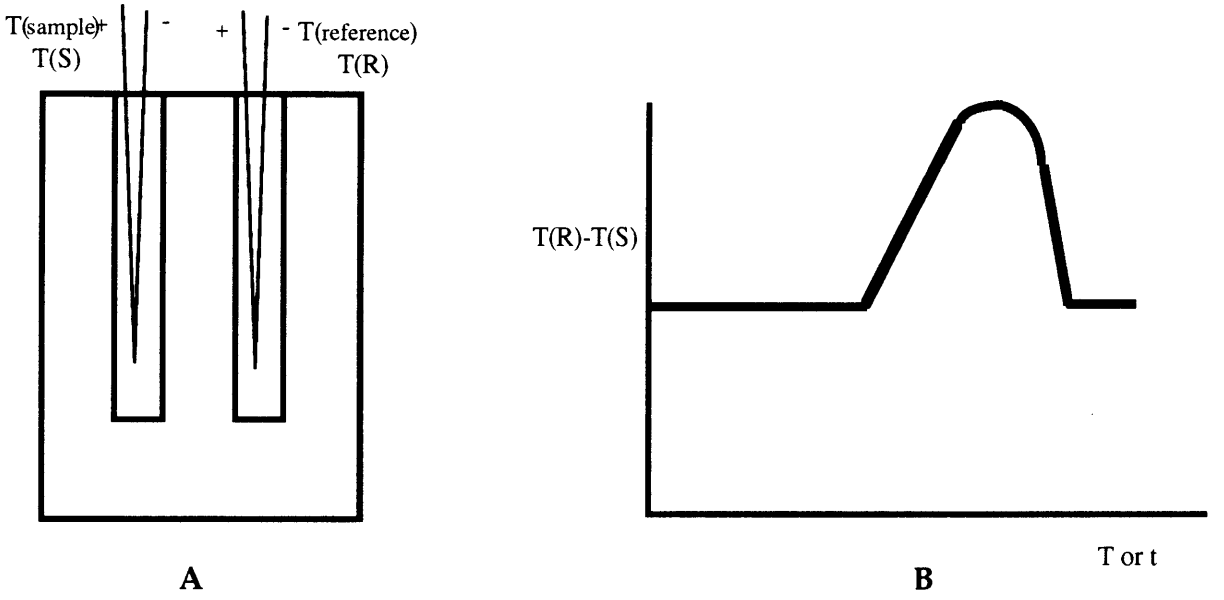

Figure 2.2.2. *Differential Thermal Analysis* **A.** Schematic of DTA apparatus. The temperature is measured in both the sample and the reference during cooling and warming. **B.** Schematic of an idealized endothermic (e.g. melting) curve. When the transition begins, the sample's temperature does not change (in the case of a pure material) or lags (in the case of a two or more component material) while the reference material continues to warm following the imposed warming program. The flat baseline when there is no transition occurring results when the thermal properties of the sample and the reference material are well matched.

In general, the temperature change due to a phase transition is small, on the order of 0.05°C, when a typical temperature gradient of 0.1 °C/sec (6 °C/minute) is used. If the temperature of the transition is -100 °C and the time for the transition is longer than one second, this five hundredth of a degree temperature change due to the transition can be obscured. If this same five hundredth of a degree is compared to a zero baseline between the sample temperature and the reference temperature, the effect is amplified providing a clearer indication of the phase change.

There are limitations to this technique. The measurement is a dynamic one as the temperature is always changing. Therefore questions arise about the achievement of thermal equilibrium (Rao). Very slow cooling or warming rates ensure thermal equilibrium in the sample. However because the heat effects are small, the transition is made obscure. This is because the liberated or absorbed heat, which generates the differential, is spread out over a much longer time period. This is exasperated over a steep liquidus [Rao]. Varying the environment temperature too rapidly causes substantial deviations from thermal equilibrium and decreases the accuracy of the measured transition temperature. The use of several different cooling and warming rates along with the use of small sample volumes helps balance the desire for thermal equilibrium within the sample and the ability to detect the event.

A second limitation to this technique is caused by experimental apparatus which is designed in consideration of the properties of the samples to be measured and the expected temperature range. This leads to nonuniformities in apparatus, measuring protocols, and interpretations of the results suggesting the need for a detailed description of the particular experimental design in order of the results to be reproducible in different laboratories [Vassallo].

2.2.2 Experimental Design

2.2.2.1 Sample Holder

The DTA apparatus used in this work follows the guidelines of Vassallo and Harden [Vassallo] and is shown in figure 2.2.3. The key factor in designing such a system is temperature uniformity so that the cooling and warming is uniform across the sample and the reference. In an ideal system, the only cause of a temperature difference would be a phase transition. To help promote uniformity a copper block was used. It was easily machined and had a high thermal conductivity. Ideally, the reference material will have the same thermal characteristic, in particular its heat capacity, as the sample throughout the measuring temperature range. This again promotes a uniform temperature profile in the apparatus. Initially, pure butyronitrile and chloroethane were tested as reference materials. The thermal qualities of the pure liquids were superior, but the open sample/reference wells and non-zero vapor pressures caused compositional changes in the samples that were unacceptable. Alumina powder was tested next and found to give suitable and consistent curves. The sample was mixed with alumina powder to better equate the thermal characteristics of the test and reference wells. Well-liners were used and were made of 12mm long 3mm i.d. Pyrex® tubing that was sealed and ground to a flat surface on one end. The liners held approximately 0.1ml of liquid which was found to be an adequate volume to indicate a clear transition. The small sample sizes used give small heat effects, but allow more uniform temperatures within the sample. The small sample sizes also allowed a more rapid return to the block temperature after a phase change. The glass-liners served two purposes: first to amplify the thermal effects by thermally isolating the reference and the sample, second to prevent contamination of the samples. The small sample size gave a

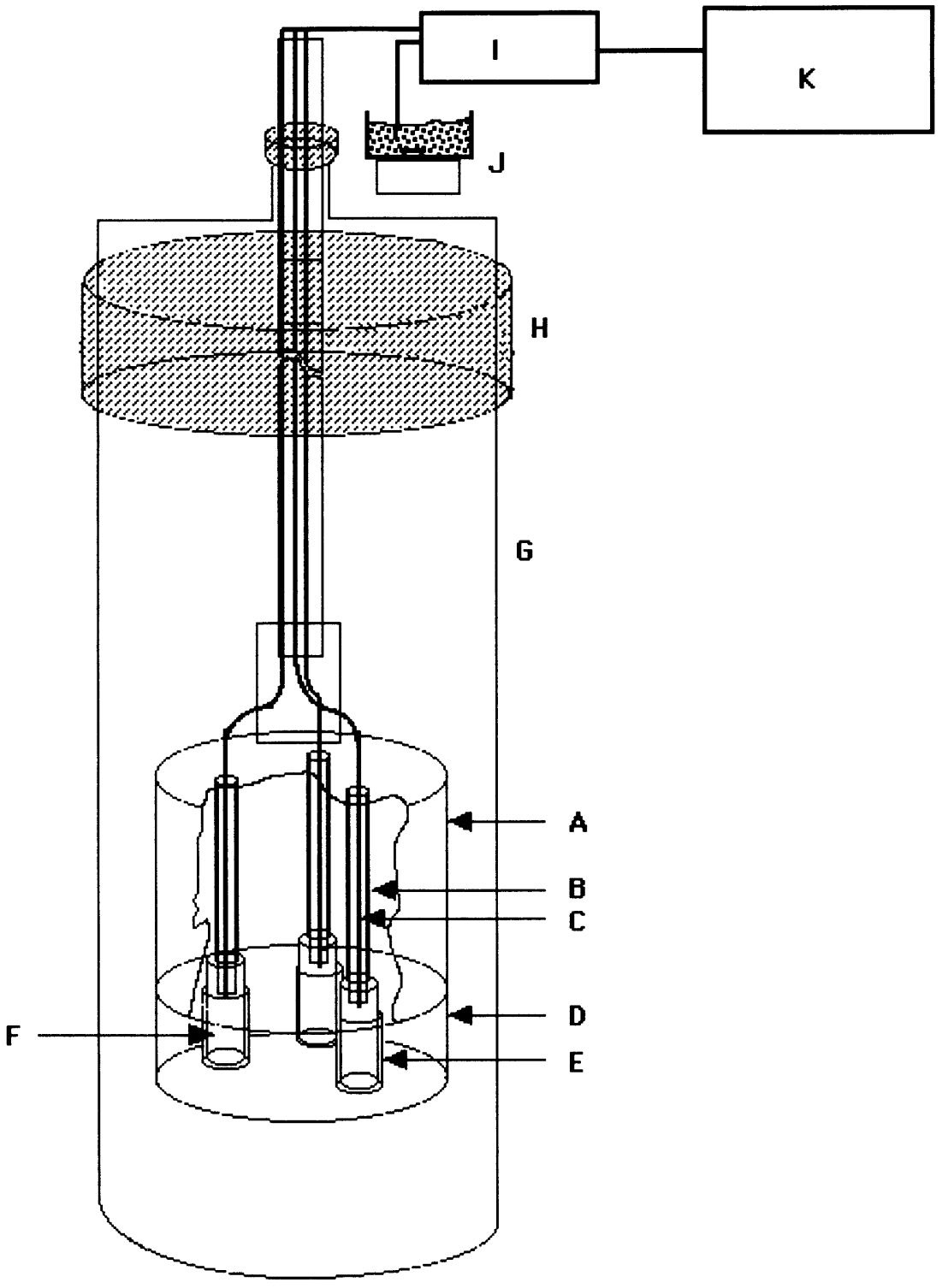

Figure 2.2.3. *Phase Diagram Apparatus*. **A**. Upper half of copper holder. **B**. Glass tubes that align the thermocouples in the reference and sample wells. **C**. Thermocouples (type T). **D**. Lower half of copper holder. **E**. Sample and reference wells. **F**. Glass liner to hold sample and reference materials - fits into E. **G**. Outer glass cylinder. **H**. Teflon® fitting. **I**. Digital multimeter. **J**. Ice-water referece bath and its thermocouple. **K**. Computer.

glass, being a poor thermal conductor, slows temporarily the return of the test sample to the reference temperature [Taylor]. The glass liners were removable allowing a clean surface before each measurement.

2.2.2.2 Thermocouples

The temperature was measured using calibrated thermocouples. There does not exist a thermocouple with linear temperature-voltage characteristics at subambient temperatures . The type T (copper - constantan) thermocouple is the most nearly linear and is recommended for low temperature work. Periodically the thermocouples were recalibrated by measuring the emf at five different temperatures and comparing it with a calibrated silicon diode that is precise to 0.15°C. Calibration curves were constructed for each thermocouple.

Each thermocouple weld was fixed into the top of the copper holder and was positioned in the center of the well with glass tubing. The glass tubes prevented the tips from being bent and assured that the tip positions were reproducible in the center of the well from one measurement to the next. The thermocouples were fed through a glass tube at the top of the cell (figure 2.2.3) and sealed with epoxy. The correspondance of measured values of pure butyronitrile and pure chloroethane with literature values confirmed the reliability of the apparatus.

2.3 Procedure

2.3.1 Experimental

The protocol for measurements was as follows. Prior to use, the glass wells and the various glass tools used in assembling the apparatus were vacuum dried. Then, the parts were placed in an inert gas filled glove bag. Chloroethane,

a gas at room temperature, required the use of an external liquid nitrogen source to prevent the solution composition from changing due to boiling. All the parts of the experiment and those required for its assembly were also cooled in the external liquid nitrogen bath. This was accomplished by immersing the parts to be cooled, while in the glove bag, into a container filled with liquid nitrogen.

The reference wells were first filled with the alumina powder reference. Then, the sample well was half-filled, by volume, with the alumina powder. All three were placed in their respective positions in the copper block. Some of the alumina powder was placed at the bottom of the outer glass chamber to enhance thermal transport during cooling and warming cycles. Butyronitrile was poured into a covered vial. Then the vial was placed in the external liquid nitrogen bath until solid. The butyronitrile weight was measured just prior to adding the chloroethane which had also been chilled in the liquid nitrogen bath. As the chloroethane melted, some was withdrawn and added to the vial of butyronitrile. When the appropriate solution was made, it was added to the alumina powder in the sample well. The entire ensemble was then place in a glass chamber and sealed with a Teflon® fitting. The experiment was assembled in an inert atmosphere (argon or nitrogen) which was maintained throughout the experiment in this sealed cell.

Once sealed, the cell was wrapped in aluminum foil which served as a Faraday shield. The cell was cooled and warmed at various rates in the temperature gradient above a liquid nitrogen pool. Linear cooling was more difficult to attained than linear warming. The voltages were measured with a Keithley 199 digital multimeter with a scanner card and were recorded by a computer with in-house software. The three thermocouples in the apparatus were referenced to a fourth type T thermocouple that was maintained in an ice-water bath. Having a fourth thermocouple was designed to make the set up less

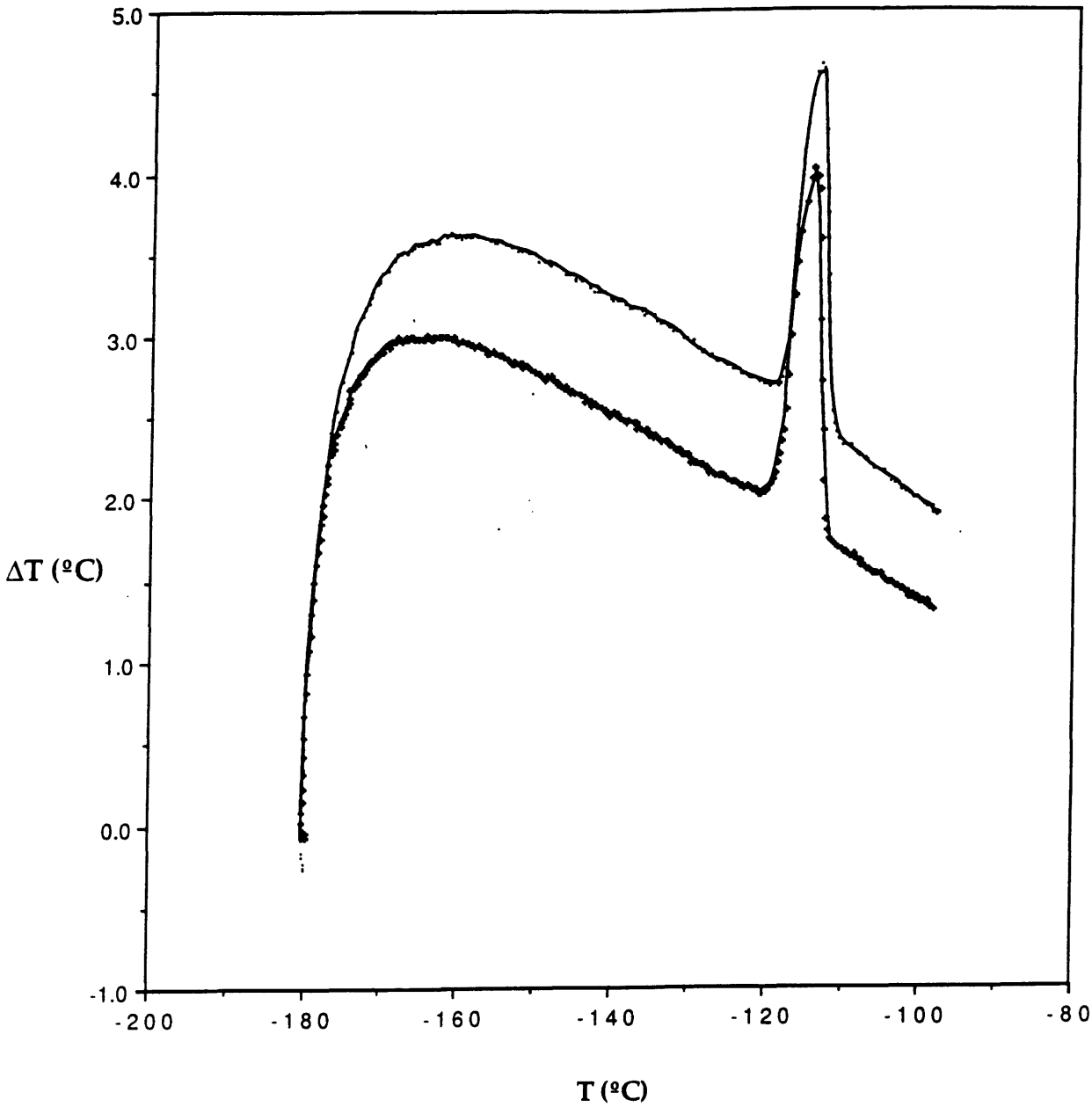

Figure 2.3.1. A Typical Warming Curve. The reference temperature appears as the abscissa; the ordinate is the temperature differential taken as the reference minus the sample temperature.

cumbersome than having a reference junctions for all of the measuring thermocouples in the ice-water.

2.3.2 Data Analysis

The measured voltages were first referenced to the zero of the ice-water bath. Then, using the calibration curve measured for the particular thermocouple, the voltages were converted to degrees centigrade. Subtracting the sample temperature from the reference temperature gave the differential temperature. This difference was than graphed as shown in figures 2.3.1 with the reference temperature as the abscissa and the differential temperature as the ordinate. As there were two reference wells, two differential curves were constructed. The closeness of the transition temperatures was an indication of the thermal uniformity across the copper block.

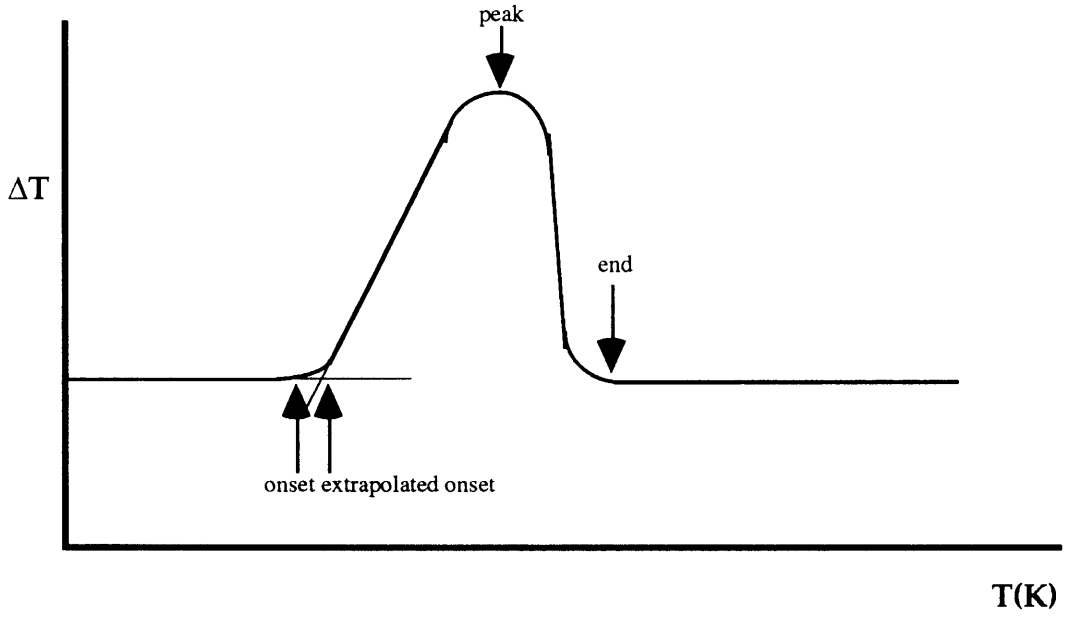

Figure 2.3.2. *Methods for Determining the Transition Temperature.* Different methods are used to determine the transition temperature. The onset is the most reasonable choice, but it is often difficult to evaluate. The peak temperature is commonly used because of its ease of determination.

There are a variety of methods used to select the transition temperature as figure 2.3.2 indicates. Typical points include the onset of the change, an

extrapolated onset which extends, as indicated, along the rise of the curve, the peak of the curve, and the end of the transition with the return to the baseline temperature [Wunderlich]. The deflections from the baseline should indicate the onset and completion of the transition, but these points are often ambiguous. The least ambiguous point, with no theoretical significance, is the peak. This point often appears in the literature as the transition temperature.

Generally, the onset of cooling is used to define the liquidus, and onset of melting defines the solidus (Mackenzie). However, butyronitrile supercools as a pure solvent and causes supercooling in a solution even with alumina powder as a nucleation source. Because cooling data gave spurious results, only warming curves were used in developing the phase diagram. The peak temperatures of the differential curve defined the liquidus. This proved reasonable as peak temperatures were consistent with at least three different warming rates. For the solidus, the onset of melting is typically used. However, due to the limitation in achieving thermal equilibrium, as described earlier and in more detail by Rao, solidus values were only reproducible in select solutions. Using these protocols the butyronitrile-chloroethane phase diagram was constructed and is shown in figure 2.3.3.

2.3.3 Temperature Error of the Thermocouples

A variety of factors contributed to the error in measuring the absolute temperature. The first was the 0.15°C error of the commercially calibrated silicon diode used to calibrate the thermocouples. A second source was the inability to control the environmental temperature during the calibration. The third source of error was due to the finite number of calibration points used to compute a

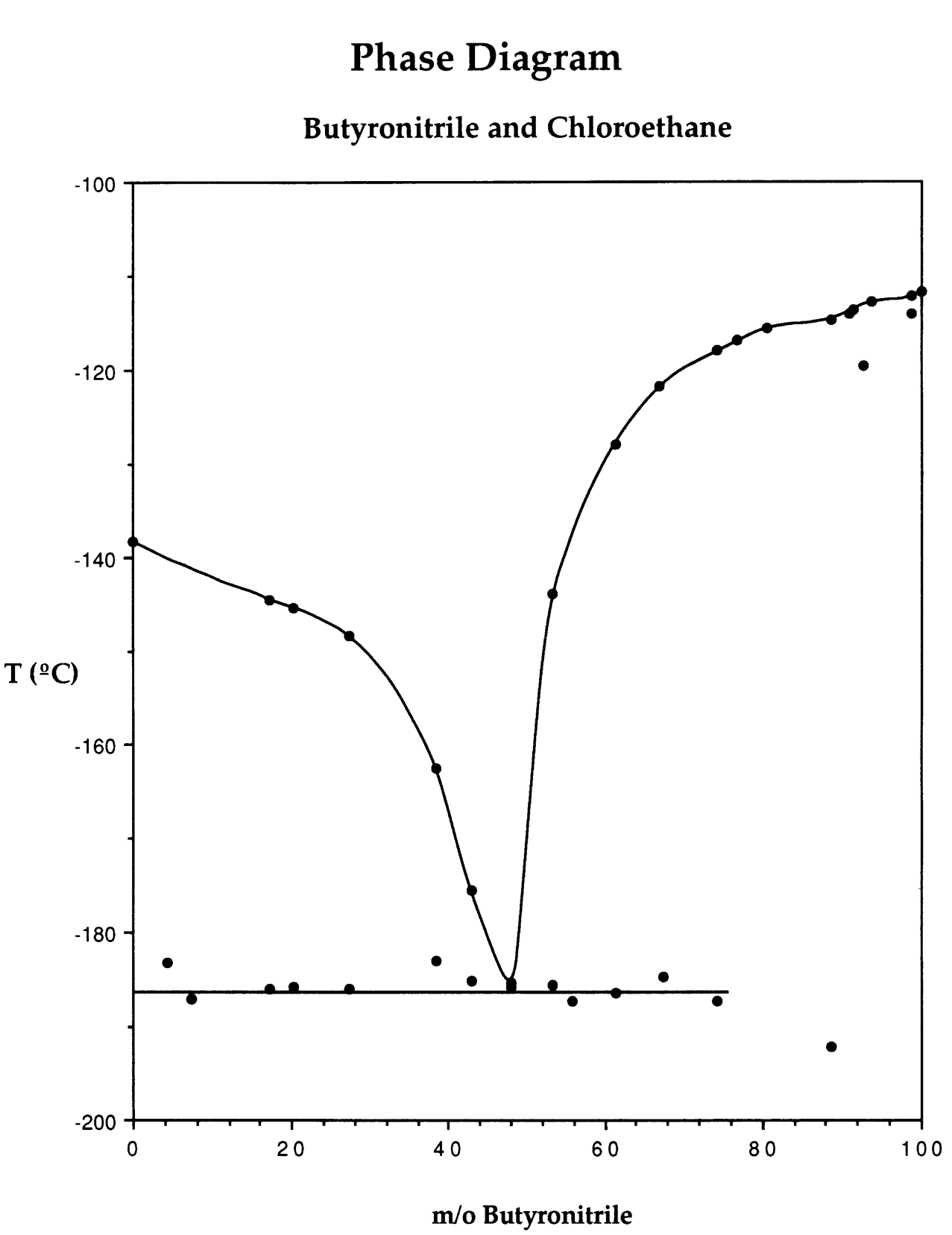

Figure 2.3.3. Phase diagram of butyronitrile and chloroethane measured by DTA.

calibration curve over a large temperature range. Table 2.3.1 shows the instability of the environment temperature as measured by the silicon diode and the difference between the temperature as measured by the silicon diode and the temperature computed using the calibration curve. The voltage used for the calculation is the same value used to compute the curve.

Table 2.3.1. Calibration Error of Thermocouples

$T_{Si\ Diode}$ (°C)	$T_{Computed}$ (°C)
-100.00 + 0.20	-100.00
-125.00 + 0.25	-124.99
-150.00 + 0.10	-150.01
-195.71 + 0.01	-195.93

Summing these errors, the overall temperature error is considered to be $\pm$0.3 °C.

2.3.4 Error of Phase Diagram Data

The error in the phase diagram points include errors due to the interpretation of the transition temperature and to errors in the measured composition. The error in the temperature was found by least squares fitting of the measured points. This uncertainty was greater on the chloroethane rich end than on the butyronitrile rich end and may be attributed to compositional changes over time due to evaporation of the chloroethane. For the butyronitrile rich end, the error, including thermocouple errors, was 0.52 °C. For the chloroethane rich end the error was 1.2 °C.

The error in the computed mole fractions due to weighing errors is determined by the following

$$\delta x_1 = \frac{\partial\left(\frac{w_1}{M_1}\Big/\frac{w_1}{M_1}+\frac{w_2}{M_2}\right)}{\partial\frac{w_1}{M_1}}\delta w_1 .$$

A weighing error was determined based on calibration measurements of the balance. The error in measuring the weight was no greater than 0.05 grams. The average overall weight of the measured samples was 5 grams. A maximum error in the computed mole fractions occurs at the extreme ends of the phase diagram. Using a weighing error of 0.05 grams and reported values for the molecular weights of the molecules, the maximum error in the computed mole fractions is 0.01.

Lack of vapor pressure measurements made the calculation of compositional changes due to evaporation impossible. The effects of evaporation on the composition was detectable for solutions in the chloroethane rich end and in particular the extreme end of the phase diagram. As a result, liquidus data below a mole fraction of 0.1 butyronitrile could not be determined. For the remainder of the solutions the estimated error due to evaporation was assumed to be 0.006 which was determined based upon the deviation of the actual temperature composition relationship from that computed by a fitted curve at compositions where the van't Hoff equation was valid. The net overall error in mole fraction is approximately 0.02.

2.4 Discussion

2.4.1 Qualitative Analysis

A liquid phase or a liquid-solid two-phase mixture existed over almost the entire composition range at the required -181 ℃ (92K) where $Ba_2YCu_3O_{7-x}$ begins to superconduct. The eutectic composition was approximately 47.87 m/o butyronitrile with a eutectic temperature of -185 ℃ (88K). From the phase diagram it is seen that butyronitrile is practically insoluble in solid chloroethane, while chloroethane is somewhat soluble in solid butyronitrile.

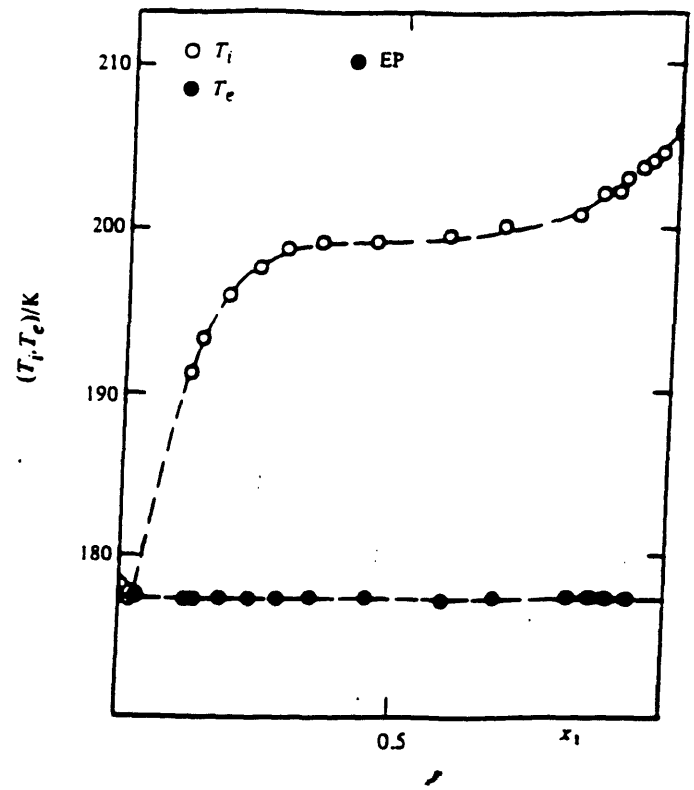

Figure 2.4.1.1 *2-Methypyridine-Hexane Phase Diagram.* Reproduction of organic phase diagram from literature. As with the measured phase diagram, there is a sharp change in the slope of the liquidus. -°C.

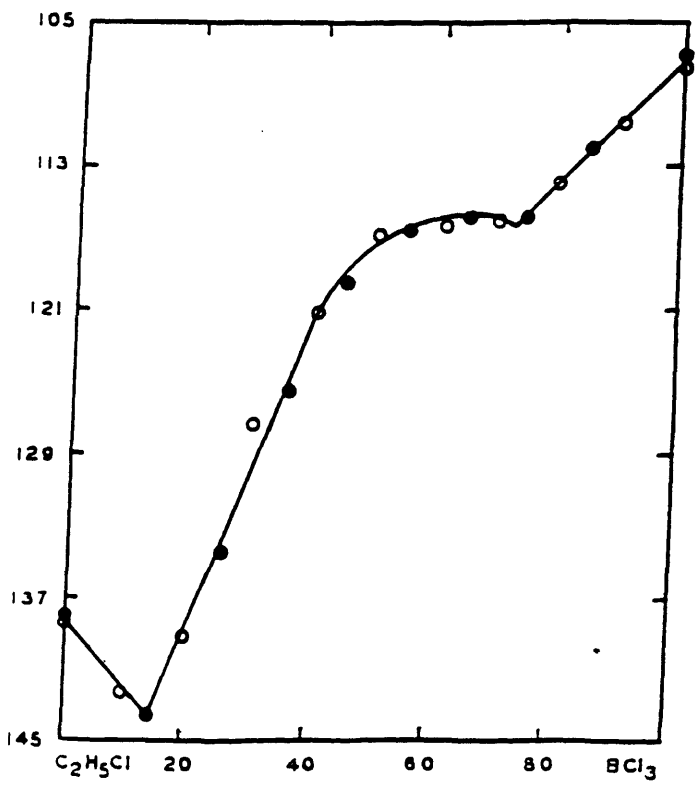

Figure 2.4.1.2 *Boron trichloride and Chloroethane.* Reproduction of organic phase diagram from literature. As with the measured phase diagram, there is a sharp change in the slope of the liquidus.

From a metallurgical perspective, the shape of the liquidus is suspect. Unlike typical metallic phase diagrams, there is an abrupt change in the liquidus slope between approximately 30 and 60 m/o butyronitrile. However, a comparison of the measured phase diagram to those of other organic systems, supports the validity of the measured data. Figure 2.4.1.1 reproduces the solid-liquid equilibrium diagram of 2-methylpyridine [C_6H_7N], a ring-shaped molecule, and hexane [C_6H_{14}], a linear molecule [Kehiaian]. No solid-liquid equilibrium diagrams were found in the literature with butyronitrile as one of the components; however, a phase diagram of chloroethane and boron trichloride was located [Martin]. This equilibrium diagram is reproduced as figure 2.4.1.2. Here again the plausibility of the shape of the liquidus curve is confirmed. In fact, the phase diagrams for chloroethane-butyronitrile and chloroethane-boron trichloride are remarkably similar considering the differences in the molecular structure of butyronitrile and boron trichloride (figure 2.4.1.3).

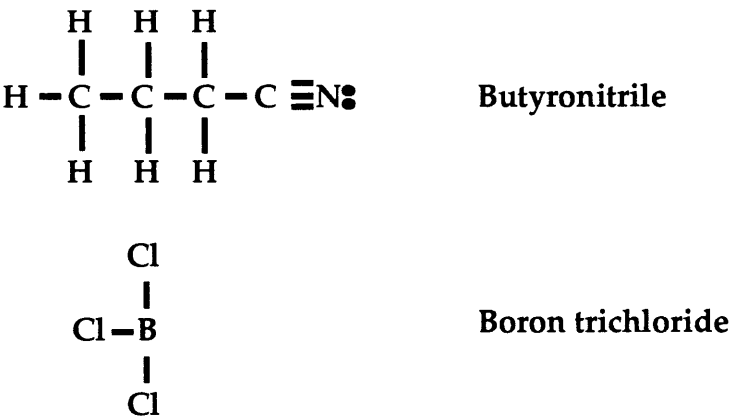

Figure 2.4.1.3. *Molecular Structures.* Molecular structures of butyronitrile and boron trichloride. Though different, they share similar phase diagrams with chloroethane. The boron of the boron trichloride [Martin] may interact with the chloroethane in a similar fashion as the nitrogen of the butyronitrile even though the former is an electron pair acceptor and the latter an electron pair donor.

2.4.2 Quantitative Analysis

From the measured butyronitrile-chloroethane phase diagram, thermodynamic information about the pure solvents can be determined. Fitting the liquidus points at dilute solutions should give a straight line (figure 2.4.2.1). The van't Hoff equation (equation 2.1.1) relates the concentration of added solute to the inverse temperature. From the slope of these lines, the heat of fusion can be computed for the pure solvent. These values are shown in Table 2.4.1. and compared to the literature value.

Table 2.4.1 Measured and Literature Values of the Heat of Fusion

	ΔH_{fusion} [Dauber]	ΔH_{fusion} (this study)	% Difference
Chloroethane $\Delta H_{(this\ study)}$ +400J -400J	4.4518kJ/mole	4.7362kJ/mole 5.1362kJ/mole 4.3362kJ/mole	6.38 15.37 -2.66
Butyronitrile $\Delta H_{(this\ study)}$ +400J -400J	5.0208kJ/mole	5.0308kJ/mole 5.4308kJ/mole 4.6308kJ/mole	0.22 8.17 -8.42

Referring to figure 2.4.2.1b, the solution data points used begin at 17 m/o and extend to nearly 30 m/o. The variation of the liquidus is linear to very high concentrations. Measurements of solutions with compositions between 0 and 10 m/o butyronitrile were suspect due to the difficulty of maintaining compositional control.

Using the van't Hoff equation (eq. 2.1.1), the heat of fusion was determined for both components and was found to conform to the literature. According to Timmermans, an error of one hundred calories, approximately four

Butyronitrile Rich End

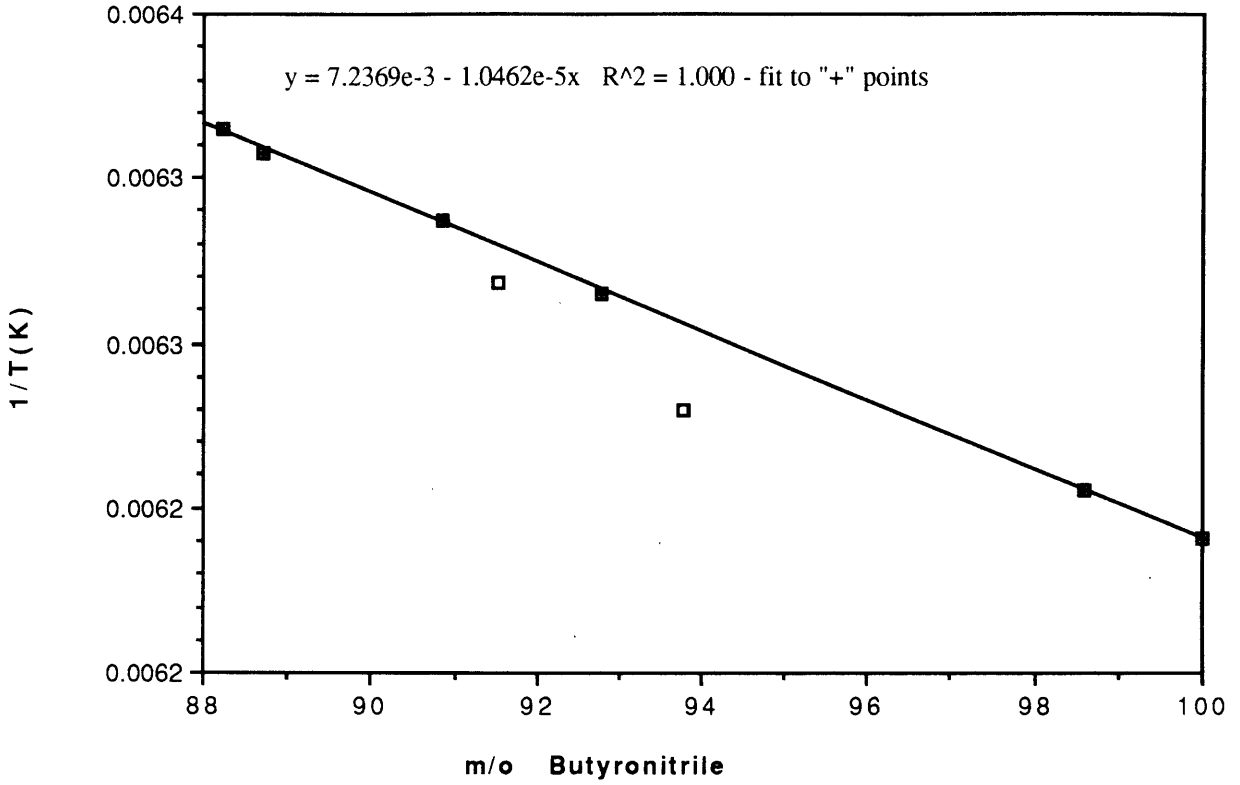

Chloroethane Rich End

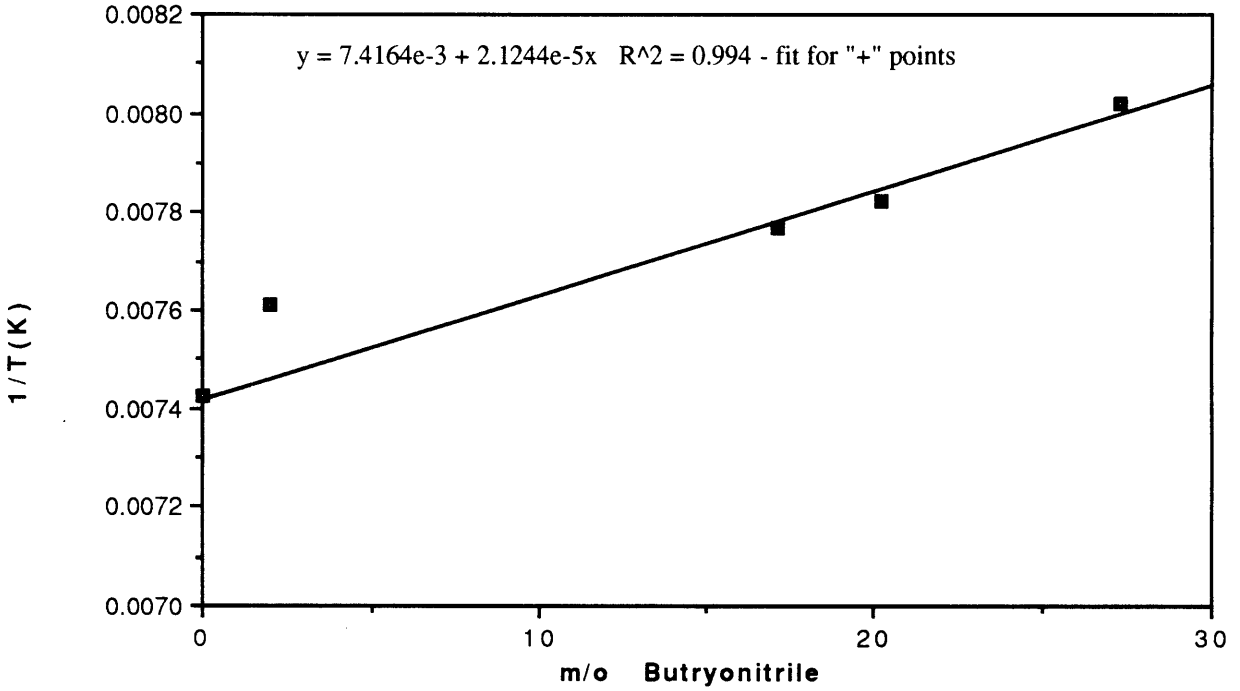

Figure 2.4.2.1. Phase Diagram Data. Displays dilute solutions in accordance with the van't Hoff equation.

hundred joules, in the heat of fusion computed from data acquired by cooling and warming curves as a function of concentration is to be expected [Timmermans]. Considering this, the values calculated from these measurements are within the expected error.

Using the more generalized form of the van't Hoff equation (eq.2.1.2) a calculated phase diagram [eutectic at 31m/o butyronitrile at 123K] with the previously listed assumption is superimposed upon the measured phase diagram (figure 2.4.2.2). The most striking feature is the shift of the eutectic composition by approximately twenty mole percent butyronitrile and a lowering of the eutectic temperature by over thirty five degrees celsius in the measured phase diagram as compared to the ideal phase diagram.

The many assumptions used in equation 2.1.2 contribute to the difference in the calculated and measured curves. The first is the use of a constant heat of fusion and a constant entropy of fusion. There is no reason to expect that over a nearly seventy five degree temperature range the heat of fusion would remain constant. For both sides of the calculated curve, the value of the heat of fusion for the pure component in the majority was used. The effects of the second component on the heat of fusion were ignored. Likewise, the effects of non-ideal mixing, typically framed as activity coeffecients, on the entropy were neglected. The derivation of this equation, **(Appendix A)**, incorporated the entropy of fusion at the normal melting point of the pure component. The use of temperature and concentration independent factors in the van't Hoff equation limits its ability to model real phase behavior.

For the system studied, the variation of the enthalpy of fusion of the pure components has not been determined as a function of temperature. In figure 2.4.2.3, three different variations of the heat of fusion are formulated and plotted. In curve *b* the weighted average of the heats of fusion was used. For curve *c* at

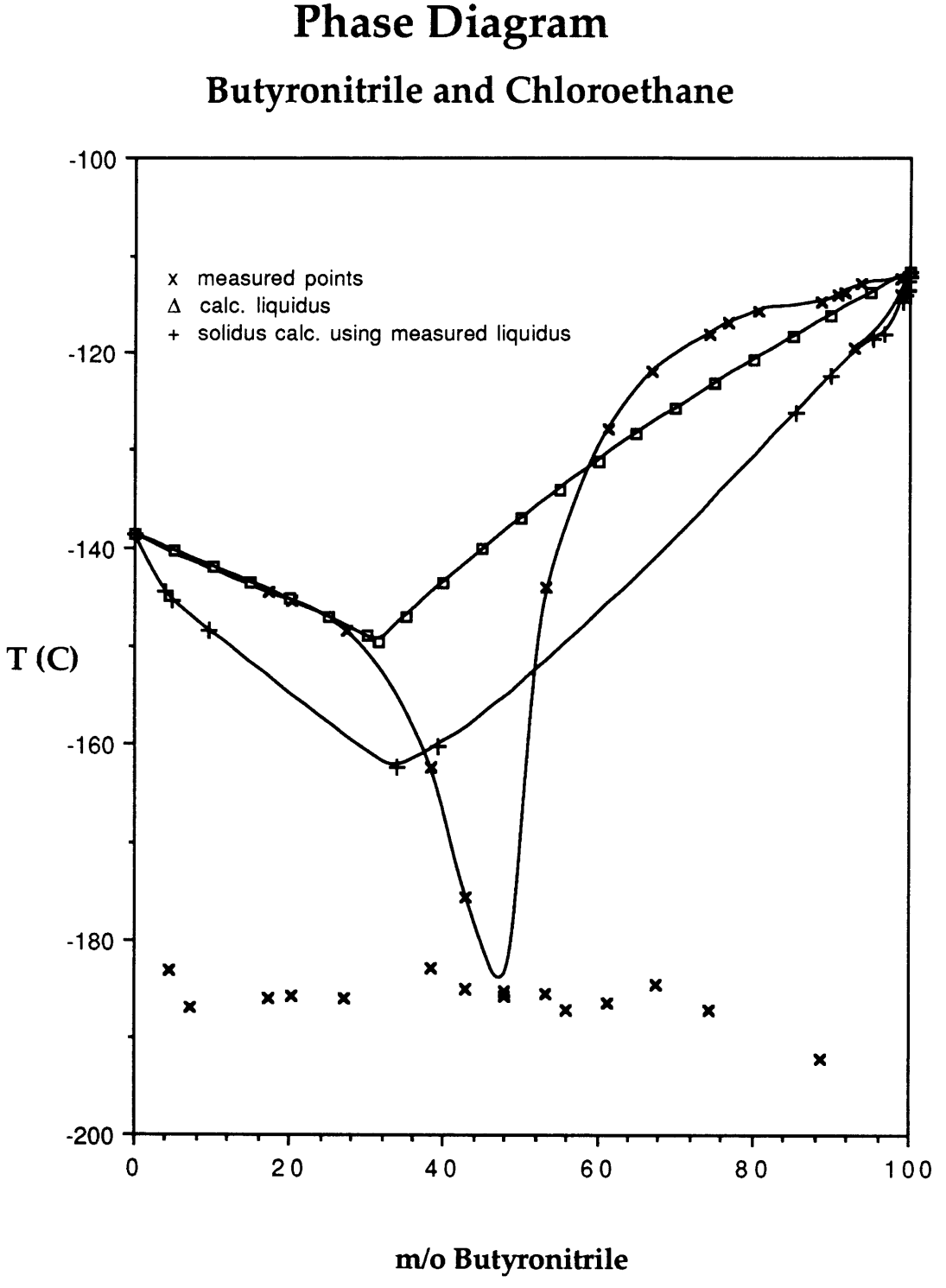

Figure 2.4.2.2. Measured and Simulated Phase Diagram. The simulated liquidus was calculated using the van't Hoff equation. Zero solid-solid solubility was assumed. The solidus was calculated using the measured liquidus compositions/temperature.

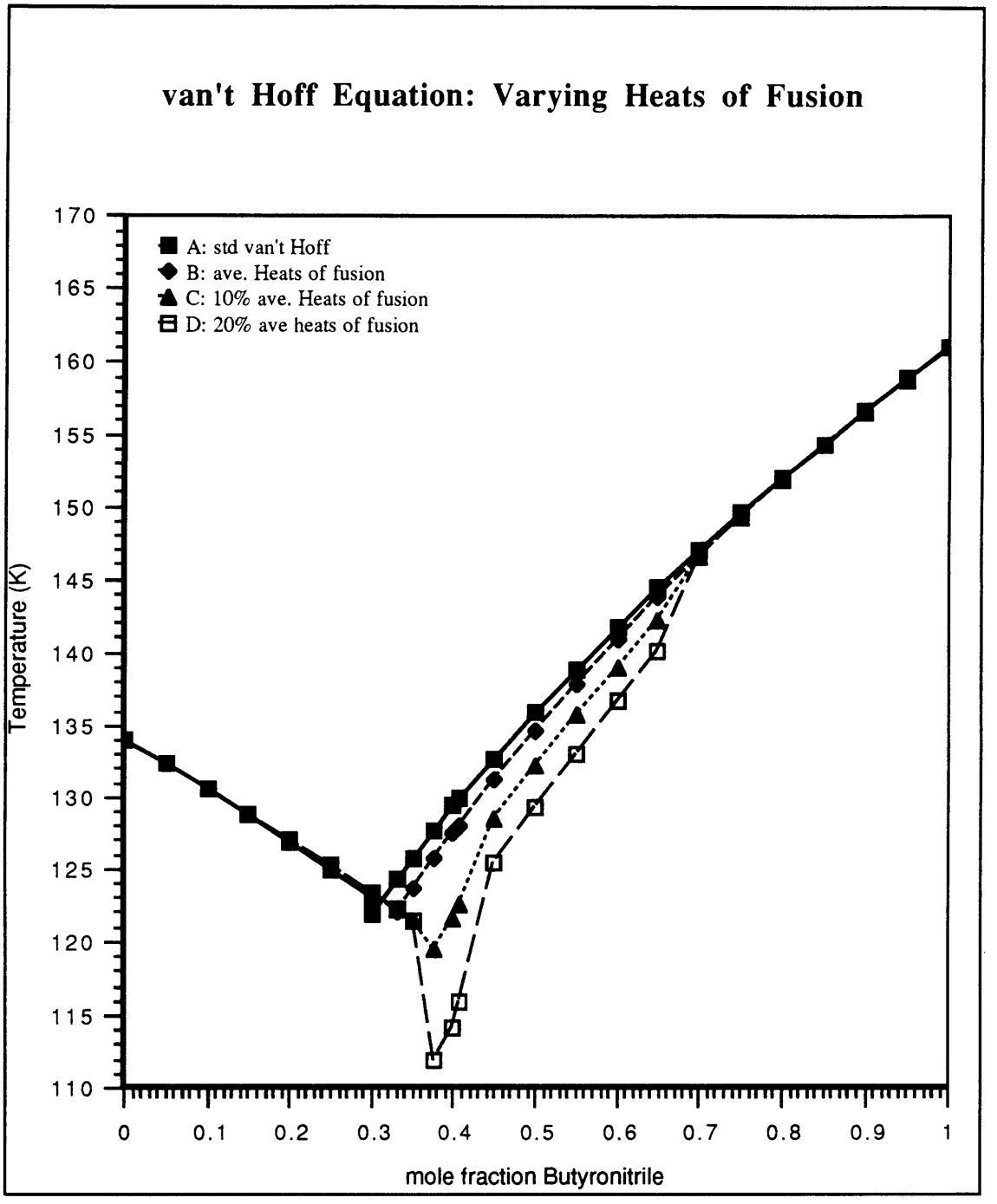

Figure 2.4.2.3. Variation of heat of fusion on the van't Hoff equation. **A.** pure component values of ΔHf used. **B.** weighted average of the ΔHf used. **C.** every 10% temperature interval, reduce weighted average of ΔHf by 10% **D.** every 10% temperature interval, reduce weighted average of ΔHf by 20%.

10% temperature intervals, the weighted heat of fusion was reduced by 10%. Curve *d* had the weighted heat of fusion reduced by 20% at 10% temperature intervals. Table 2.4.2 shows the variation of the eutectic point for these curves.

Table 2.4.2 Computed Eutectic Point When ΔH_{fusion} is Varied		
ΔH_{fusion}	**eutectic composition m/o butyronitrile**	**eutectic temperature K**
pure component values	31.4	122.8
weighted average	33.2	122.1
10% weighted average	37.6	119.5
20% weighted average	40.7	116.0

As can be seen, the magnitude of the heat of fusion changes the eutectic composition to a large extent. For the eutectic temperature, the change is less dramatic. The enthalpy is related to the heat content. The results indicated in Table 2.4.2 and in figure 2.4.2.3 suggest that the energy change of the solution is less than predicted from the pure component values. The change in the eutectic composition with heat content reflects the variations in the interaction energy between like [A-A and B-B] and unlike pairs [A-B]. Since the reduction in the "heat of fusion", which was based upon pure component values, gives a more symmetric and deeper eutectic, the unlike pairs must be more energetically favored than like pairs. For if like pairs were favored, a molecule in the system is more likely to be in a "pure" component environment. The energy content of the more concentrated solutions, which are less like a "pure" component, would be expected to be greater.

The ordering of the liquid points contradicts the ideal mixing that is assumed. In the solid phase there is also ordering. The eutectic of the phase diagram (figure 2.3.3) shows that the solid phase is made up of two immiscible

components, one nearly pure butyronitrile and the other nearly pure chloroethane. So while the liquid phase favors unlike ordering, the solid phase favors like ordering. The prominence of ordering in this analysis suggests the importance of entropic changes on mixing.

For a system where the molecules of the solution are similar in size and lack a permanent dipole, the system is more nearly ideal. In dilute solution, even when the molecules are vastly different, the assumption of ideality is reasonable allowing the determination of the pure component properties as was done at the start of this section. In more concentrated solutions, the solute molecules are no longer far enough apart that intermolecular and intrasolute interactions may be neglected. As seen in table 2.4.3, butyronitrile and chloroethane molecules are very different. These differences must be considered in order to understand the phase behavior of the butyronitrile-chloroethane system.

Table 2.4.3 Properties of Butyronitrile and Chloroethane [Daubert]

Property	Butyronitrile	Chloroethane	% Difference
Molar Volume	0.0879 m^3/kmole	0.07118 m^3/kmole	19.02
van der Waals Volume	0.04883 m^3/kmole	0.03552 m^3/kmole	49.60
Dipole Moment	1.3576×10^{-29} C-m	6.8381×10^{-30} C-m	27.26

2.4.3 Modeling of Phase Diagram

The preceding analysis assumed ideal behavior and incurred all the limitations of this assumption. The system measured is far from ideal. Many theories attempt to account for this non-ideal behavior. In the thermodynamic approaches all non-ideal behavior is grouped into an excess free energy and is

related to the bulk properties of the pure components [Malanowski]. Thus, the free energy is the sum of the ideal and excess free energies.

$$G\ (\text{liquid}) = G^{id} + G^{xs}$$
$$G\ (\text{solid}) = G^{id} + G^{xs}$$

The goal is to create a model that enables the prediction of phase relationships in unmeasured liquid solutions. These models incorporate the size difference of the molecules and interaction energies between like and unlike molecules. Due to the complexities of the liquid state, lack of long range order (gas-like) while interacting locally (solid-like), the models all fail at some level to describe the nature of a real system [Malanowski]. Attempts have been made to overcome these failures, often by the addition of extra constants, limiting the predictive powers of the model.

The models can be loosely grouped into two types. The first lumps all the excess free energy into an enthalpic term. Thus, though the excess enthalpy suggests ordering of some type the assumption of random mixing is maintained for the entropic term. In the second group, the non-random factors are considered in modeling the excess free energy. In this second case an excess enthalpy is sometimes also added. The measured butyronitrile-chloroethane phase diagram is fit to those empirical relationships commonly used to model organic liquid solutions.

2.4.3.1 Excess Enthalpy Models

2.4.3.1.1 One Term Redlich-Kister Model

The thermodynamic approaches for the free energy can be expressed with the Redlich-Kister phenomenological equation [Marcus]

$$g^{xs} = x_1 x_2 \sum_j b_j (T,P)(x_1 - x_2)^{j-1} (1 \le j \le k) \qquad \text{eq. 2.4.3.1}$$

where the b_j's are constants at a given temperature and pressure and are often associated with the interaction energies between pairs of molecules [Redlich]. The temperature variation of the b_j values, at constant pressure, often takes the form

$$b_j = \alpha_j + \beta_j T + \gamma_j T \ln T \qquad \text{eq. 2.4.3.2}$$

As seen in eq. 2.4.3.1, even values of the exponent j cause asymetries with respect to composition for the excess free energy while odd values are symmetric with respect to composition. Typically, no more than four terms of the expression are used [Marcus].

Using only the first term with no temperature or presssure dependence to the b_1 constant, reduces the Redlich-Kister equation to the regular solution equation. The regular solution model assumes ideal mixing and attributes all non-ideal behavior to an excess enthalpy ($h^{xs,mix}$). It further assumes ideal volumetric behavior, i.e. a zero excess volume. In this formulation, the molar volumes of the two components are assumed identical [Scatchard, 1935a]. The excess free energy is:

$$g^{xs,mix} = x_{BN} x_{CE} b \qquad \text{eq. 2.4.3.3}$$

where x_i is the mole fraction of butyronitrile (BN) or chloroethane (CE)
b is a constant.

This initial version of the model explained the behavior of very few systems [Malanowski]. Later versions of the model allowed for changes in the regular solution constant, b, with temperature [Marcus].

Following the later version using the Gibbs' method [Scatchard 1935b], free energy curves for both the liquid and the solid state were simulated (figure 2.4.3.1) and the resultant phase diagram superimposed on the measured diagram as seen in figure 2.4.3.2. In simulating the excess quantities, zero solid-solid solubility was assumed. [*N.B.* This assumption is used throughout section 2.4.3.] Compared to the ideal model (figure 2.4.2.2), the eutectic temperature, 100K, and composition, 41 m/o butyronitrile, better approach the measured values, 85K and 47.87 m/o butyronitrile respectively. The approach to the eutectic does not share the sudden decrease as found in the measured curve between 30 and 60 m/o butyronitrile. This simplified model, which does not account for dipole interactions, does not replicate the measured diagram due to the presence of significant dipole moments to the components. The temperatures are also low enough that the association, orientation, and/or other inter- and intramolecular forces no longer are overwhelmed by thermal energy [Scatchard 1935a, Hildebrand 1933].

In figure 2.4.3.1, the value for the regular solution constant for the solid and liquid is listed for a given temperature. The positive value for the solid state gives a spinodal curve. A spinodal shaped solid free energy curve is consistent with the eutectic point found in the measured phase diagram. An invariable value of the regular solution constant was found for the solid excess free energy of mixing.

For the liquid state, figure 2.4.3.1 indicates negative values for the constant, *b*. This implies that the liquid solution is more stable than ideal mixing would predict. The values of the constant for the liquid state were found to be linear with temperature as shown in figure 2.4.3.3.

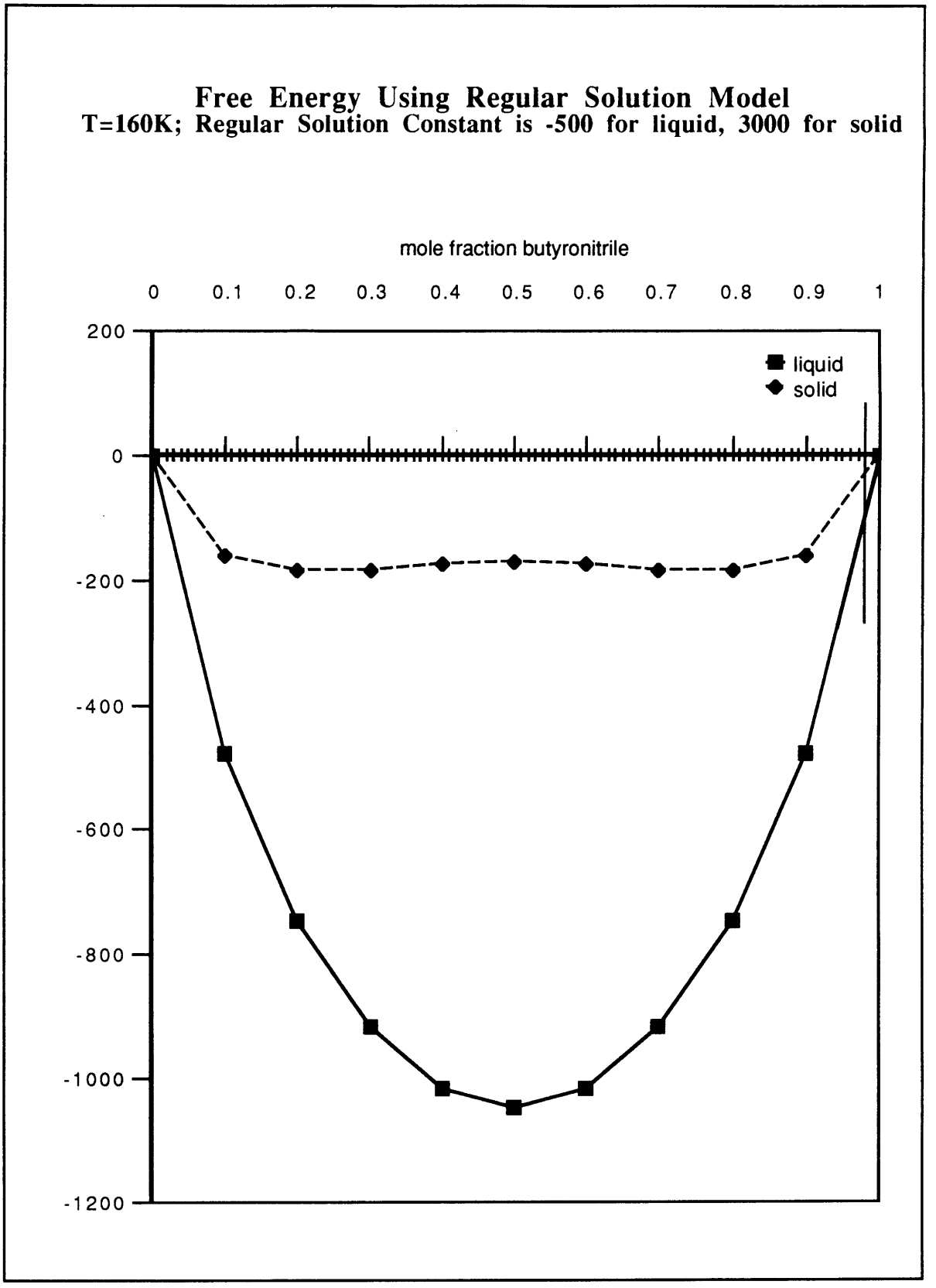

Figure 2.4.3.1a. *Free Energy Curve for Regular Solution Model.* Liquid and solid free energy curves simulated using the regular solution model where the regular solution constant is a scaled value.

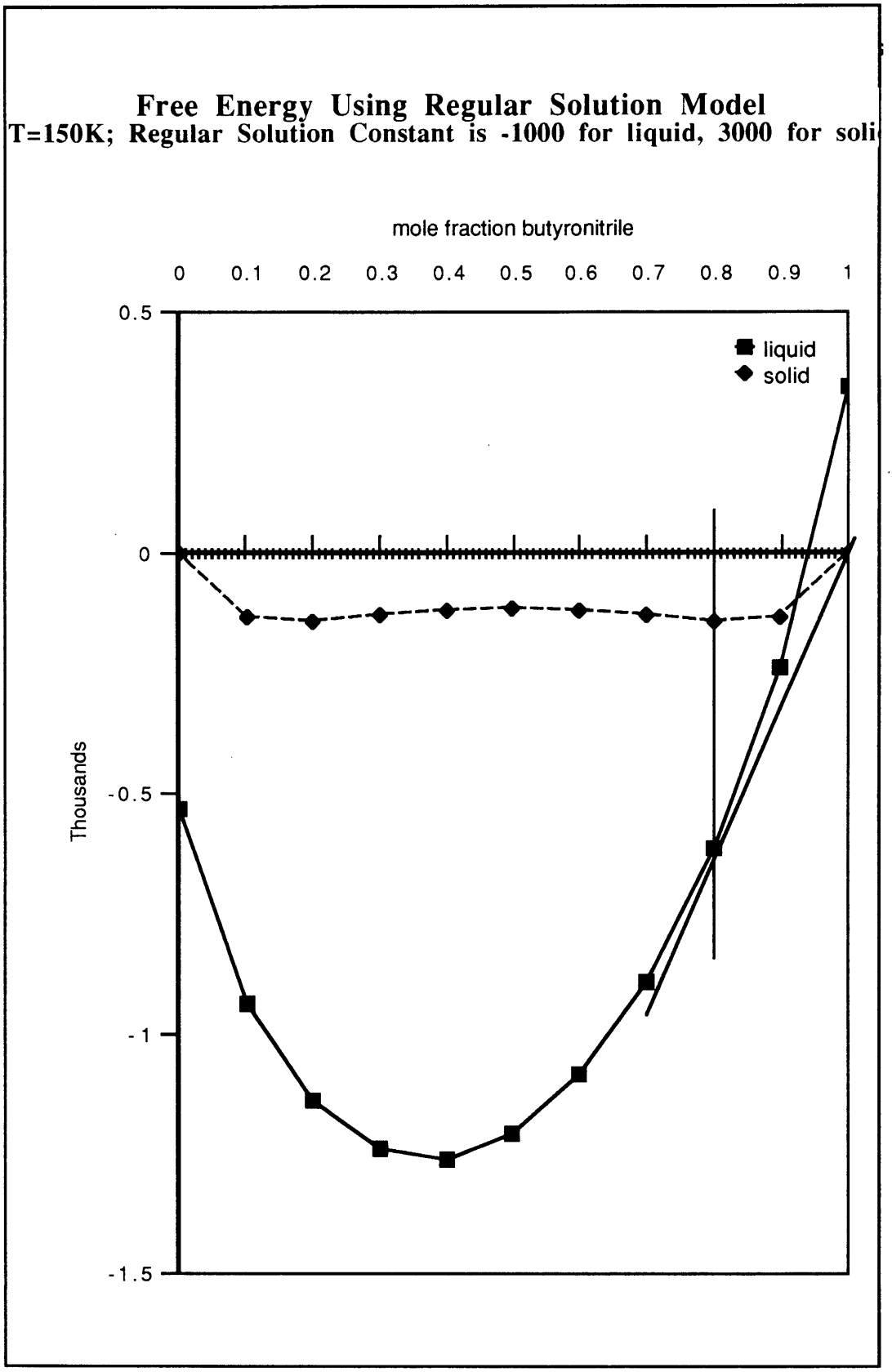

Figure 2.4.3.1b. *Free Energy Curve for Regular Solution Model.* Liquid and solid free energy curves simulated using the regular solution model where the regular solution constant is a scaled value.

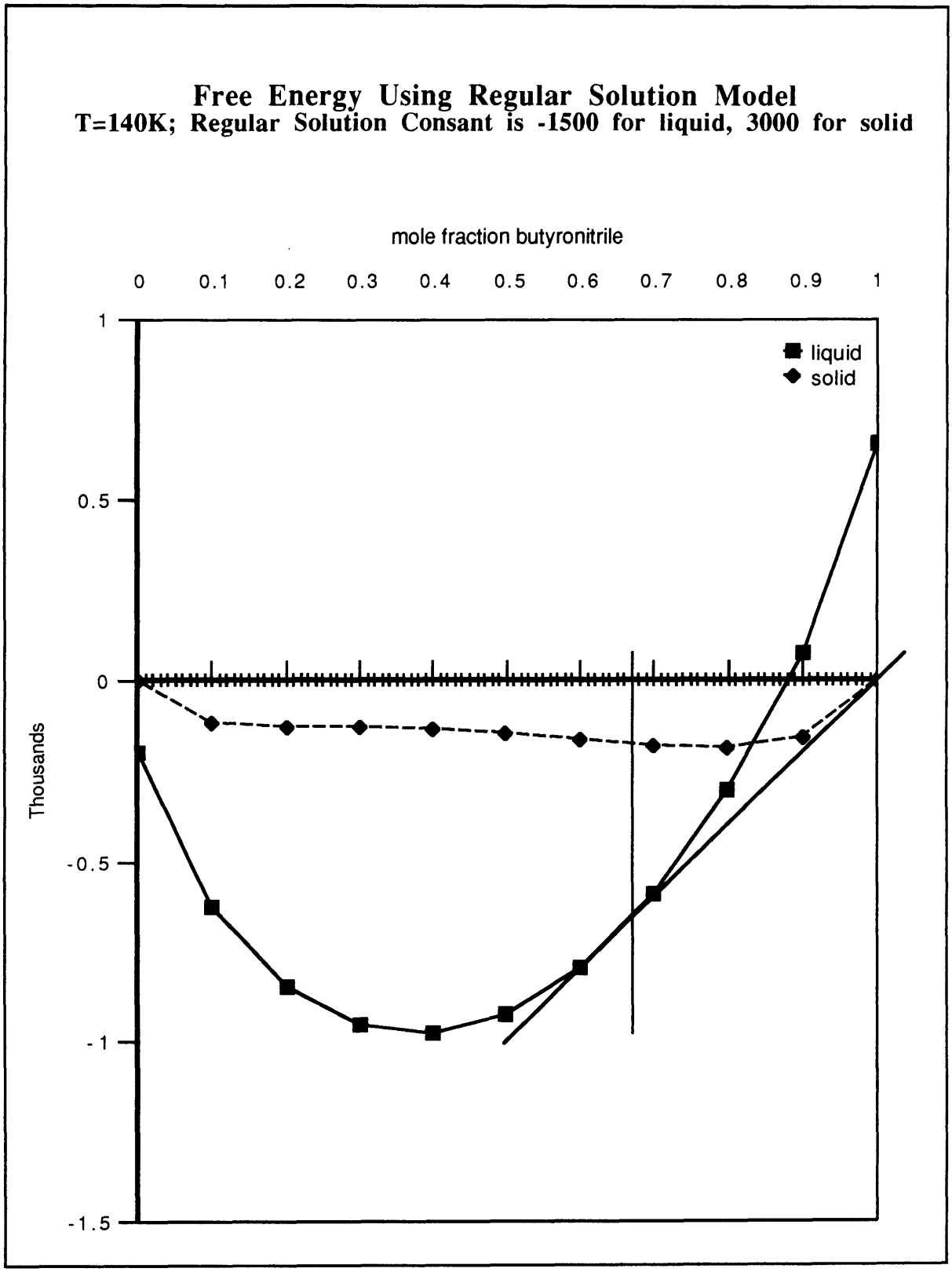

Figure 2.4.3.1c. *Free Energy Curve for Regular Solution Model.* Liquid and solid free energy curves simulated using the regular solution model where the regular solution constant is a scaled value.

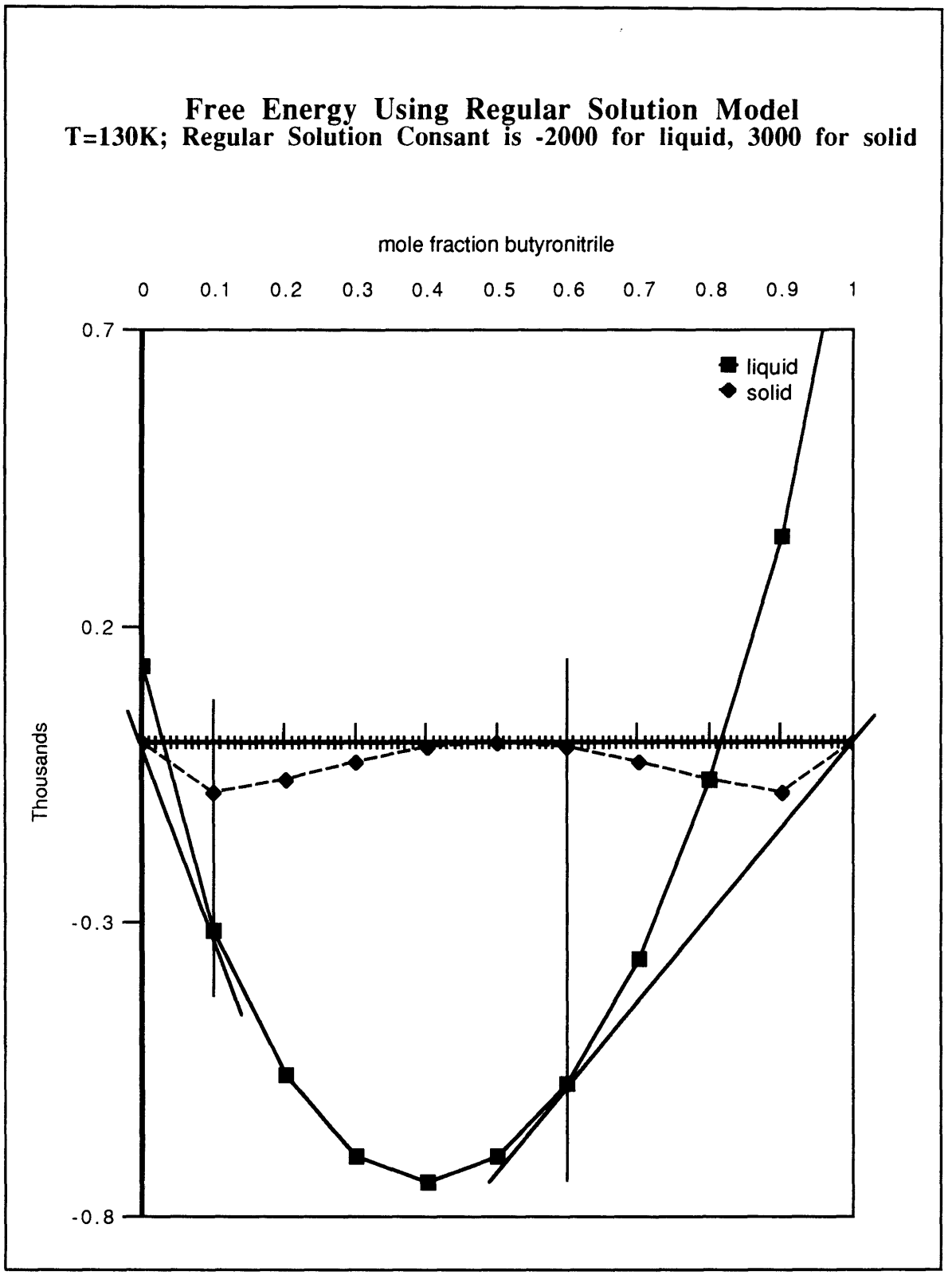

Figure 2.4.3.1d. *Free Energy Curve for Regular Solution Model.* Liquid and solid free energy curves simulated using the regular solution model where the regular solution constant is a scaled value.

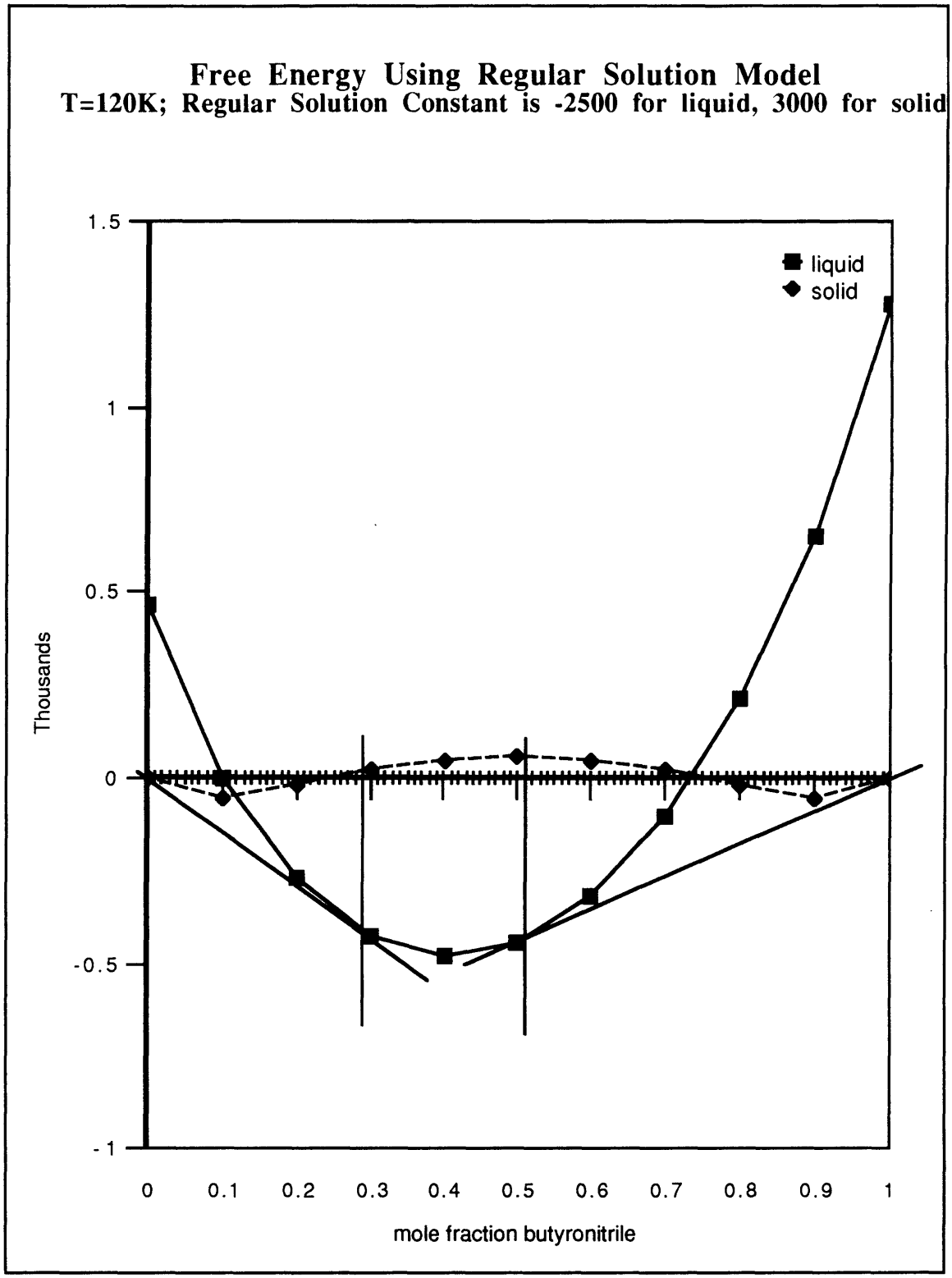

Figure 2.4.3.1e. *Free Energy Curve for Regular Solution Model.* Liquid and solid free energy curves simulated using the regular solution model where the regular solution constant is a scaled value.

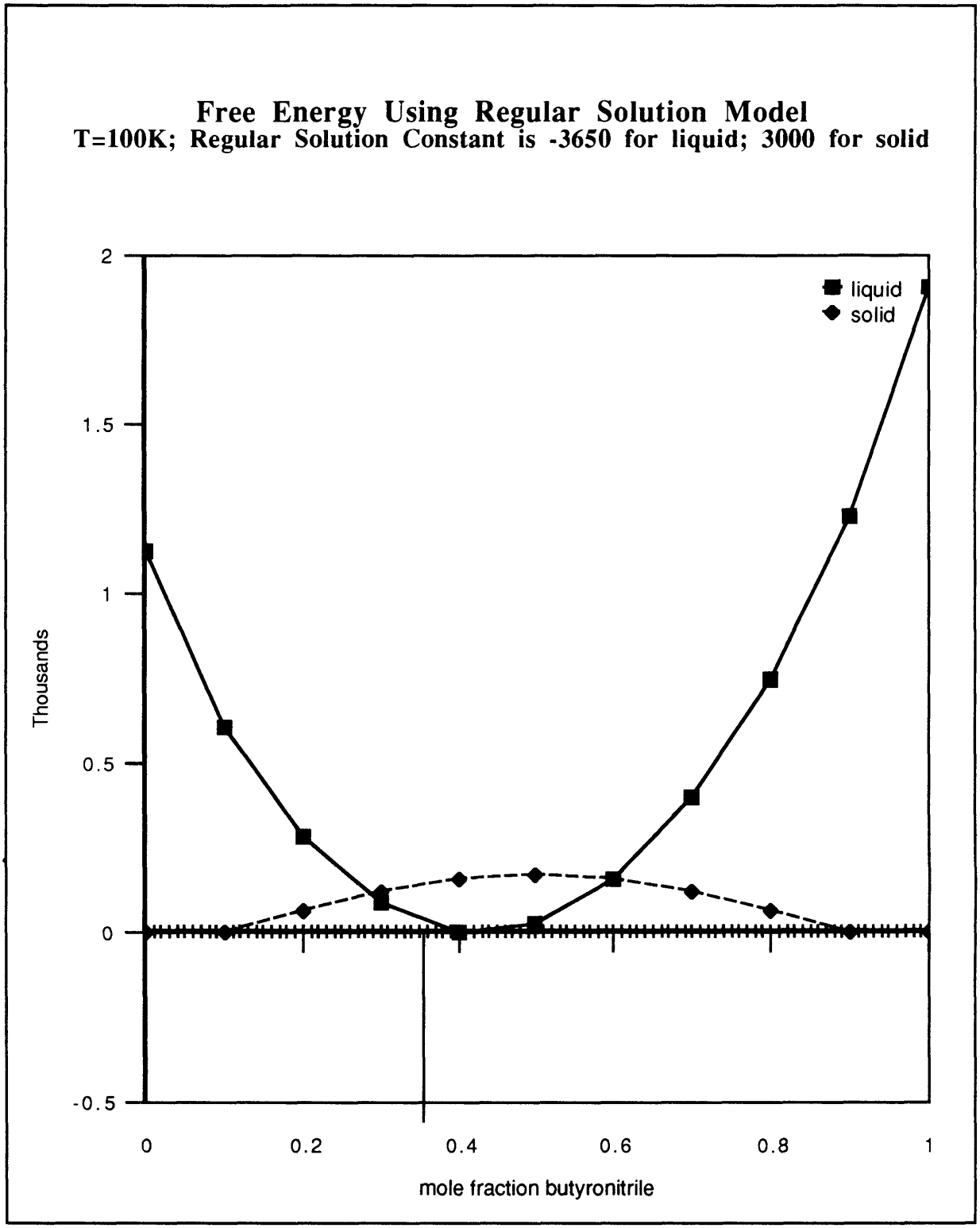

Figure 2.4.3.1f. *Free Energy Curve for Regular Solution Model.* Liquid and solid free energy curves simulated using the regular solution model where the regular solution constant is a scaled value.

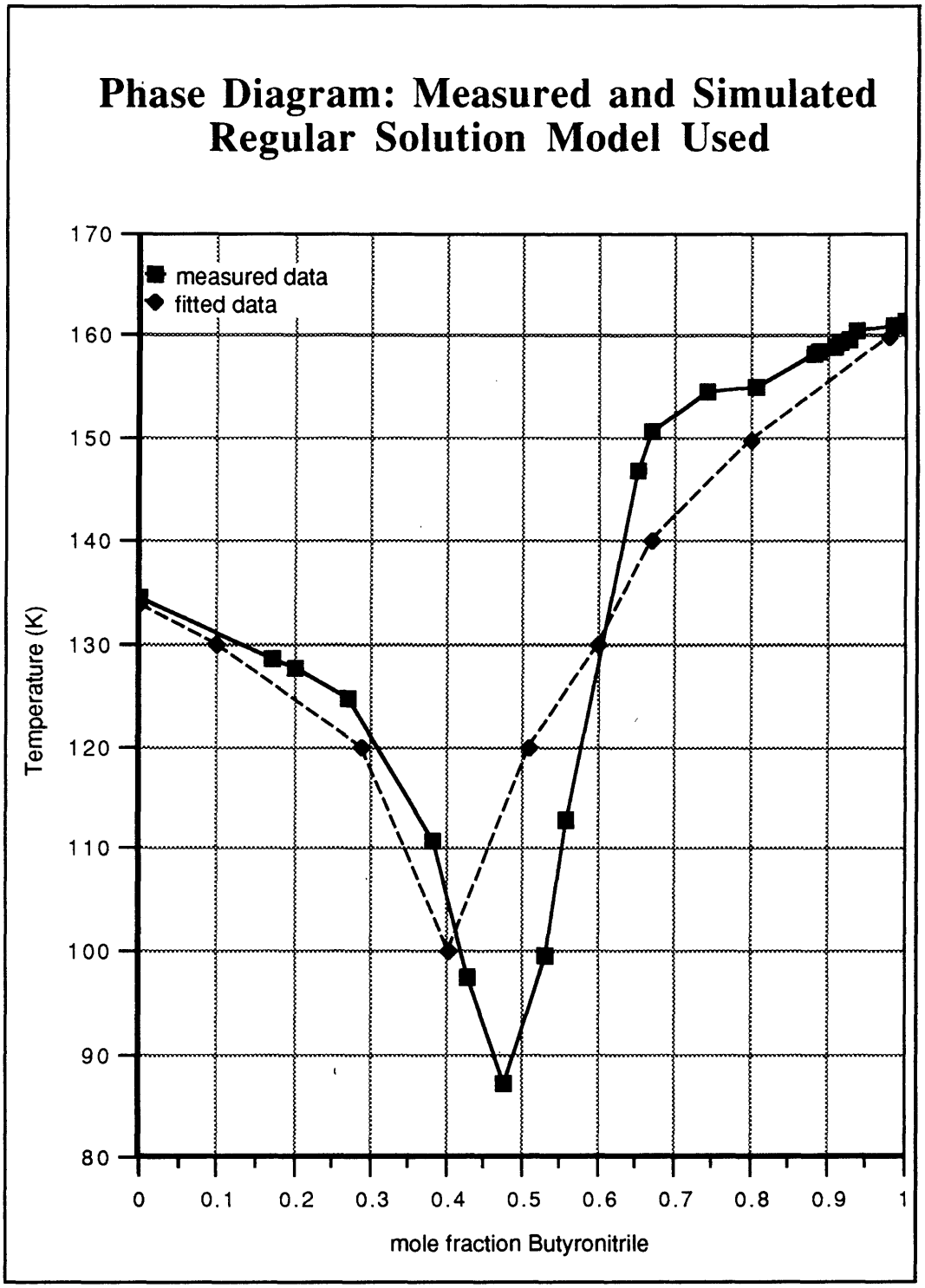

Figure 2.4.3.2. *Phase Diagram Simulated with Regular Solution Model.* Superimposed measured and simulated phase diagrams. The regular solution constant was scaled to give the best fit of the measured data.

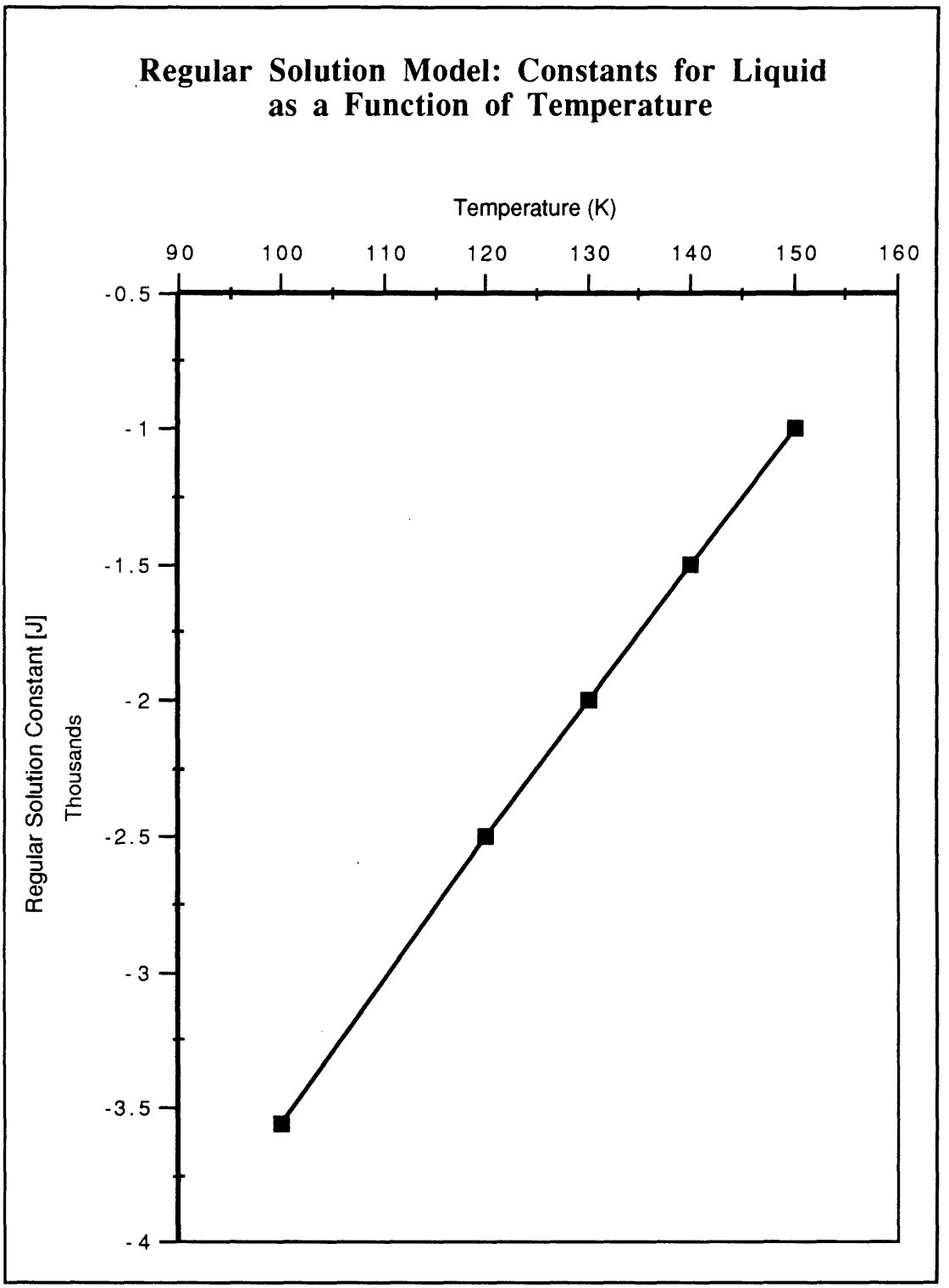

Figure 2.4.3.3. *Scaled Regular Solution Parameter.* Regular solution constant was selected to give the best fit to the measured data. For the solid, a constant value of 3000 was chosen. For the liquid, the value was found to vary linearly as a function of temperature as shown here.

2.4.3.1.2 Hildebrand-Scatchard Regular Solution Model

The regular solution model discussed above was initially posed by Hildebrand in 1929 to explain the behavior of iodine in various solvents [Hildebrand 1970]. The regular solution constant for a binary solution, according to Hildebrand and Scatchard, maintains a volumetric component which was neglected above and excess free energy assumes the form [Scatchard 1935a, Hildebrand 1933, 1970]

$$g^{xs} = (x_1 v_1 + x_2 v_2)(\delta_1 - \delta_2)^2 \varphi_1 \varphi_2 \qquad \text{eq. 2.4.3.4}$$

where δ_i is the solubility parameter of component i $[J/m^3]^{1/2}$
v_i is the molar volume of component i $[m^3/mole]$
φ_i is the volume fraction of component i
x_i is the mole fraction of component i

The solubility parameter was related by Hildebrand to the square root of the cohesive energy density as defined by Scatchard [Hildebrand, 1970]. This is related to the energy required to remove a molecule from its own liquid [Hildebrand, 1970]

$$\delta_i = \left(\frac{H_{v,i}}{v_i} \right)^{1/2} \qquad \text{eq. 2.4.3.5}$$

where $H_{v,i}$ is the heat of vaporization of component i
v_i is the molar volume.

From this equation, it can be seen that the excess energy of mixing, the enthalpy or heat content, is taken as a molar volume averaged sum of the energy to remove a molecule from its pure liquid. A phase diagram simulated using this model is shown superimposed on the measured data in figure 2.4.3.4. In this

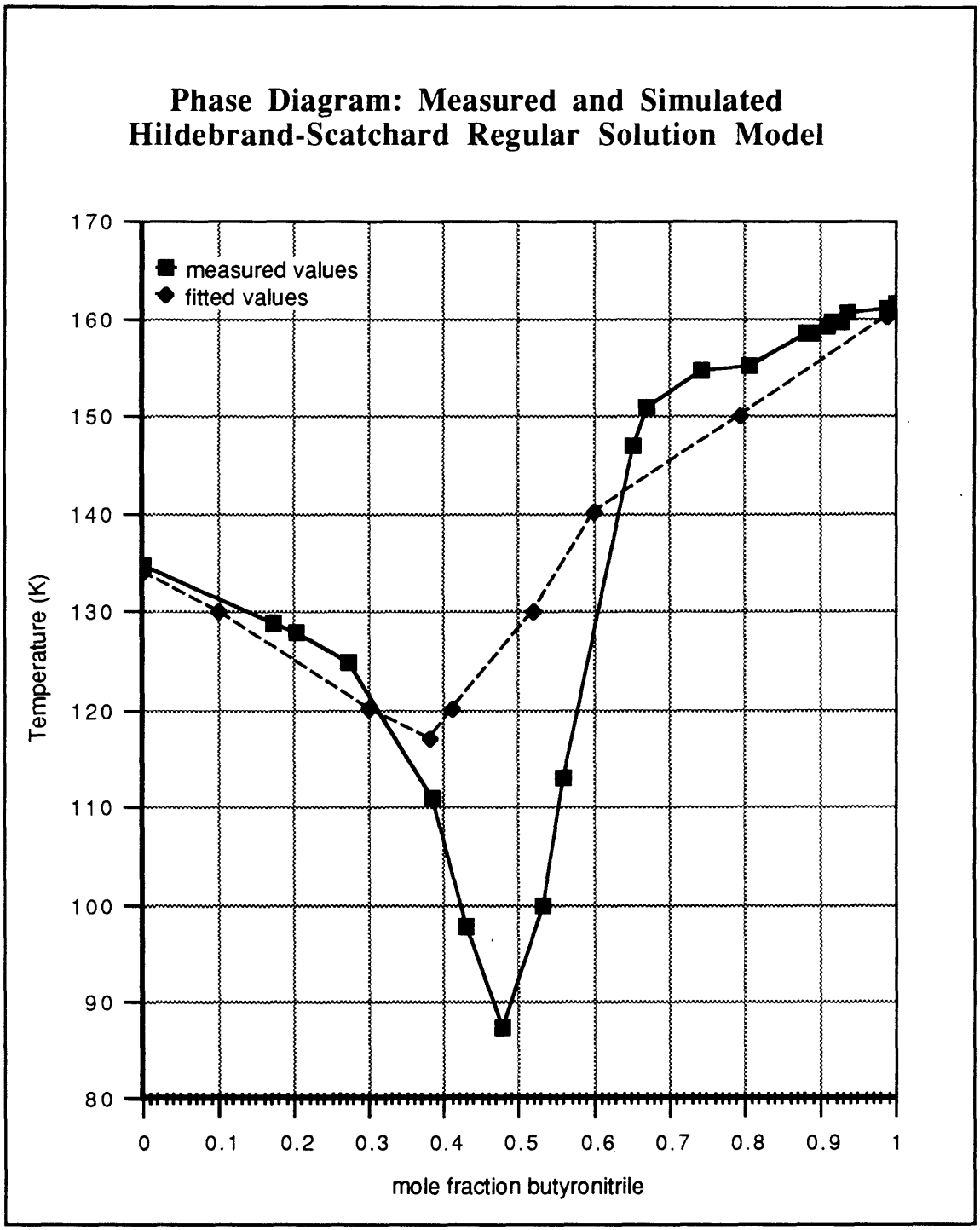

Figure 2.4.3.4 *Hildebrand-Scatchard Regular Solution Model.* Comparison of the regular solution model to the measured phase diagram.

model and in all subsequent models, the value of the molar volume was extrapolated to lower temperatures from an empirical relationship of the density of the pure component found in the literature [Daubert].

$$\varphi_i = \rho_i^{-1} = \left\{ A / B^{\left[1+(1-T/C)^D\right]} \right\}^{-1} \qquad \text{eq. 2.4.3.6}$$

where A_{BN}= 0.87533; A_{CE}= 0.87533
B_{BN}= 0.24331; B_{CE}= 0.27464
C_{BN}= 582.25; C_{CE}= 460.35
D_{BN}= 0.28586; D_{CE}= 0.3140

In this simulation, the excess free energy of the liquid was multiplied by -1 in order to better represent the data. For the solid phase, the parameter values at 80K were used.

The eutectic point following the regular solution model as put forth by Hildebrand and Scatchard is at 38 m/o butyronitrile and 117K. The model is a better approximation than the ideal model (figure 2.4.2.2) but not as good as the prior model and still fails to completely represent the measured system. The model was not developed to define polar, associated, and/or hydrogen bonded solvents where mixing is not random [Hildebrand, 1970, Redlich, Scatchard, 1935a]. Nor is it applicable when the thermal energy does not dominate over other molecular interactions [Hildebrand, 1933].

The enthalpy of mixing used depends on the solubility parameter of the pure component. The solubility parameter is defined through the heat of vaporization of the component and is extrapolated to lower temperatures via the following equation based on the ideal gas law [Hildebrand, 1970]

$$\delta = \sqrt{\frac{\Delta H_v - RT}{v}} \qquad \text{eq. 2.4.3.7}$$

where ΔH_v is the heat of vaporization and the other factors have their earlier meanings.

Though it should account for the dipole interactions of the pure solvent, it does not consider the change in dipole interactions in a solution. As a result the excess energy of the liquid for the measured phase diagram is underpredicted when compared to the scaled values of the one-parameter Redlich-Kister model (eq. 2.4.3.3). For the solid phase, the spinodal curve is not predicted contrary to the measured phase diagram .

The Hildebrand-Scatchard regular solution model demonstrates the effects of the molecular volumes (i.e. the lack of random mixing) in the measured system. Though the energies due to the solubility parameters are far lower than those used in the one term Redlich-Kister model, the Hildebrand-Scatchard model results in a eutectic composition of very nearly the same value. In the former model, much larger energies were required to skew the eutectic composition closer to the measured value (47.87m/o butyronitrile) from the ideal value (31m/o butyronitrile). The volumetric effects in the latter model results in the same eutectic composition with a much smaller energy requirement.

2.4.3.1.3 Weimer-Prausnitz Polar Regular Solution Model

Because the components of the measured phase diagram have permanent dipoles, a successful model must account for the polarity of the solvents. Weimer and Prausnitz as well as others have sought to expand the cohesive energy term of the regular solution model of Hildebrand and Scatchard to consider the effects of the dipoles [Malanowski]. The cohesive energy is divided into two parts. The first represents the dispersive forces (non-polar contribution), and the second accounts for the polar effects.

$$\delta_i^2 = \tau_i^2 + \lambda_i^2 \qquad \text{eq. 2.4.3.8}$$

where λ_i is the nonpolar part
τ_i is the polar part.

The excess free energy, maintaining the assumptions of the regular solution model, becomes [Marcus, Malanowski]:

$$g^{xs} = (x_1 v_1 + x_2 v_2)\varphi_1\varphi_2\left[(\lambda_1 - \lambda_2)^2 + (\tau_1 - \tau_2)^2 - 2\psi_{12}\right] \qquad \text{eq. 2.4.3.9}$$

where $\psi_{12} = \lambda_1\lambda_2 + \tau_1\tau_2 - C_{12}$ is the binary interaction term.

Defining this term is problematic. In the case of a polar-nonpolar solution, $\psi_{12} = 0.4\tau_{polar}^2$ is often used [Marcus]. The phase diagram of figure 2.4.3.5 was simulated from free energy curves where the excess free energy was defined as

$$g^{xs} = (x_1 v_1 + x_2 v_2)\varphi_1\varphi_2[C] \qquad \text{eq. 2.4.3.10}$$

where C is a scaled constant.

In figure 2.4.3.6, these constants are plotted as a function of temperature. It was found to vary as:

$$C\left[J/cm^3\right] = -177.929 + 1.106T(K) \qquad \text{eq. 2.4.3.11}$$

Comparison with equation 2.4.3.9 (Weimer-Prausnitz model) with eq. 2.4.3.4 (Hildebrand-Scatchard model) the form of the constant, C, is the difference of the solubility parameter terms less twice an interaction term. For the

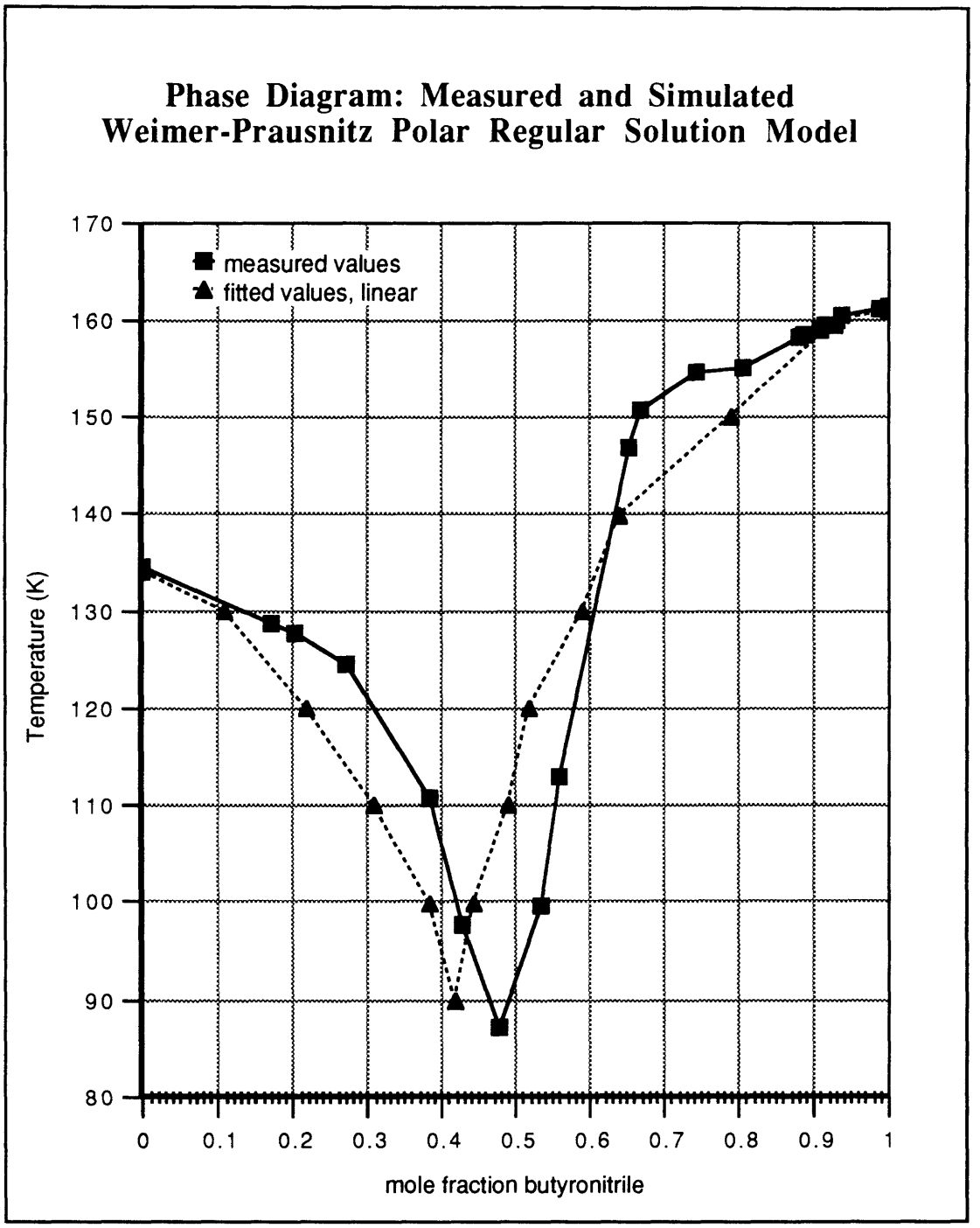

Figure 2.4.3.5 *Hildebrand-Scatchard Regular Solution Model.* Contrast of the regular solution model with a fitted constant to the measured phase diagram.

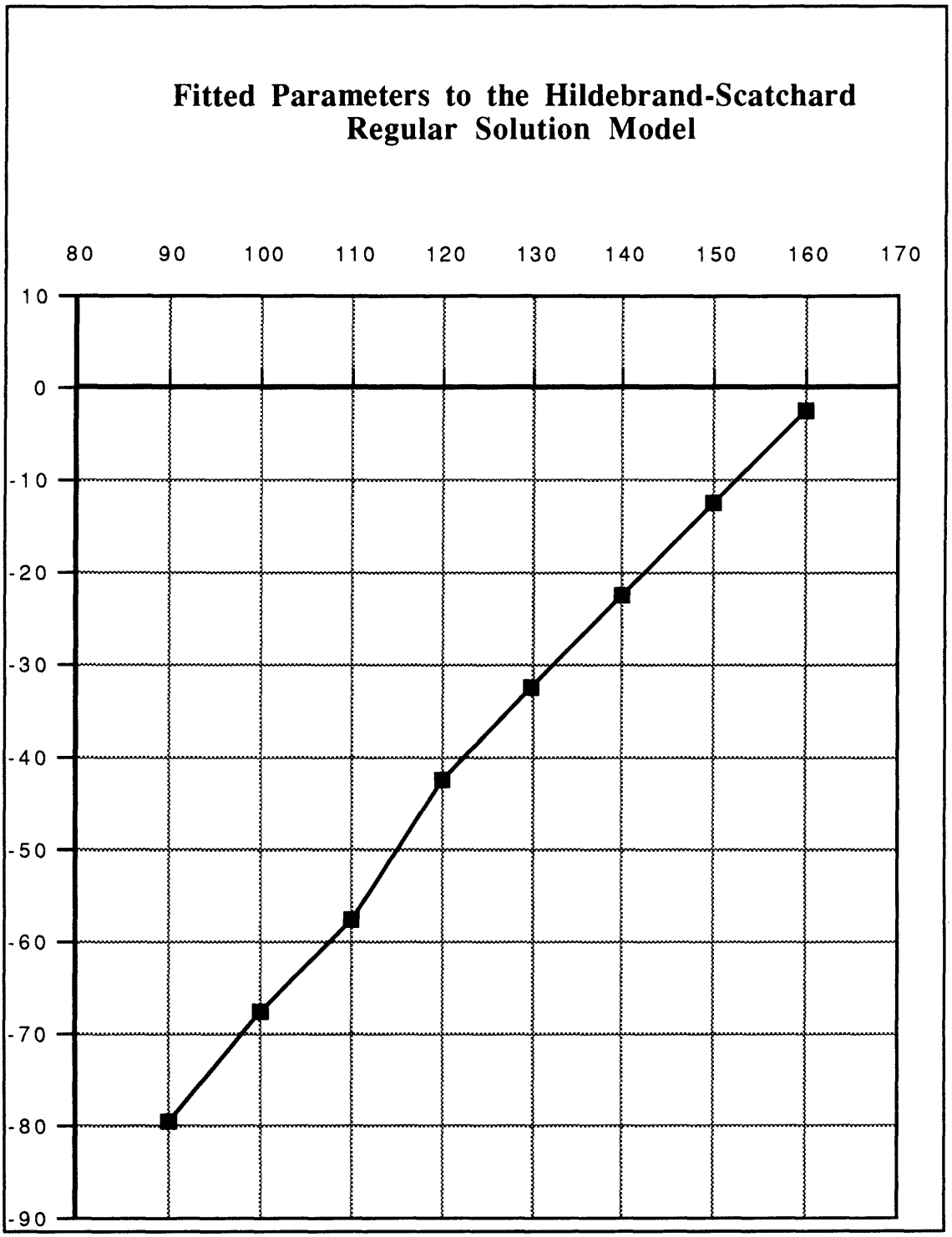

Figure 2.4.3.6 *Polar Solubility Constant.* Fitting the Hildebrand-Scatchard model to a scaled constant instead of one based upon the solubility parameter. The resultant constant as a function of temperature is related to the polar solubility constant found in equation 2.4.3.12.

measured system, the factors of the solubility parameter (eq. 2.4.3.8) have not been measured as a function of temperature nor is there a viable representation of the binary interaction term. Using equation 2.4.3.7, the solubility parameter can be computed as a function of temperature. If the interaction term is related to the geometric mean of the two components and the Weimer and Prausnitz *polar* solubility parameter (equation 2.4.3.8) is used, an expression for C may be obtained as follows.

$$C = (\delta_{BN} - \delta_{CE})^2 - 2(\delta_{BN}\delta_{CE}) \qquad \text{eq. 2.4.3.12a}$$
$$= (\lambda_{BN} + \tau_{BN} - \lambda_{CE} - \tau_{CE})^2 - 2[(\lambda_{BN} + \tau_{BN})(\lambda_{CE} + \tau_{CE})]$$
$$= (\lambda_{BN} - \lambda_{CE})^2 + (\tau_{BN} - \tau_{CE})^2 - 2[\lambda_{BN}\lambda_{CE} + \tau_{BN}\tau_{CE} - \lambda_{BN}(\tau_{BN} - 2\tau_{CE}) - \lambda_{CE}(\tau_{CE} - 2\tau_{BN})]$$

The binary interaction term becomes

$$\psi_{12} = \lambda_{BN}(\tau_{BN} - 2\tau_{CE}) + \lambda_{CE}(\tau_{CE} - 2\tau_{BN}) \qquad \text{eq. 2.4.3.12b}$$

The temperature relationship of eq. 2.4.3.12a is

$$\left\{(\delta_{BN} - \delta_{CE})^2 - 2(\delta_{BN}\delta_{CE})\right\}[J/cm^3] = -1155.092 + 1.083T(K) \qquad \text{eq. 2.4.3.13}$$

which compares well with the C values computed in the simulated phase diagram. The solubility parameter values were computed at temperatures far below the applicability of equation eq. 2.4.3.7, yet the temperature dependence of the computed (eq. 2.4.3.13) and scaled (eq. 2.4.3.11) regular solution constant (C in eq2.4.3.10) were similar. This also suggests that the size of the molecules is of great importance in considering the thermodynamics of this system [Recall, $\delta = f(T,v)$]. Equation 2.4.3.12b suggests complex interactions exist between the molecules. As expected, the model reflects the measured diagram well, but is not perfect.

2.4.3.1.4 Two Term Redlich-Kister Model

The regular solution model is a special case of the Redlich-Kister relationship (eq. 2.4.3.1). If two terms of the equation are used, free energy takes the form

$$g^{xs} = x_1 x_2 \left[b(1) + b(2)(x_1 - x_2) \right] \qquad \text{eq. 2.4.3.14}$$

and the free energy curves can be simulated resulting in the phase diagram shown in figure 2.4.3.7. For the solid phase the constants were invariant with temperature. For the liquid, the values of the constants are plotted in figure 2.4.3.8 as a function of temperature. The computed phase diagram is a better representation of the measured data as compared to the ideal and regular solution models. The addition of the second term, where *j-1* is odd, skews the free energy curves and the phase diagram causing a better match to both the eutectic temperature and composition.

As the molar volumes of the two components differ by less than 50%, the Scatchard equation may be used to generate the constants, $b(1)$ and $b(2)$ [Redlich, 1948]. The relationships are

$$b(1) = 2A v_1 v_2 / (v_1 + v_2) \qquad \text{eq. 2.4.3.15a}$$

$$b(2) = -b(1)(v_1 - v_2)/(v_1 + v_2) \qquad \text{eq. 2.4.3.15b}$$

where A is related to the solubility parameter and the other functions have their previously defined meanings.

For A, the *polar* solubility parameter, equation 2.4.3.13, was used. When eq. 2.4.3.15a was allowed to vary with temperature through the solubility parameter, δ, and the molar volume, v, the following relationship results

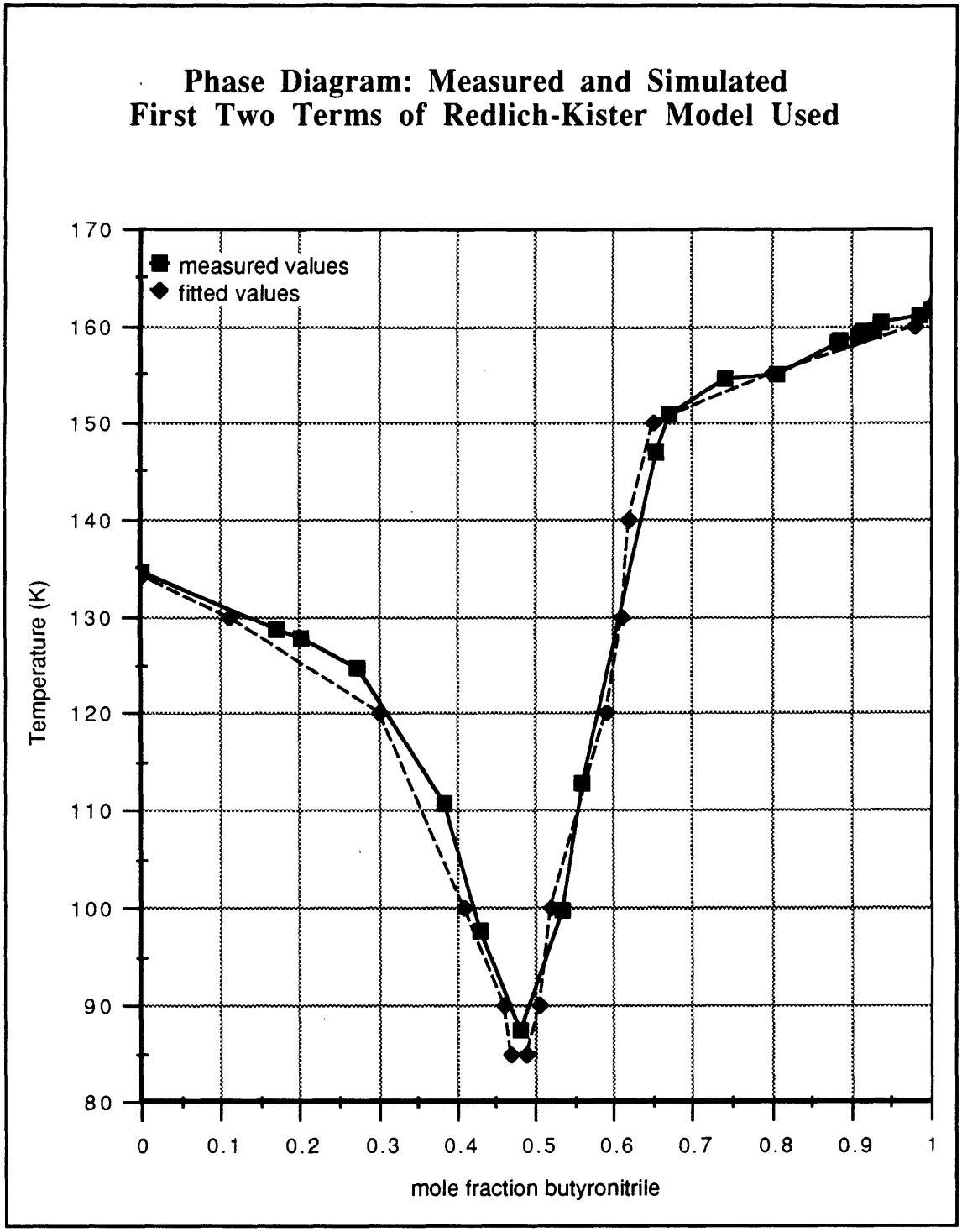

Figure 2.4.3.7. *Two Term Redlich-Kister Model.* Simulated phase diagram using two terms of the Redlich-Kister model is superimposed on the measured data. The scaled parameters were selected to best fit the measured data.

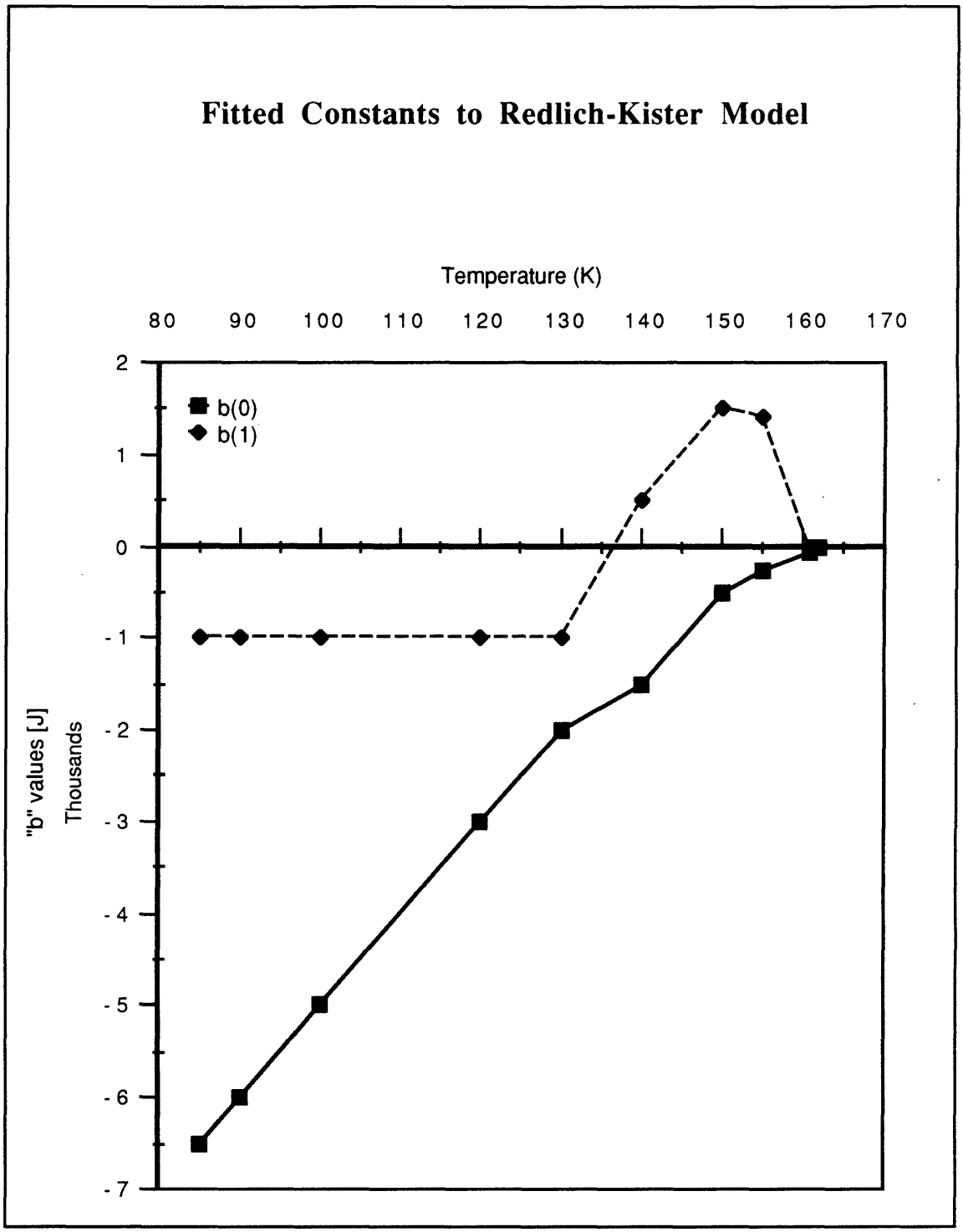

Figure 2.4.3.8 *Constants for Two-term Redlich-Kister Model.* These constants were used to simulate the free energy curves that generate the phase diagram shown in figure 2.4.3.7.

$$b(1)_{\text{model}}[J/mole] = -69{,}971 + 19T \qquad \text{eq. 2.4.3.16a}$$

which compared poorly to the fitted curve variation with temperature

$$b(1)_{\text{fit}}[J/mole] = -14{,}060.8 + 90.45T. \qquad \text{eq. 2.4.3.16b}$$

For the second constant the temperature variation of the model is

$$b(2)_{\text{model}}[J/mole] = -7241.41 - 0.340T. \qquad \text{eq. 2.4.3.17}$$

At the lower temperatures, $b(2)$ was found to be invarient with temperature with a value of -1000. Again, the fit is fairly poor and the model does not explain the fairly large variation at higher temperatures. The poor fit is in part due to the use of a model that is inappropriate near the freezing points of a liquid. The Hildebrand-Scatchard model, as mentioned earlier, was developed with the assumption that thermal forces dominate all other forces. Again, the assumption of random mixing is a short-coming of this and the previous models.

2.4.3.1.5 Z-fraction

The molecule size has been accounted for in a number of other models. In place of the mole fraction, x_i, a z-fraction is often used [Marcus]

$$z_1 = \frac{x_1}{x_1 + rx_2} \qquad \text{eq. 2.4.3.18a}$$

$$z_2 = \frac{rx_2}{x_1 + rx_2} \qquad \text{eq. 2.4.3.18b}$$

where r is a constant. When r is taken as the ratio of the molar volume of the components, $r = v_2/v_1$, the z-fraction reduces to the volume fraction of the component. Using only the first term of equation 2.4.3.1 (Redlich-Kister equation), the excess free energy in terms of z-fractions is now

$$g^{xs} = z_1 z_2 b \qquad \text{eq. 2.4.3.19}$$

When

$$r = \frac{v_2}{v_1}$$

$$b = b'\left[\frac{\left(x_1 v_1 + x_2 v_2\right)^2}{v_1 v_2}\right] or \qquad \text{eq. 2.4.3.20a}$$

$$b = b'\left(x_1 v_1 + x_2 v_2\right)$$

reduces to the excess free energy with z-fractions to the first term Redlich-Kister equation (eq. 2.4.3.3) when b' is a constant dependent on temperature and the Hildebrand-Scatchard equation (eq. 2.4.3.4 and eq. 2.4.3.9) when b' is difference of the solubility parameter squared respectively.

When

$$r = \frac{v_1}{v_2}$$

$$b = b'\left[\frac{\left(x_1 v_2 + x_2 v_1\right)^2}{v_1 v_2}\right] or \qquad \text{eq. 2.4.3.20b}$$

$$b = b'\left[\frac{\left(x_1 v_2 + x_2 v_1\right)^2}{\left(x_1 v_1 + x_2 v_2\right)}\right]$$

to reduce the excess free energy in terms of z-fractions to the Redlich-Kister and Hildebrand-Scatchard equations respectively.

Free energy curves were generated and the resulting phase diagram superimposed on the measured data is shown in figure 2.4.3.9a where the r-parameter equals the ratio of the molar volumes of chloroethane divided by butyronitrile. The inverse relationship is used in figure 2.4.3.9b. As seen, the latter is a far better fit. The b values are plotted as a function of temperature in

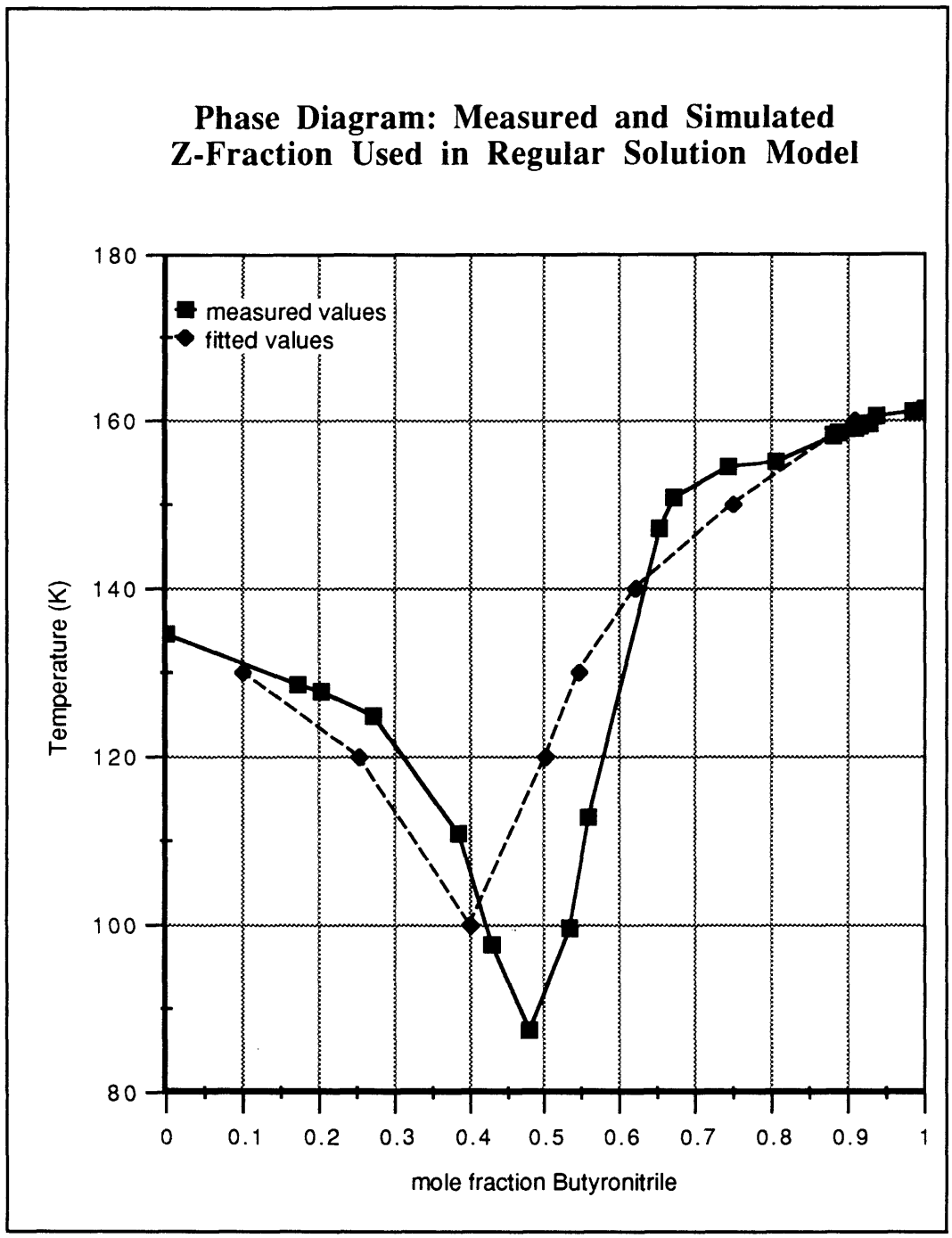

Figure 2.4.3.9a. *Z-fraction Simulated Phase Diagram.* Phase diagram computed using z-fraction in place of the mole fraction in the excess free energy term. The r-parameter used is the ratio of the molar volume of chloroethane to butyronitrile, MV(CE)/MV(BN), evaluated at the required temperature. The molar volumes were extrapolated to low temperatures with an

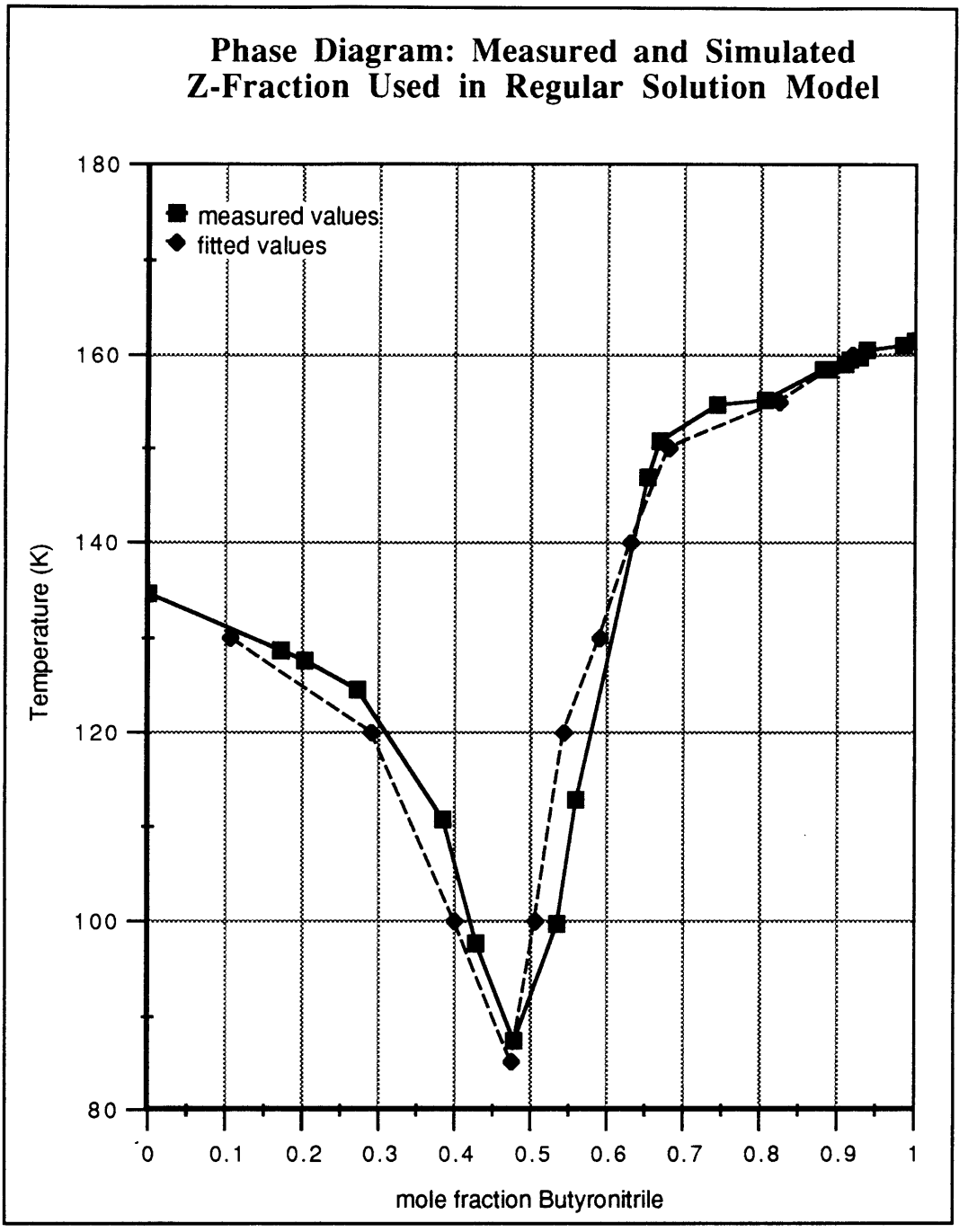

Figure 2.4.3.9b. *Z-Fraction Simulated Phase Diagram.* Phase diagram computed using z-fraction in place of the mole fraction in the excess free energy term. The r-parameter used is the ratio of the molar volume of butyronitrile to chloroethane, MV(BN)/MV(CE), evaluated at the required temperature. The molar volumes were extrapolated to low temperatures with an experimental relationship found for the pure components. [Dauber]

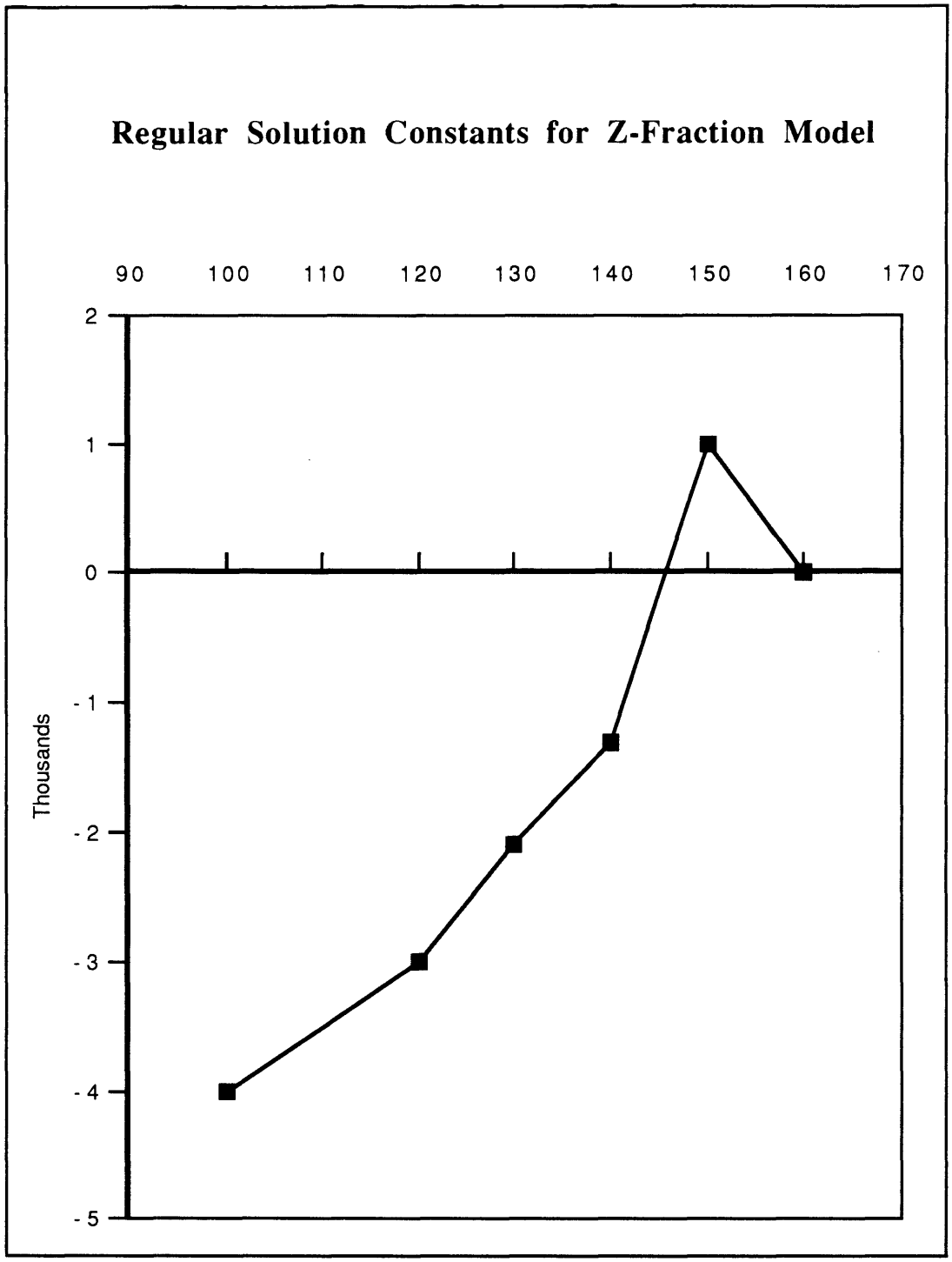

Figure 2.4.3.10a. *Regular Solution Constant for Z-fraction Model.* Value of the regular solution constant for the liquid phase when z-fraction is used instead of the mole fraction in computing the excess free energy. The value of the r-parameter used is the molar volume ratio of chloroethane to butyronitrile evaluated at the required temperature.

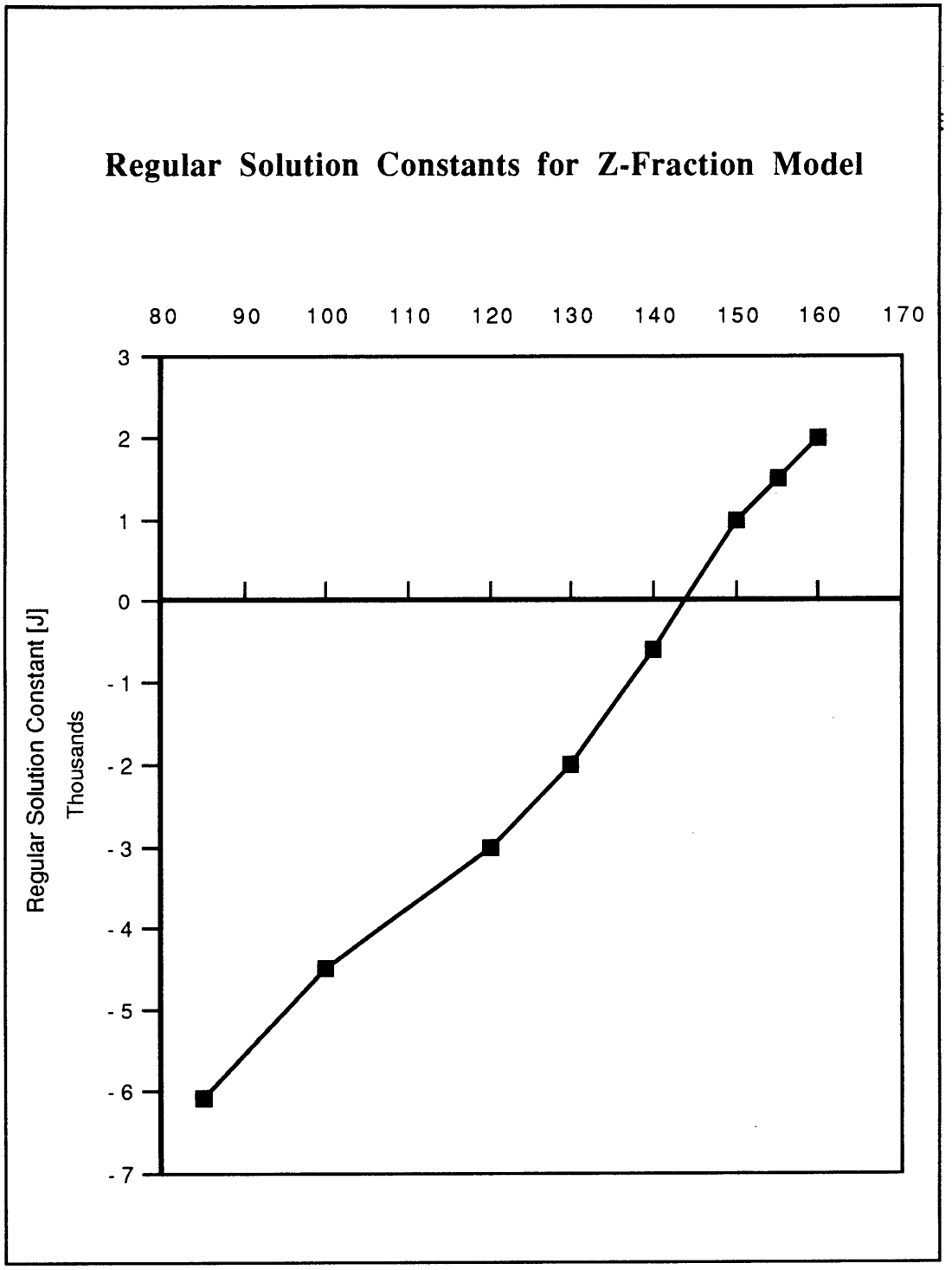

figure 2.4.3.10b. *Regular Solution Constant for Z-fraction Model.* Value of the regular solution constant for the liquid phase when z-fraction is used instead of the mole fraction in computing the excess free energy. The value of the r-parameter used is the molar volume ratio of butyronitrile to chloroethane evaluated at the required temperature.

figures 2.4.3.10a and b. In the latter case, where the fit of the model and the measured data are close, the b values vary with temperature as

$$b[J/mole] = -15646.7 + 109.11T(K) \qquad \text{eq. 2.4.3.21}$$

This is similar to the $b(1)$ variation with temperature of the two term Redlich-Kister equation (eq. 2.4.3.16b). That this model requires only one term to give a reasonable fit to the measured data indicates the importance of the different molar volumes of the components in determining the liquid phase thermodynamics.

3.4.3.2 Excess Entropy Models

3.4.3.2.1 Flory Model

The preceding models attributed all the excess properties to an excess enthalpy. Their neglect of nonrandom mixing leads to deviations of the fitted curve to the measured data. They also required large enthalpies of mixing to best fit the measured diagram. The importance of the molecular volume, which would cause nonrandom mixing, is magnified in the z-fraction model, where the r parameter assumes an inverse form of the molar volume ratios to produce a good representation of the liquidus.

When the volumes of the molecules in a solution are of significantly different sizes, the mixing is unlikely to be random. This alters the entropy of mixing. Using a free volume model [Hildebrand, 1947, Marcus], the entropy of mixing may be written as

$$\Delta s^m = -R\left\{N_1 \ell n \frac{V - N_1\left(N_A v_1'\right) - N_2\left(N_A v_2'\right)}{N_1\left[v_1 - \left(N_A v_1\right)\right]} + N_2 \ell n \frac{V - N_1\left(N_A v_1'\right) - N_2\left(N_A v_2'\right)}{N_2\left[v_2 - \left(N_A v_2\right)\right]}\right\} \quad \text{eq. 2.4.3.22}$$

where $N_A v_i'$ = the volume of component i in solution (i.e. It may not equal the molar volume.)
V= the volume of the solution
all other terms have their previous meanings

This can be rewritten as

$$\Delta s^m = -R\left[x_1 \ell n \frac{x_1}{\left(x_1 + r x_2\right)} + x_2 \ell n \frac{r x_2}{\left(x_1 + r x_2\right)}\right] = -R\left[x_1 \ell n z_1 + x_2 \ell n z_2\right] \quad \text{eq. 2.4.3.23}$$

where the terms have the same meaning as earlier [Marcus].

As can be seen, r is the ratio of the volume difference of component 2 in its pure state and in solution to the volume difference of component 1 under the same circumstances. For the case where the free volume of the components share the same proportionality to the total volume, r is the ratio of the molar volumes of component 2 to component 1.

$$s^m = -R[x_1 \ln \varphi_1 + x_2 \ln \varphi_2] \quad \text{eq. 2.4.3.24}$$

(*N.B.* In the case of chain molecules, the rotational entropy, which can not be separated from the configurational entropy, must also be considered [Marcus].)

A model that incorporates these effects was proposed by Flory in 1942 [Flory, Hildebrand 1947] and is often used to interpret the excess free energies of polymer-solvent solutions. In the lattice type model from which it was developed, the larger molecules are divided into segments which occupy more than one lattice site which must be adjacent. Different packing results than if ideal random packing occurred. The size factor is also incorporated into the excess enthalpy, again represented by a regular solution model.

$$g^m = x_1 g_1^\circ + x_2 g_2^\circ + RT\left[x_1 \ell n \varphi_1 + x_2 \ell n \varphi_2\right] + x_1 \varphi_2 b \qquad \text{eq. 2.4.3.25}$$

where the terms have their earlier meanings [Gallego].

Using this relationship, free energy curves were again generated for the solid and liquid phases with the resultant phase diagram superimposed on the measured curve and the regular solution constant shown in figures 2.4.3.11 and 2.4.3.12 respectively.

The model is a fairly good representation of the measured data. The Flory model uses an assumption that effectively cancels out the rotational component of the entropy. For polymers where the number of nearest neighbors in the solution is large and where the chains are very long, this is a good approximation [Marcus]. For the measured system, where the chain lengths may be considered as 2 for chloroethane and 4 for butyronitrile, this is not true Still, the model does fit the data well.

For the regular solution component of eq. 2.4.3.25, the curve can be broken up into three segments. [It should be noted that the *b* values of figure 2.4.3.12, were chosen to fit to the composition of the liquidus but are defined in terms of temperature only.] The segments suggest that the heat of mixing is composed of at least two types of molecular interactions: the energy associated between like molecules [A-A or B-B] and between unlike molecules [A-B]. Segment one represents the higher temperature points where the liquid is a dilute solution of chloroethane in butyronitrile. Under these conditions, like molecular interactions [A-A] predominate. Though of fewer number, unlike [A-B] molecular interactions, which have been concluded to be strong based upon the high energies of the enthalpic models, cause nominally all of the low concentration species to be complexed. In segment three, representing concentrated solutions,

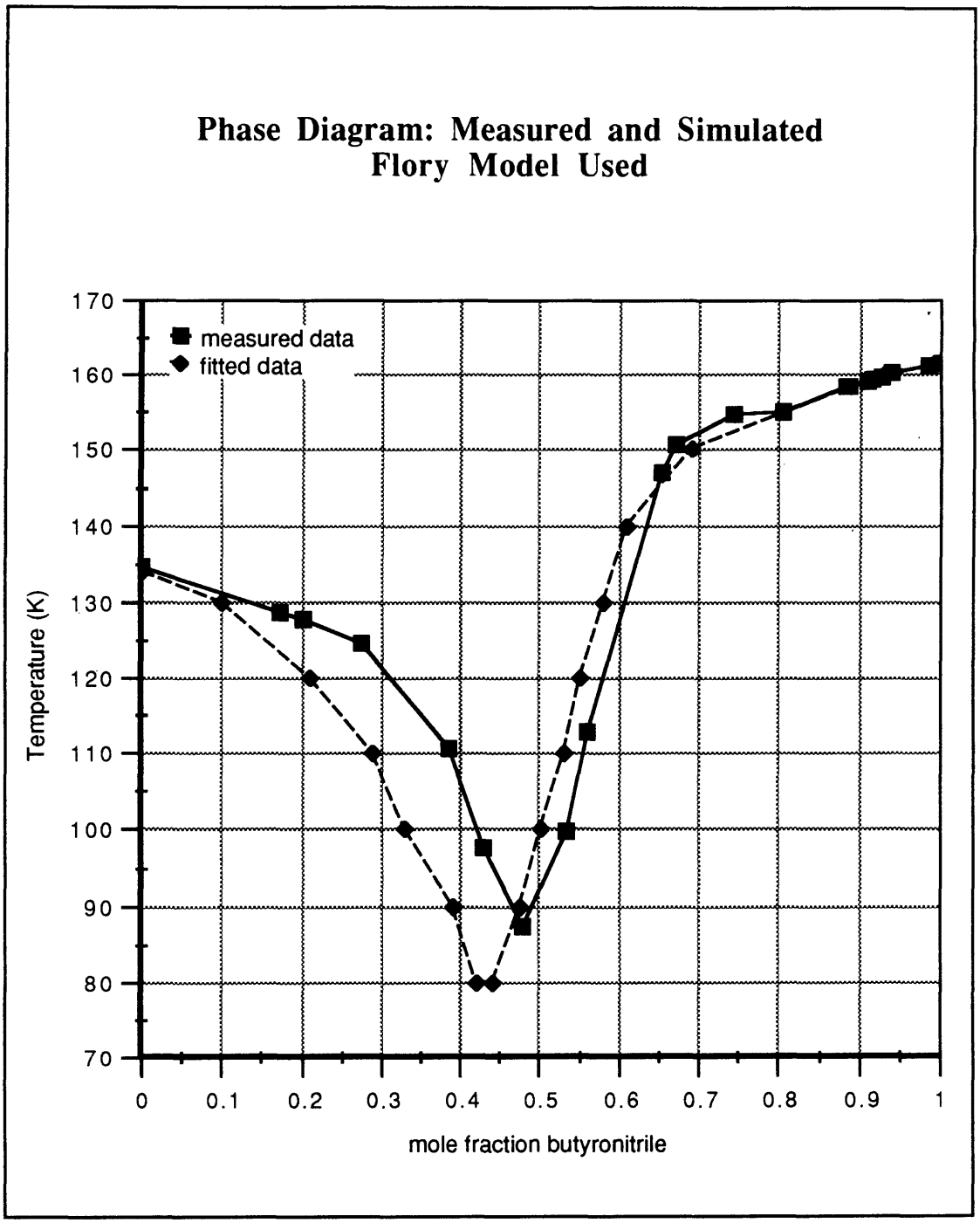

Figure 2.4.3.11. *Flory Model.* Simulated phased diagram using the Flory model superimposed on the measured data. The model incorporates a regular solution excess enthalpy with the models formulation of the excess entropy. The regular solution constants were selected to best fit the measured data.

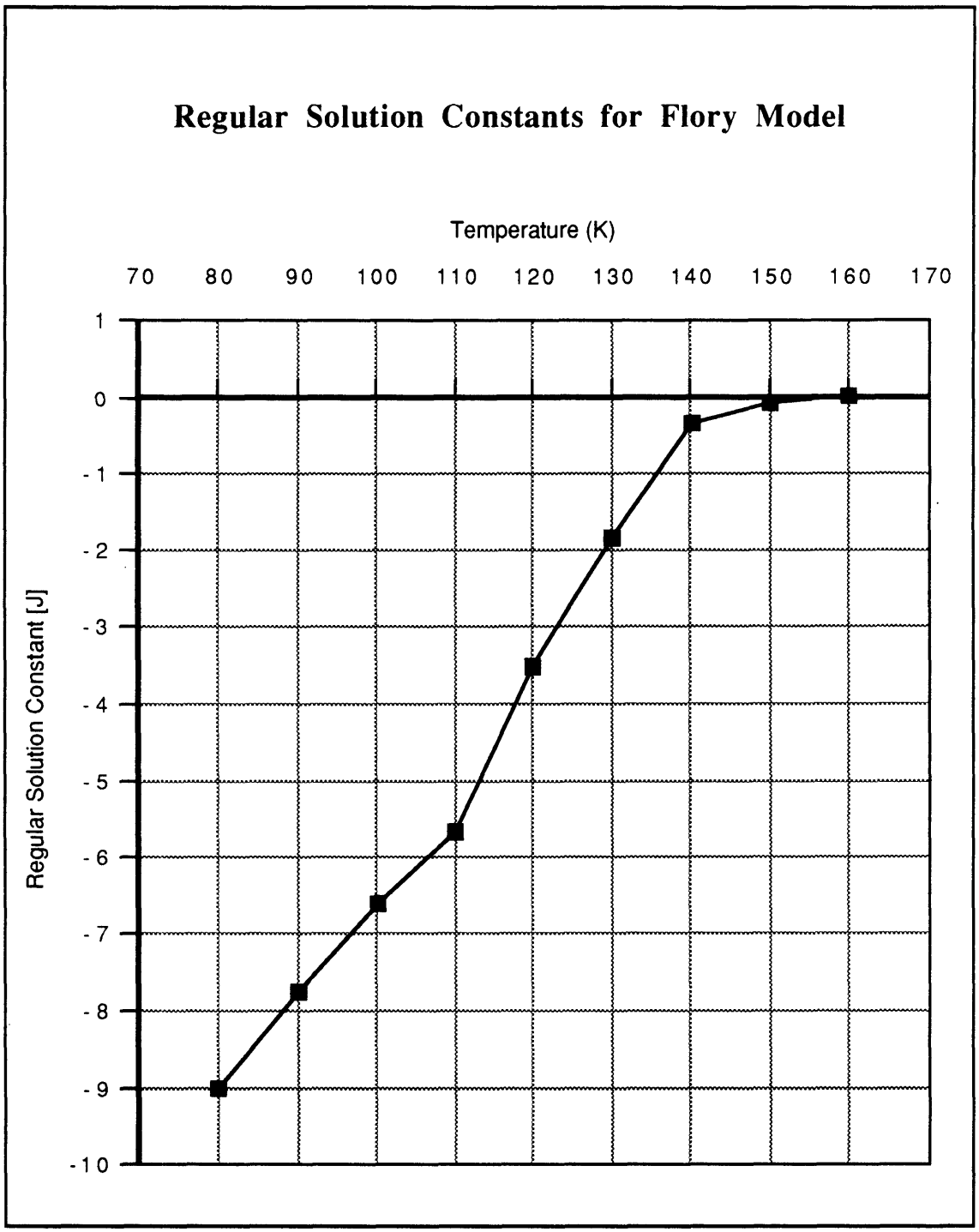

Figure 2.4.3.12. *Regular Solution Constants for Flory Model.* Regular solution constants were selected so that the simulated phase diagram (figure 2.4.3.11) best fit the measured data.

most of the species are expected to be part of unlike [A-B] complexes. The result is very little like [A-A or B-B] molecular complexes. The middle segment represents the transition between these two energetic effects of the molecular configurations.

2.4.3.2.2 Associated Solutions

From the preceding analysis, both nonrandom mixing and molecular interactions are of importance in understanding the thermodynamics of the butyronitrile-chloroethane phase diagram. In the above approaches, the solutions are considered to be comprised of individual butyronitrile and/or chloroethane molecules with the composition and mole fraction represented as n_A, n_B, x_A, x_B respectively. These models, the enthalpic effects depicted in figure 2.4.2.3, and the shape of the measured phase diagram are suggestive of unlike complexes [A-B] forming in the liquid. The liquid phase, then, may be considered to contain components A, B, and A_iB_j with the composition and mole fraction represented as $(n_{A_1}, n_{B_1}, n_{AB}, x_{A_1}, x_{B_1}, x_{A_iB_j})$ respectively. The entropy from a two component or stoichiometric view is non-random. If modeled from a many component standpoint, the solution may be considered random mixing of these species. The liquid, when viewed in this manner, is an associated solution.

The excess free energy may be written in terms of the activity coefficients as

$$g^{xs} = RT\left[x_A \ell n\gamma_A + x_B \ell n\gamma_B\right]. \qquad \text{eq. 2.4.3.26}$$

In the associated solution model, it can be shown that

$$\mu_A^\circ + RT\ell n x_A\gamma_A = \mu_{A_1}^\circ + RT\ell n x_{A_1} \qquad \text{eq. 2.4.3.27}$$

The difference of the chemical potentials when the mole fraction of *A* tends to one is

$$x^{\circ}_{A_1} = \exp\left(-\frac{\mu^{\circ}_{A_1} - \mu^{\circ}_{A}}{RT}\right) \qquad \text{eq. 2.4.3.28}$$

which is the mole fraction of uncomplexed species in the pure solution.

Therefore, the activity coefficient of species ***i*** of non-random mixing is related to the mole fraction of i_1 in the associated solution through [Prigogine]

$$\gamma_i = \frac{1}{x^{o}_{i_1}} \cdot \frac{x_{i_1}}{x_i} \qquad \text{eq. 2.4.3.29}$$

where $x^{o}_{i_1}$ is the mole fraction of uncomplexed *i* in the pure liquid (i.e. self - associates may exist in pure phase).
x_{i_1} is the mole fraction of uncomplexed *i* in the solution.
x_i is the stoichiometric mole fraction of *i* (i.e. the total mole fraction of *i* in the solution whether complexed or not).

For the butyronitrile-chloroethane system, the formation of dimolecular self-associates of butyronitrile and unlike dimolecular [A-B] complexes of one butyronitrile and one chloroethane is anticipated [Murray, chapter three of this thesis]; therefore, an equilibrium of A, B, A_2, and AB [BN, CE, BN_2, and BNCE] is expected. Lack of information about the nature and number of each of the associated species makes the mathematics unwieldy. By assuming a model in which only the unlike dimolecules of one butyronitrile and one chloroethane form, the mathematics may be solved. The resulting equilibrium constant would in actuality reflect the combined equilibrium of the two associated species. This will be discussed in more detail after the discussion of the three species [A, B, AB] model.

For the equilibrium $AB \Leftrightarrow A + B$ $\{BNCE \Leftrightarrow BN + CE\}$, the mole fraction of the uncomplexed species in solution is

$$x_{A_1} = \frac{n_{A_1}}{n_{A_1} + n_{AB} + n_{B_1}} . \qquad \text{eq. 2.4.3.30}$$

The equilibrium is represented by an equilibrium constant which follows Gibbs-Helmholtz behavior with temperature where

$$K = \frac{x_{A_1} x_{B_1}}{x_{AB}} = \frac{x_{BN} x_{CE}}{x_{BNCE}} = \frac{n_{A_1} n_{B_1}}{n_{AB}\left(n_{A_1} + n_{B_1} + n_{AB}\right)} = e^{-\Delta G^\circ / RT} = e^{\Delta S^\circ / R} \cdot e^{-\Delta H^\circ / RT} \qquad \text{eq. 2.4.3.31}$$

where ΔG° is the standard free energy [J/mole].

This is solved for

n_{A_1} in terms of n_{B_1}, n_{AB}, and K,

n_{B_1} in terms of n_{A_1}, n_{AB}, and K,

and n_{AB} in terms of n_{A_1}, n_{B_1}, and K.

Then, the mole fraction of the uncomplexed species can be determined in terms of the stoichiometric mole fractions and the equilibrium constant [Prigogine]. As an example

$$x_{A_1} = \frac{x_A - x_B + \sqrt{x_A^2 + x_B^2 - 2x_A x_B\left(\frac{1-K}{1+K}\right)}}{1 + \sqrt{x_A^2 + x_B^2 - 2x_A x_B\left(\frac{1-K}{1+K}\right)}} . \qquad \text{eq. 2.4.3.32}$$

This is then incorporated into the excess free energy expression (eq. 2.4.3.26).

Using equation 2.4.3.26, free energy curves were again generated. The equilibrium constant is the only scaling factor. The resulting phase diagram and the equilibrium constants as a function of temperature are shown in figures 2.4.3.13 and 2.4.3.14 respectively. As seen, the fit of the measured data is very close. The dramatic descents of the liquidus between 30 and 60 mole percent butyronitrile are produced in this model without resorting to large excess energies or, in the z-fraction model, to unusual volume effects. The effects of the

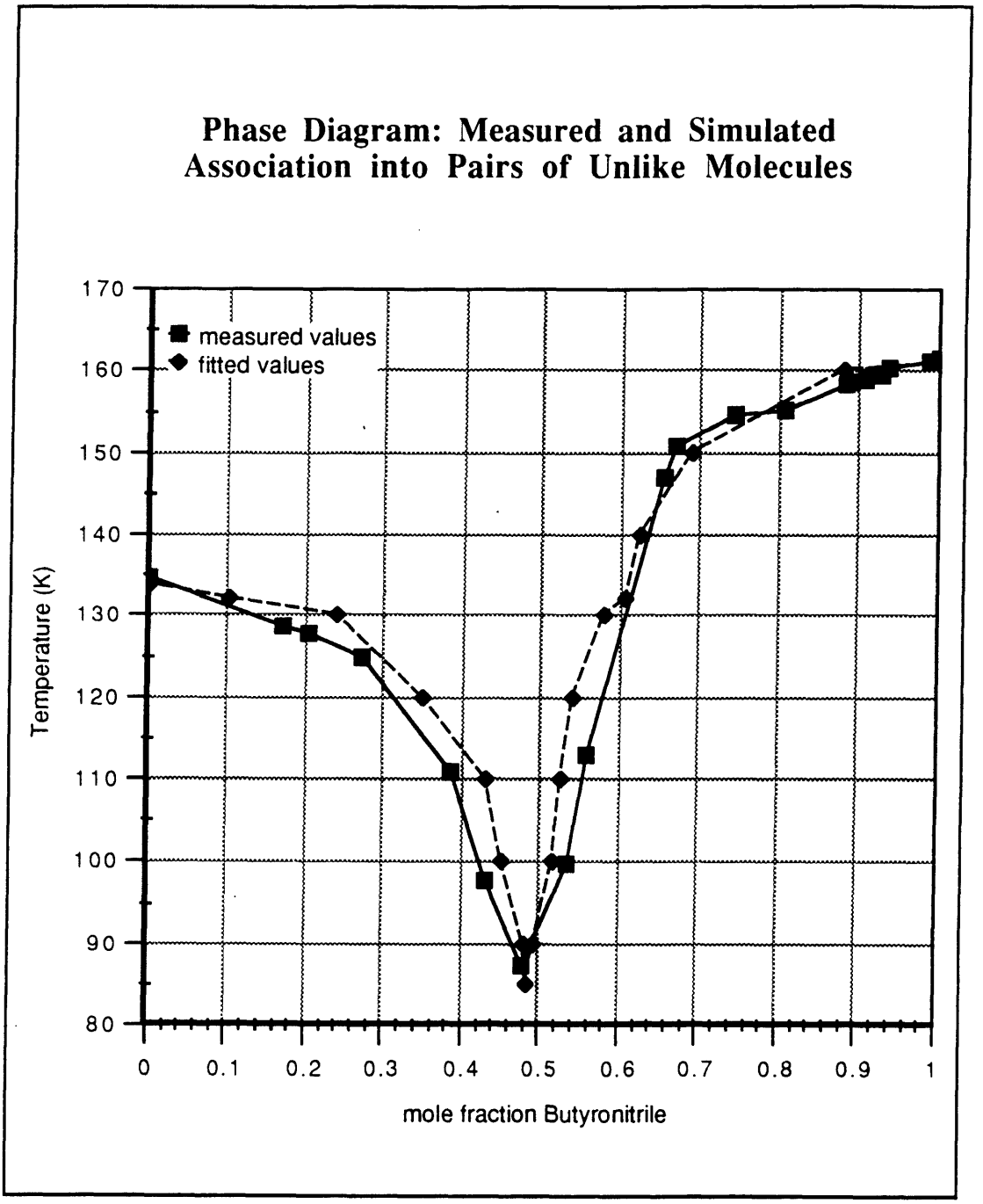

Figure 2.4.3.13 *Associated Phase Diagram Simulation.* Butyronitrile and chloroethane are assumed to associate into unlike pairs. No like pair-associates are assumed. The degree of association is a function of the equilibrium constant for the associate.

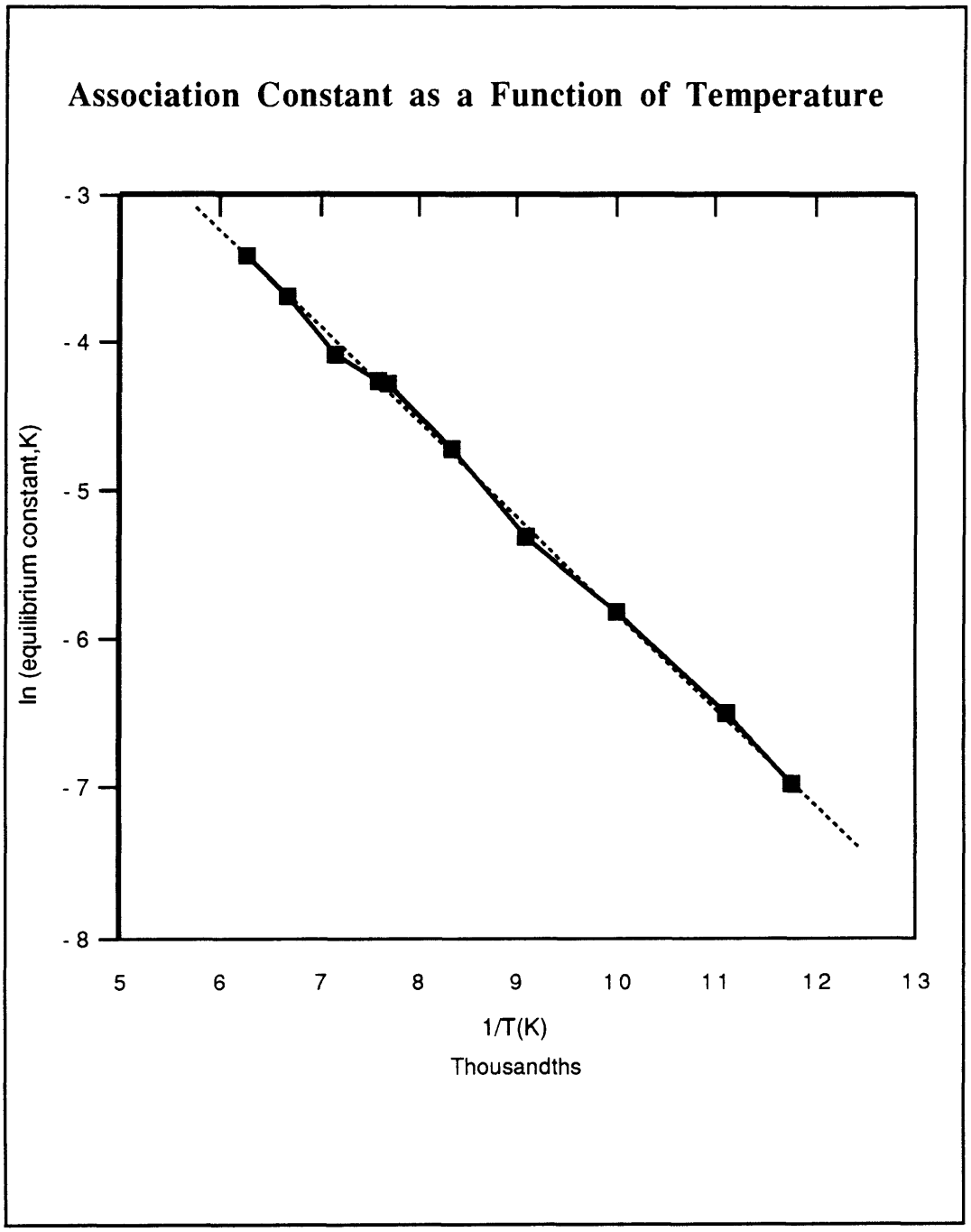

Figure 2.4.3.14 *Association Constant.* Butyronitrile and chloroethane are assumed to associate into unlike pairs. The degree of association is a function of the equilibrium constant for the associate and is expected to follow Gibbs-Helmholtz behavior.

molecular and excess volumes, neglected in the above treatment, contribute less than 1% to the error in the activity coefficients [Sarolea-Mathot].

The equilibrium constant as seen in figure 2.4.3.14 follows Gibbs-Helmholtz behavior where

$$K = 0.62 exp\left(-\frac{5351.3}{RT}\right) \qquad \text{eq. 2.4.3.33}$$

The value of the enthalpy (ΔH°) may be related to the energy between the dipoles written in MKS units for isolated dipoles as [Rhoads]

$$E = \frac{\mu_{BN}\mu_{CE}}{4\pi\varepsilon_{\circ}r^3} \qquad \text{eq. 2.4.3.34}$$

where μ_i is the dipole moment (Table 2.4.3)
r is the distance between the dipoles
ε_o is the permittivity of vacuum (8.854×10^{-12} F/m)

From equation 2.4.3.6, the molar volume of the components is determined. If the molecules are assumed to be spheres, an average center to center distance can be computed and used for r. The resulting energy is 477.22 J/mole. The calculated energy is only an order of magnitude smaller than the enthalpy of the equilibrium constant. If the same considerations are maintained, but with the separation of the molecules decreased from 10.174×10^{-10} m to 4.545×10^{-10} m, the measured value of the interaction energy is attained. It is reasonable for the separation to be reduced because the molecules are expected to be oblong not spherical. It also should be recalled that the enthalpy term in the equilibrium constant represents the formation energy of both dimolecular self-associates of butyronitrile and dimolecular unlike complexes of one butyronitrile and one chloroethane. The extent of the pairing is a function of temperature as defined by the equilibrium constant (eq. 2.4.3.33).

For the measured phase diagram, the sharp drop in the liquidus between 30 and 60 mole percent butyronitrile suggests that the free energy of the liquid is much lower than predicted based upon ideal mixing laws. This may be accounted for by excessively high enthalpies of mixing or by a positive value for the excess entropy of mixing ($g^{xs} = -Ts^{xs}$) or both. The energy to form the complex is large and is on the order of the enthalpies required in the other thermodynamic models. This suggests the excess enthalpy dominates the liquid free energy. In general, solutions with large enthalpies of mixing are termed associated solutions [Prigogine].

When $n_{AB}<n_A+n_B$, the excess entropy is positive. When $n_{AB}=n_A+n_B$, the excess entropy is zero. And when $n_{AB}>n_A+n_B$, the excess entropy is negative [Prigogine, Sarolea-Mathot]. From the magnitude of the equilibrium constant with the initial assumption that there are three species in solution [BN, CE, BNCE], the number complexed is far greater than the number uncomplexed and so there is a negative excess entropy. For the four species model [BN, CE, BN_2, BNCE], the excess entropy would be positive.

Without other information, the thermodynamics of the butyronitrile-chloroethane system may be evaluated with a three species [BN, CE, BNCE] model. As mentioned, there is support in the literature for the formation of four species [BN, CE, BNCE]. The mathematical expression for the equilibrium constant (eq. 2.4.3.33) may be reevaluated to consider a more realistic equilibrium of species in solution.

The equilibrium may be written as

$$Cx_{BN_2} + Dx_{BNCE} \Leftrightarrow Ax_{BN} + Bx_{CE} \qquad \text{eq.2.4.3.35}$$

with

$$K_{dissoc.} = \frac{x_{BN}^{A} x_{CE}^{B}}{x_{BN_2}^{C} x_{BNCE}^{D}}. \qquad \text{eq. 2.4.3.36}$$

This is related to the measured equilibrium constant (eq. 2.4.3.31) if

$$x_{AB} = x_{BN_2}^{C} x_{BNCE}^{D}. \qquad \text{eq. 2.4.3.37}$$

The energy term of the equilibrium constant now reflects the energy of formation of the butyronitrile self-associate and the butyronitrile-chloroethane complex. Using the simplistic dipole-dipole energy as a model (eq. 2.4.3.34), the energy for the butyronitrile self-associate is 854.179J/mole. More information would be required to separate the contributions to the enthalpy due to the self-associates and the complexes.

Based upon the closeness of the modeled behavior to the measured data, the associated solution model just discussed is judged to be the best representation of this system. The value of the computed equilibrium constant as a function of temperature is deemed physically reasonable. The assumption of dipole-dipole interactions as the cause of the complexing is also consistent with the value of the enthalpy. The formation of a complex explains the very large excess enthalpies of the other models tested. Finally, based upon the discussion of the relative dielectric constant measurements of the butyronitrile-chloroethane system, the assumption of the existence of butyronitrile-chloroethane complexes and butyronitrile self associates is supported by the data.

From this model it is possible to predict the vapor pressure properties as a function of temperature and composition. This is accomplished using equations 2.4.3.29 and 2.4.3.32 to determine the activity of butyronitrile and chloroethane. If it is assumed that the vapor pressure of the pure components may be extrapolated to lower temperatures and that ideal mixing occurs in the vapor, then the total vapor pressure may be computed with the following.

$$P_{total} = a_{BN} p^{\circ}_{BN} + a_{CE} p^{\circ}_{CE} \qquad \text{eq. 2.4.3.38}$$

where a_i is the activity of i

p_i° is the partial pressure of i of the pure component

Estimated values for the vapor pressure as a function of composition at two different temperatures are shown in Appendix E. As seen, the chloroethane dominates the vapor pressure, and at the eutectic composition, there is a significant decrease in the estimated vapor pressure when compared to Raoultian behavior.

One can speculate as to the value of the eutectic liquid as a candidate working fluid in a cryogenic refrigeration system. At 120K the eutectic has a vapor pressure of 0.0005Pa. The enthalpies of evaporation at 120K are 48.9kJ/mole and 28.89kJ/mole for the butyronitrile and chloroethane, respectively [Daubert].

A summary of the models discussed in this section is shown in Table 2.4.4.

Table 2.4.4 Summary of Thermodynamic Models

Model	Governing Equation	Scaled Parameter	Eutectic m / o	Eutectic T(K)
Redlich - Kister (1 - term)	$g^{ex} = x_1 x_2 b$	$b(0)\left[J/\overline{m}\right] = -8810.7 + 52.1T(K)$	40	100
Redlich - Kister (2 - terms)	$g^{ex} = x_1 x_2 \left[b(0) + b(1)(x_1 - x_2)\right]$	$b(0)\left[J/\overline{m}\right] = -14,061 + 90.45T(K)$ $b(1)\left[J/\overline{m}\right] = -1000$	48	83
Regular Solution	$g^{ex} = (x_1 v_1 + x_2 v_2)\varphi_1\varphi_2[C]$	$C\left[J/\overline{m}\right] = -177.93 + 1.106T(K)$	42	90
I Hildebrand - Scatchard	$C = (\delta_1 - \delta_2)^2$		38	117
II Wiemer - Prausnitz	$C = \left[(\lambda_1 - \lambda_2)^2 + (\tau_1 - \tau_2)^2 - 2\psi_{12}\right]$			
III Author's	$C = \left[(\delta_1 - \delta_2)^2 - 2\delta_1\delta_2\right]$ where $\delta_i = \lambda_i + \tau_i$	$C\left[J/\overline{m}\right] = -1155.1 + 1.083T(K)$		
Z - fraction	$g^{ex} = z_1 z_2 b(r = v_2/v_1)$ $g^{ex} = z_1 z_2 b(r = v_1/v_2)$	$b\left[J/\overline{m}\right] = -15,646.7 + 109.1T(K)$	40 47.5	100 85
Flory	$g^{ex} = \sum x_i g_i^* + RT\left[\sum x_i \ell n\varphi_i\right] + x_1\varphi_2 b$		43	83
Associated Solution	$g^{ex} = RT\left[\sum x_i \ell n\gamma_i\right]$ where $\gamma_i = \frac{1}{x_{i_1}^*} \cdot \frac{x_{i_1}}{x_i}$	$K = 0.58 exp\left[\frac{-5351.3}{RT}\right]$	48	85

3.0 Relative Dielectric Constant

There are many factors to consider when selecting the appropriate solvent for an electrolyte. For studies involving cryogenic electrochemistry, the state of the solvent is important as was described in section 2 of this document. Another key factor is the ability of the solvent to ionize a solute, a property that is related to the medium's relative dielectric constant.

The Nernst-Thompson law [Schlundt] correlates an increase in the relative dielectric constant to an increase in the ionizing power of a solvent. Though there are many exceptions, this rule of thumb is still a good measure of the ionizing ability of a solvent. In the case of nitriles, Schlundt determined that the ionizing ability is far greater than expected based solely on the relative dielectric constant. However, he did determine that within the homologous family of nitriles the Nernst-Thompson rule is obeyed, where the relative dielectric constant varies directly with the ionizing ability of a solvent [Schlundt]. This ability of a solvent to ionize a solute can also be related to the potential for dissolved ions to interact. The higher the relative dielectric constant, the less likely it is that the ions will form pairs, triplets, and higher order ion clusters [Fuoss]. The net result is that for the same concentration of ions, a solvent with a higher relative dielectric constant will tend to have a higher conductivity because of the greater number of net charge carriers.

Both butyronitrile and chloroethane, the solvents under study, are considered polar solvents as they have permanent dipole moments of 1.3576×10^{-29} C-m and 6.8381×10^{-30} C-m [Daubert] respectively. The relative dielectric constant is related to the dipole moment of a molecule. In the liquid state the molecules are close enough to interact which may, in the

absence of thermal motion, result in a parallel or antiparallel alignment of the molecules. The alignment leads to a net increase or decrease of the effective dipole moment, and therefore, of the relative dielectric constant. This may account for higher ionizability of the nitrile solvents as determined by Schlundt. The electrical attributes of a solvent that are responsible for the ionization of a salt are related to the local properties (e.g., the dipole moment) not the bulk properties. Because of anti-parallel alignment of the dipoles, the measured relative dielectric constant is lower than that predicted based upon the nitrile solvent's ability to ionize a salt. Similarly, the difference between the dipole moment as measured in the gaseous state and that computed from the liquid state dielectric properties (i.e. the effective dipole moment), leads to speculation about the molecular configurations of the liquid and interdipole interactions [Hill, Kirkwood]. In a binary solution, the variation of the relative dielectric constant as a function of composition leads to speculation on how the molecules of the solution are arranged due to these electrical interactions [Dannhauser, Papanastaslou, Marcheselli, Meyer].

3.1. Theory

3.1.1 Pure Polar Solvent

The dielectric properties represent the ability of a material to be polarized under an applied electric field. If a dielectric medium is placed between two parallel plates with a voltage, V, across the plates, a polarization charge P, within the dielectric forms in response (figure 3.1.1). The

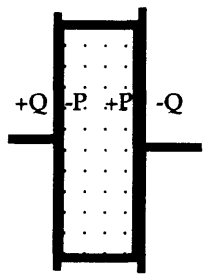

Figure 3.1.1 *Capacitance.* The capacitance is the measure of the amount of charge that accumulates in response to an applied voltage, V. [C=Q/V]. If a material exists between the plates, it polarizes in response to the charge on the electrodes. Now, for the same applied voltage, a total charge of Q+P can accumulate on the plates with a resultant capacitance of C '= [Q+P]/V. If C is the capacitance measured in vacuum, then the relative dielectric constant, ε_r, is defined as the ratio of the capacitance measured with the material divided by the capacitance measured in vacuum. [ε_r = C'/C]

polarization of a polar liquid is a sum of electronic, atomic and orientational contributions which stem respectively from motion of the electron cloud about the nucleus, the relative positions of the atoms, and the rotation of permanent dipoles in response to the applied field. The time for the polarization to be complete, i.e. the time for one of these contributions to respond to the applied field, is manifest as a frequency dependence of the dielectric response to the applied field. This time is 10^{-14} -10^{-15} s, 10^{-11} -10^{-14} s, 10^{-10}-10^{-12} s for the three contributions respectively [Hill]. Their effects with frequency on the measured dielectric properties are shown in figure 3.1.2.

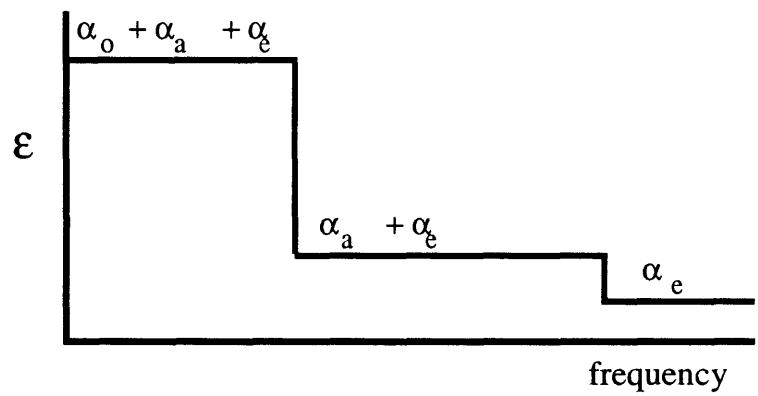

Figure 3.1.2 *Polarization.* The contributions of polarization to the dielectric properties vary as a function of frequency. At low frequencies, all polarizations contribute; at higher frequencies only the atomic (α_a) and electronic (α_e) polarizations contribute; at still higher frequencies only the electronic part contributes to the dielectric properties of the medium. α_o is the orientational polarization part of the total polarization.

The relative dielectric constant, also called the static permittivity, is a measure of these properties of the material when all three of these contributions to the polarization are in effect (i.e. at frequencies below 10 GHz). For a polar liquid, the orientational contribution tends to predominate [Hill].

In the gaseous state the dielectric properties of a polar medium are completely defined by the Debye equation, written in rational MKS units as

$$\left[\frac{\varepsilon_r - 1}{\varepsilon_r + 2}\right] = \frac{N_1(\alpha + \mu_g^2 / 3kT)}{3\varepsilon_o} \qquad \text{eq. 3.1.1}$$

where ε_r is the relative dielectric constant
N_1 is the number of dipoles per unit volume = $N\rho / M$
N is Avogadro's number =6.02×10^{23} $mole^{-1}$
ρ is the density [kg/m^3]
M is the molecular weight [kg/mole]
μ_g is the dipole moment in the gas phase [C-m]
ε_o is the permittivity of free space (8.85×10^{-12} F/m)
α is the distortion polarizability [$F\text{-}m^2$] (electronic and atomic parts of the polarization).

The assumptions made in the development of this equation, in particular the lack of directional forces between dipoles, and the lack of dipole interactions, restricts this equation to gases and dilute solutions of polar molecules in nonpolar solvents [Hill].

Onsager sought to overcome the limitations of the Debye equation by placing a point dipole within a cavity and considering the effects of the exterior on the dipole (cavity field) and the polarization of the dipole on its environment (reaction field). The resulting relationship, also written in rationalized MKS, as eq. 3.1.2 does not consider strong interactions of

neighboring dipoles, but better defines the relationship of non-polar fluids and dilute solutions of polar solvents in non-polar solvents.

$$\frac{(\varepsilon_r - n^2)(2\varepsilon_r + n^2)}{\varepsilon_r(n^2+2)^2} = \frac{N_1 \mu_g^{\,2}}{9kT\varepsilon_o} \qquad \text{eq. 3.1.2}$$

where n, the internal refractive index, defines the polarizability

$$\frac{n^2-1}{n^2+2} = \frac{\alpha}{\varepsilon_o a^3} \qquad \text{eq. 3.1.3}$$

(Note. Often the refractive index measured using the sodium doublet is used)
a is the radius of the cavity = $\sqrt[3]{3/4\pi N_1}$ *(assumes the molecules take up all the available volume)*
all other symbols have the same meaning as before.

In his formulation, Onsager characterizes the polarization of a molecule as its "internal refractive index" [Onsager]. Others have interpreted the polarizability as the dielectric constant measured at "infinite" frequency, ε_∞ [D'Aprano]. The dielectric constant at "infinite" frequency is defined as the sum of the electronic and atomic components of the total polarization. (*N. B .* At true infinite frequency it would be expected that even the electronic part of the polarization would not contribute to the dielectric constant and so ε_∞ would be equivalent to the dielectric constant of vacuum.) The electronic polarization is the square of the refractive index; the atomic component is rarely measured and is approximatedly ten percent of the electronic part of the polarization [D'Aprano]. In general, a value of $1.1n^2$ is used for the dielectric constant at "infinite" frequency [Danhauser, D'Aprano] (*i.e.* $1.1n^2$ is inserted for n^2 in the Onsager equation and in all subsequent equations).

The Kirkwood equation, written in rationalized MKS (eq. 3.1.4), was developed via statistical methods as opposed to the macroscopic

considerations used above, and it incorporates a correlation parameter to account for the local ordering within a polar medium [Hill]. This factor reflects the enhancement or diminishment of the dipole moment of a particular dipole due to its environment. If there are no net orientations of the neighboring dipoles, the dipole in question has a moment equal to itself (g=1). If the dipoles align parallel to one another, the effective dipole moment of the dipole in question will be larger, giving a correlation factor greater than one; an antiparallel arrangement of dipoles will result in a correlation parameter less than one. Detailed knowledge of the liquid structure is required to calculate the correlation parameter from first principles.

$$\frac{(\varepsilon_r - 1)(2\varepsilon_r + 1)}{3\varepsilon_r} = \frac{N}{V\varepsilon_o}\left(\alpha + \frac{g\mu^2}{3kT}\right) \qquad \text{eq. 3.1.4}$$

where V is the volume
g the correlation parameter, a measure of local ordering and is a function of temperature
all other symbols have the same meaning

Note that μ in the Kirkwood equation (eq. 3.1.4) is now the local dipole moment [Hill]. The permittivity of a material, differing appreciably from unity, causes a reaction field as defined by Onsager which alters the dipole moment from that in the gaseous state. The local moment is related to the dipole moment as measured in the gas phase by using the Onsager relationship [Kirkwood, Onsager]

$$\mu = \frac{(2\varepsilon_r + 1)(n^2 + 2)}{3(2\varepsilon_r + n^2)}\mu_g \qquad \text{eq. 3.1.5}$$

where the symbols have the same meaning as before.

As can be seen in all of the above equations for the relative dielectric constant of polar media, the temperature is an integral factor. As the temperature is lowered, thermally induced disruption of ordering is lessened. This increases the relative magnitude of the orientational component of the total polarization. Reducing the temperature increases the density of the solvent which also results in an increase of the relative dielectric constant. Combining these factors, the overall relative dielectric constant of a polar solvent increases as the temperature is lowered.

3.1.2 Solutions of Polar Solvents

In the case of solutions of polar solvents in polar solvents, the models are greatly limited in explaining experimental data, or become unwieldy under too many variables. Often, weighted averages of the solution parameters are used [Akhadov, Nath] and substituted into the Kirkwood equation. The deviations of the correlation factor determined by the Kirkwood equation from strict additivity, are related to additional structural aspects of the solution.

$$\Delta g = g_{(observed)} - g_{(idealmixing)} = g_{(observed)} - x_1 g_1 - x_2 g_2 \qquad \text{eq. 3.1.6}$$

Often a positive value of Δg is said to indicate that the solution is more correlated tending toward increased intermolecular interactions of the molecular species than predicted based upon ideal mixing [Nath]. This is not a universal statement. Under conditions where g_i is less than unity, a value for $g_{(observed)}$ may still be less but numerically closer to unity than ideal mixing predicts. This represents a more disordered or less correlated system. In table 3.2.1, reasonable values for correlation factors are used in eq. 3.1.6. Each

system must be considered independently as a broad definition is not applicable.

Table 3.2.1 Meaning of Δg			
for $\Delta g>0$, $g_{obs} > x_1 (g_1 - g_2) + g_2$			
g	g	g	Comment
>1	>1	>1	even larger than unity so always more ordered than predicted by ideal mixing
<1	>1	>1or <1	depending on the magnitude, may be more or less ordered than predicted by ideal mixing
>1	<1	>1or <1	depending on the magnitude, may be more or less ordered than predicted by ideal mixing
<1	<1	>1or <1	depending on the magnitude, may be more or less ordered than predicted by ideal mixing
for $\Delta g<0$, $g_{obs} < x_1 (g_1 - g_2) + g_2$			
<1	<1	<1	even larger than unity so always more ordered than predicted by ideal mixing
<1	>1	>1or <1	depending on the magnitude, may be more or less ordered than predicted by ideal mixing
>1	<1	>1or <1	depending on the magnitude, may be more or less ordered than predicted by ideal mixing
>1	>1	>1or <1	depending on the magnitude, may be more or less ordered than predicted by ideal mixing

3.2 Experimental Methods

The relative dielectric constant, as stated above (figure 3.1.1), is related to the capacitance of a medium. As a result, the relative dielectric constant is determined by measuring the capacitance of the solvent of a known geometry or cell constant via the following equation:

$$C = \varepsilon_o \varepsilon_r G \qquad \text{eq. 3.2.1}$$

where C is the capacitance (F)

ε_o is the permittivity of free space (8.854×10^{-12} F/m)

ε_r is the relative dielectric constant

G is the cell constant

The cell constant can be determined from geometric considerations. However, due to fringing fields, it is more often determined through calibration with standard solutions.

There are a number of methods used to determine the capacitance. One is the Heterodyne-Beat method whereby the capacitance is determined from the capacitance change required in the external circuit to return a cavity to resonance upon the addition of the sample. Alternatives are variations of bridge methods. In such circuits, a given frequency is applied to the circuit and the required capacitance and resistance needed to balance the circuit is used for the determination of the electrical properties of the unknown sample at the applied frequency. The use of more than one frequency is standard protocol. In liquid solvents, for instance, the measured capacitance may be due to the double layer capacitance or the bulk capacitance; the latter is proportional to the relative dielectric constant. If only one frequency is used, it is not known if the measured capacitance is due to the double layer or the bulk properties. These two capacitances, however, are of different magnitudes and therefore have a distinct impedance at a given frequency. By using more than one frequency during a series of measurements on a given solvent, these different electrical phenomena may be distinguished. Taking this procedure to the next level, that of sweeping the frequency, is described in more detail below and is termed electrochemical impedance spectroscopy.

3.2.1 Electrochemical Impedance Spectroscopy

By varying the frequency and applying a constant voltage amplitude to a sample and measuring the resultant ac current, impedance as a function of frequency may be determined. The different electrical properties of the sample (e.g. conductance, double layer capacitance) respond in a manner

similar to lumped circuit elements as a function of frequency. For example, the conductance of a solution, i.e. the transfer of free charges, is not expected to vary as a function of frequency and so it is modeled by a resistor. Likewise, the double layer, an alignment of ions and solvent molecules near the charged electrodes, appears and behaves like a nonlinear capacitor. The impedance of these two circuit elements as a function of ac frequency is as follows [Bard]:

$$Z_{\text{Resistor}} = R \qquad \text{eq. 3.2.2}$$

$$Z_{\text{Capacitor}} = \frac{1}{j\omega C} \qquad \text{eq. 3.2.3}$$

A circuit is developed with these lumped elements that is assumed to represent the physical phenomena of the measured system. If the correct circuit model is chosen, the impedance of the modeled circuit and the measured system would be the same as a function of frequency. The values of the circuit elements can then be attributed to physical phenomena of the measured system. Therefore, the value of a bulk resistor of the modeled circuit, is proportional to the resistivity ($R = \rho/G$) and the value of a bulk capacitor is proportional to the relative dielectric constant ($C = \varepsilon_o \varepsilon_r G$) of the sample.

As an example, for a liquid undergoing no faradaic reactions, the assumed circuit model is shown in figure 3.2.1.

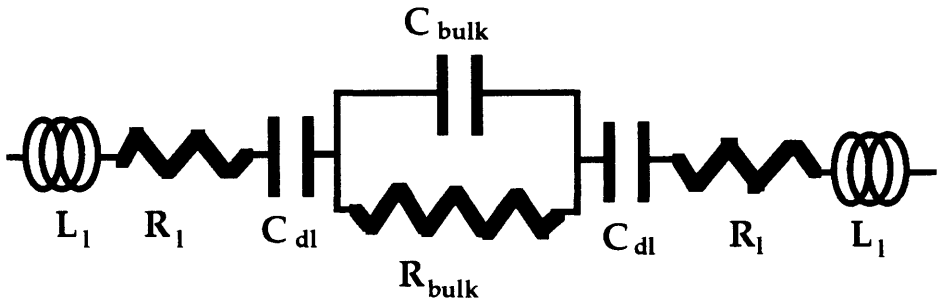

Figure 3.2.1 *Equivalent circuit.* Circuit model for impedance measurement with no faradaic or chemical effects. R_l and L_l are the lead wire resistance and inductance respectively, C_{dl} is the double layer capacitance, R_{bulk} is the bulk resistance (proportional to solvent resistivity), C_{bulk} is the solvent capacitance (proportional to relative dielectric constant).

Where Z is defined as the impedance,

$$Z_{total} = 2Z_{lead\ wire} + 2Z_{double\ layer} + \frac{Z_{bulk\ resistance} Z_{bulk\ capacitance}}{Z_{bulk\ resistance} + Z_{bulk\ capacitance}} \qquad \text{eq. 3.2.4}$$

$$Z_{total} = 2\left(R_{lead\ wire} + j\omega L_{lead\ wire}\right) + \frac{2}{j\omega C_{double\ layer}} + \frac{R_{bulk}}{1 + j\omega R_{bulk} C_{bulk}} \qquad \text{eq. 3.2.5}$$

The total impedance is seen to vary with frequency. If the magnitudes of the circuit elements are different enough, each element will dominate the total impedance in certain frequency regimes. When this occurs, the shape of the impedance-frequency curve aids in determining the circuit model. In the above circuit, for example, the measured impedance as a function of frequency is shown in figure 3.2.2 when the magnitudes are sufficiently different.

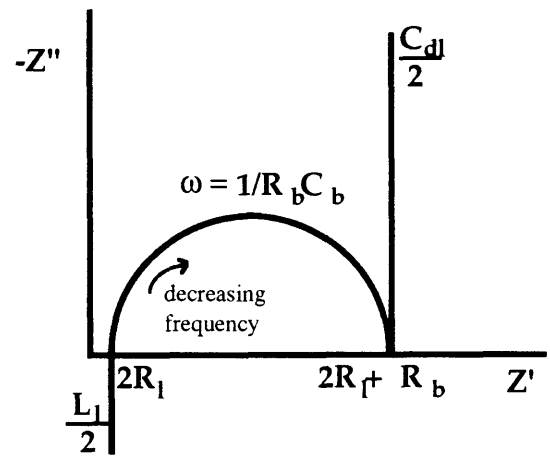

Figure 3.2.2 *Nyquist Plot* . Impedance of equivalent circuit shown in figure 3.2.1.

Likewise, when the magnitudes are sufficiently different, the determination of the unknown values of the circuit elements and their corresponding physical meaning can be better determined. This is because when the elements are close in value, the impedances overlap making differentiation difficult.

In general, and found in the measured systems of butyronitrile, chloroethane, and their solutions, the double layer capacitance is orders of

magnitude greater than the bulk capacitance. Given the inverse relationship of the impedance of a capacitor with frequency (eq. 3.2.3), at higher frequencies the double layer capacitor of figure 3.2.1 behaves as a short circuit. For the measured systems, the solvent resistance is far greater than the lead wire resistance, and so $\mathbf{R_{lead\ wire}}$ is effectively a short circuit in the circuit model for the range of frequencies used in these measurements. At the frequencies used, the impedance due to lead wire inductance is also neglible. Considering these factors, the equivalent circuit reduces to

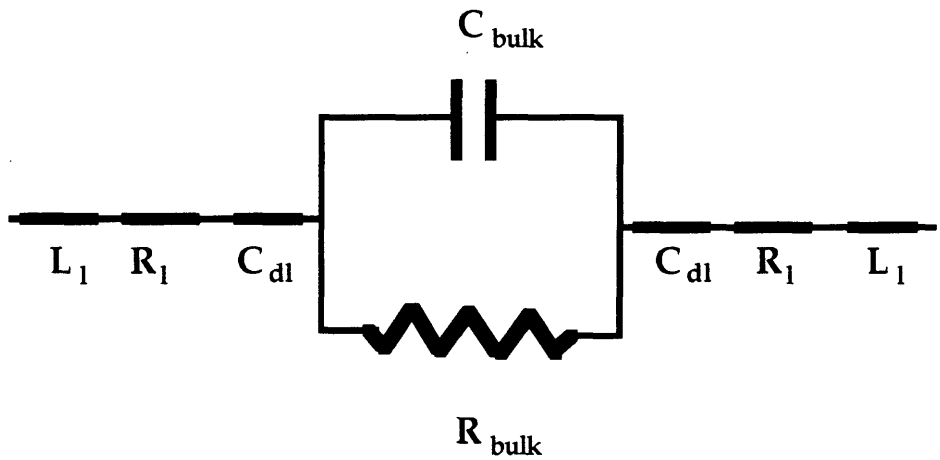

Figure 3.2.3 *Reduced Equivalent Circuit.* Equivalent circuit shown in figure 3.2.1 reduced through consideration of expected magnitudes of the circuit elements at the measured frequencies.

The impedance as a function of frequency is expected to vary as

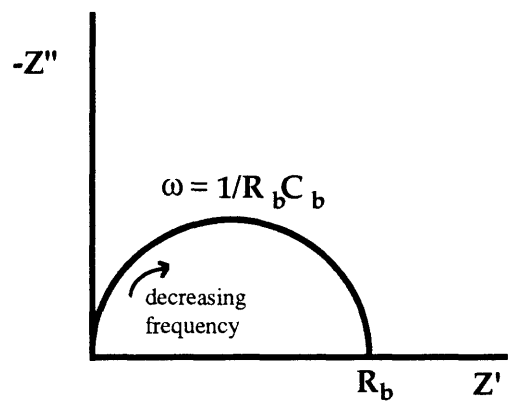

Figure 3.2.4 *Nyquist Plot* . Impedance plot for simplified equivalent circuit shown in figure 3.2.3.

In figure 3.2.5 a sample of the measured data for pure butyronitrile measured at -35°C is reproduced. As seen, the measured data is well modeled by a resistor and capacitor in parallel.

3.2.2 Experimental Design

3.2.2.1 Electrode Selection

To measure the capacitance of the sample, electrodes are required. Ideally, the electrodes would have zero electrical resistance and would be non-reactive with the solvents to be tested. The measured liquids have a very high intrinsic resistivity, and so the electrode resistance for metallic electrodes is zero by comparison. With the exception of aluminum [Ullmann] and copper [Kirk-Othmer], metals were not expected to be reactive with either butyronitrile or chloroethane. Visual examination of the electrodes between measurements supported this expectation. Unchanged values of the cell constant, a relationship of the electrode dimensions, and invariant values of the electrical conductivity of the solvents over the course of an experiment, offered further evidence of the inertness of the electrode materials. Had a corrosive process that formed a film been in effect, the electrode dimensions and/or the space between the electrodes would have changed, altering the cell constant. If a corrosive process resulted in ion formation, the conductivity of the solvent would have increased with time. The corrosion processes would also be evident from the shape of the measured impedance curve.

Electrodes made of platinum, platinum sputtered on copper, and nickel-plated brass were tested. The platinum sputtered on copper electrodes failed. This was due in large part to the poor adhesion of the platinum to the copper. This poor adhesion allowed corrosion to occur; corrosion products

Experimental Data

Pure Butyronitrile at T=238.16K

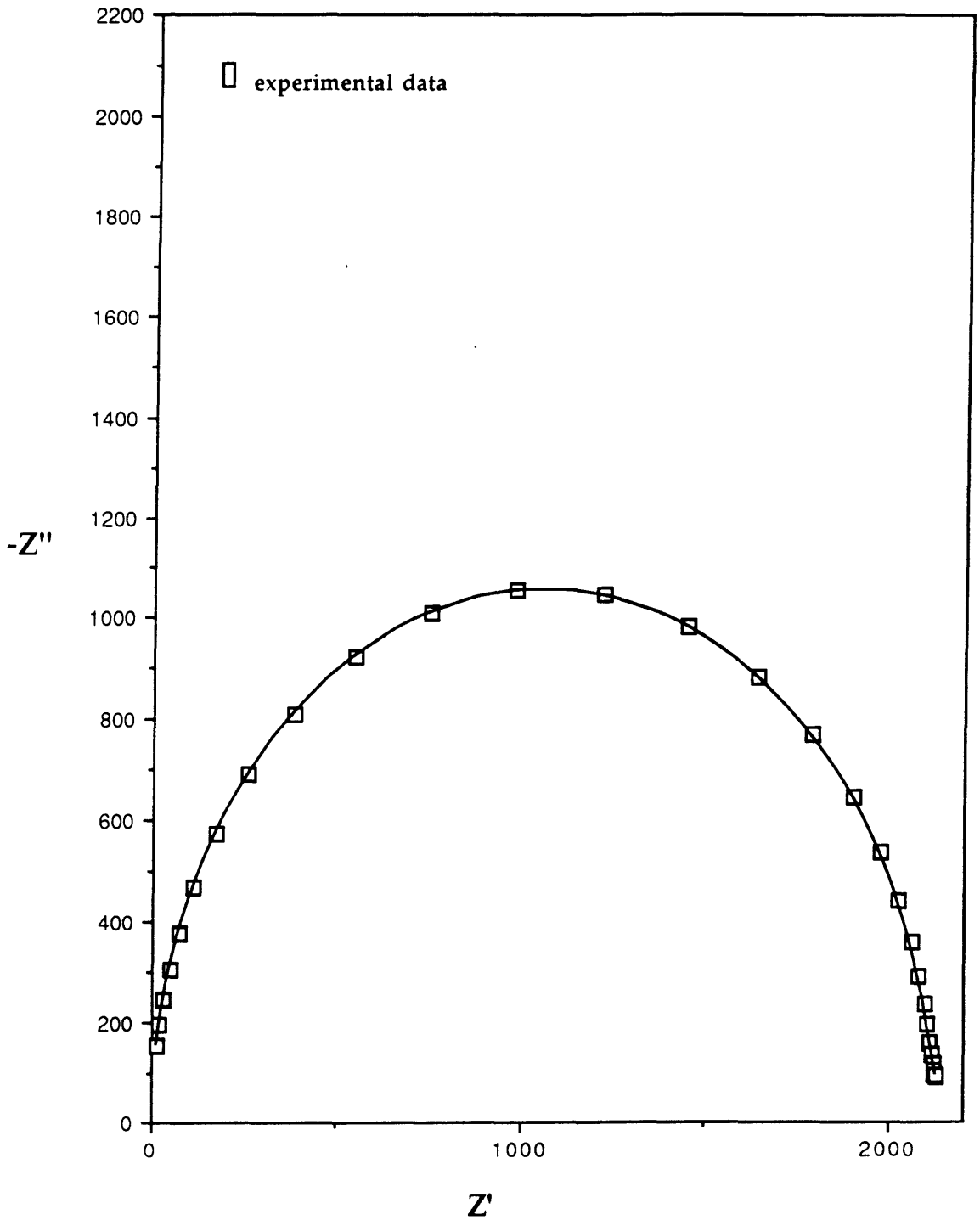

figure 3.2.5. Sample of Measured Data. The measured data forms a semi-circle which is well modeled by a capacitor and resistor in parallel.

were visible on the electrodes after exposure to aqueous KCl during calibration tests. The other two materials tested showed no signs of reaction with aqueous solutions or butyronitrile, chloroethane, and their solutions.

Aside from the materials issues, the electrode configuration is of great importance. Ideally, the current generated by the applied ac voltage should remain in the confines of the electrodes. Under such circumstances, the cell constant, the *G* in equation 3.2.1, can be computed from the electrode geometry. As an example, the parallel plate electrodes of figure 3.1.1 would have

$$G\,[\mathrm{m}] = \frac{\text{Area of electrodes } [\mathrm{m}^2]}{\text{Distance between electrodes } [\mathrm{m}]}$$

In reality there is nothing confining the current and so fringing occurs as seen in figure 3.2.6.

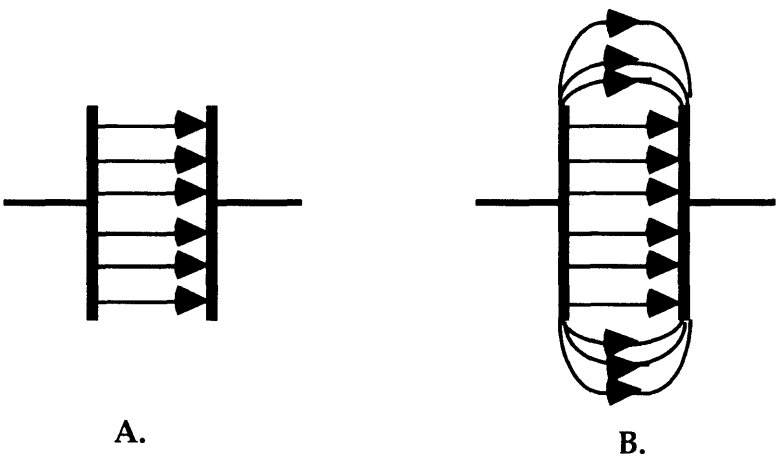

Figure 3.2.6. *Fringing fields.* **A.** Ideal scenario has linear field lines solely between the electrodes. The cell constant can be computed based on the electrode geometry. G=Area/distance. **B.** Real scenario has the field lines outside of the geometry of the electrodes. The cell constant can be approximately computed using the geometry or can be measured using solutions with known values of relative dielectric constant. [For conductivity measurements, for which the same considerations are important, solutions with known conductivities are used for the calibration. The cell constant is the same, however, it is better to calibrate using known solutions with physical properties of the same magnitude as those to be measured.]

There are two methods used to take the effects of fringing fields into account. The first is to eliminate them from the total measurement by using

a differential cell constant which is defined under the conditions of constant fringing fields. This can be achieved by varying either the area of the electrodes or their spacing while assuring that the fringing fields remain constant [Jones, Spiro]. Under these conditions, the differential cell constant is a measure of the change in cell constant as a function of the change in either the area or the interelectrode spacing. Thus the effects of the fringing field are eliminated. When the electrodes are far enough from the cell walls and the liquid surface (twice the interelectrode spacing is a good rule of thumb), the fringing fields are constant to the first order approximation. Figure 3.2.7 shows both cylindrical and parallel plate electrodes that vary the area and interelectrode spacing respectively. Both of these electrode configurations were tested and found to behave as expected. Limitations in other aspects of the cell design limited their usefulness for the desired experiments.

It is possible to avoid having the effects of the fringing fields as part of the measurement by measuring only the part of the total field that is well behaved between the electrodes. Guarding the electrodes is a method for achieving this [Hawes, Spiro]. Under this configuration, shown in figure 3.2.8, a separate electrode is placed in close proximity to the working electrode. The potential applied to this electrode is the same as that applied to the working electrode. When the guard and working electrodes are very close, the field lines generated mimic those of a continuous electrode surface. However, the current is measured only on the working electrode where the field lines are linear and can be calculated from the electrode geometry. Both parallel plate and cylindrical guarded electrodes were tested. The results were ambiguous due to the failure of other aspects of the experiment.

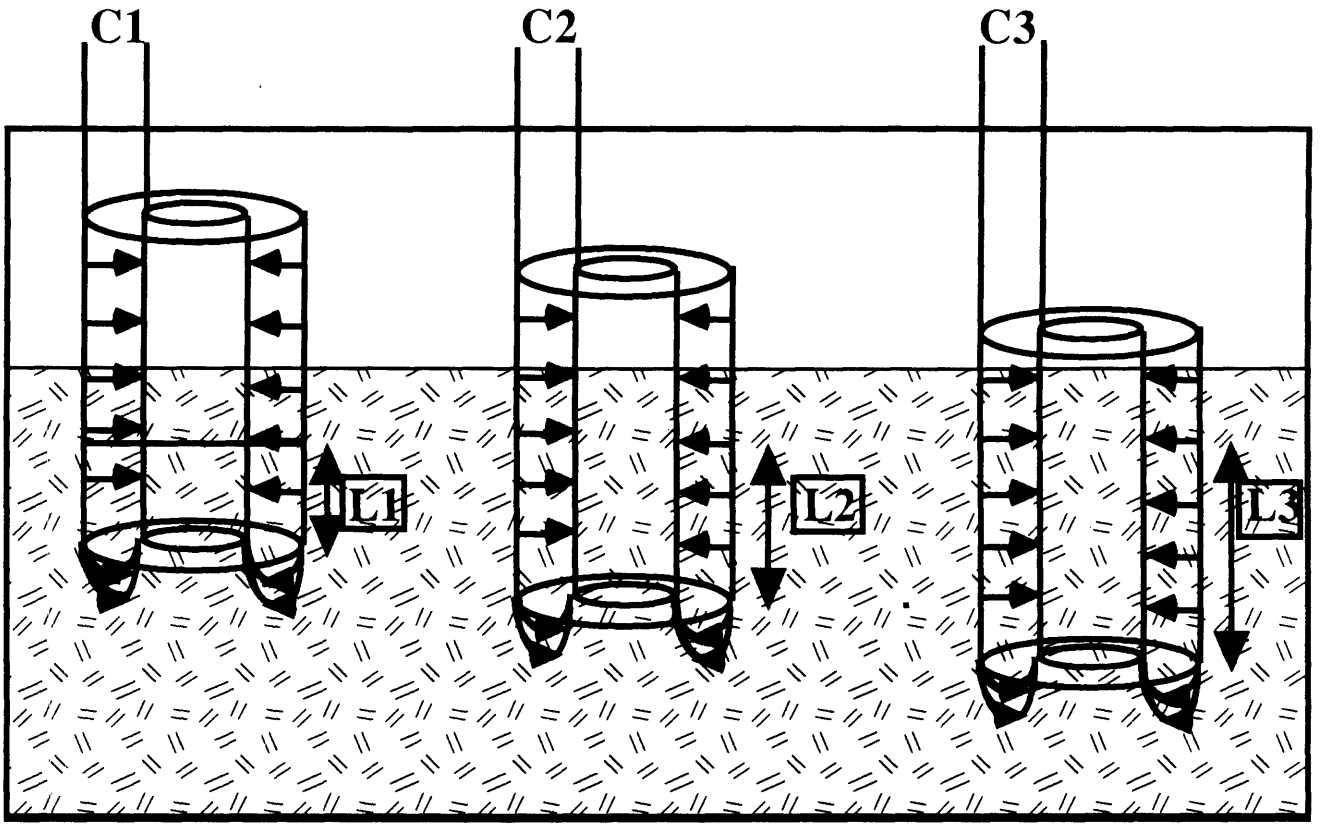

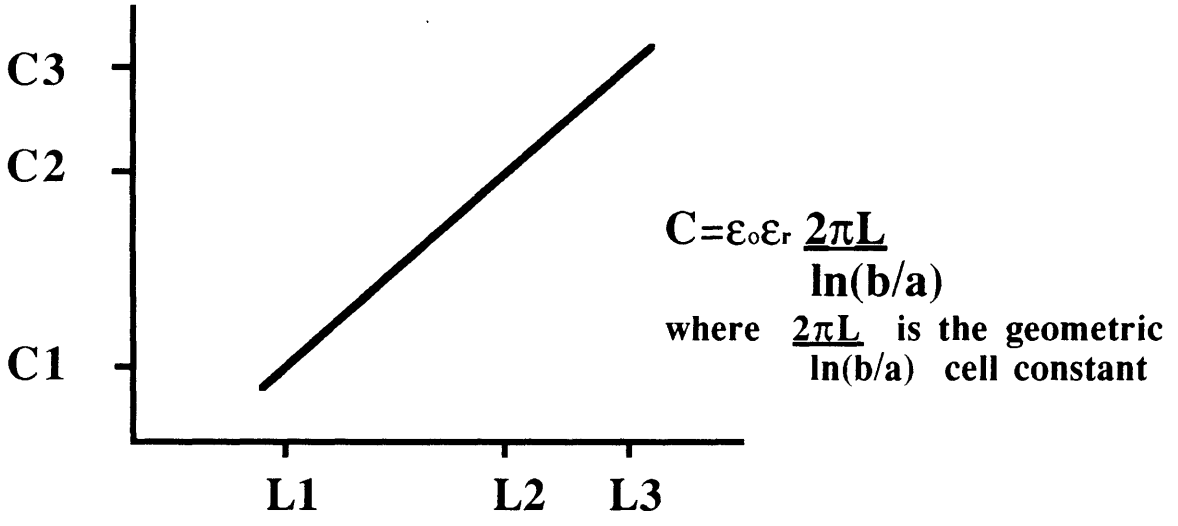

Figure 3.2.7a. *Moveable Concentric Cyclinder Electrodes.* By varying the depth of immersion of the electrodes, the area is changed. Calibration is conducted as a function of depth of immersion to give a differential cell constant. As long as the electrodes are far enough from the bottom of the cell, the fringing fields are constant and therefore are eliminated from the differential cell constant.

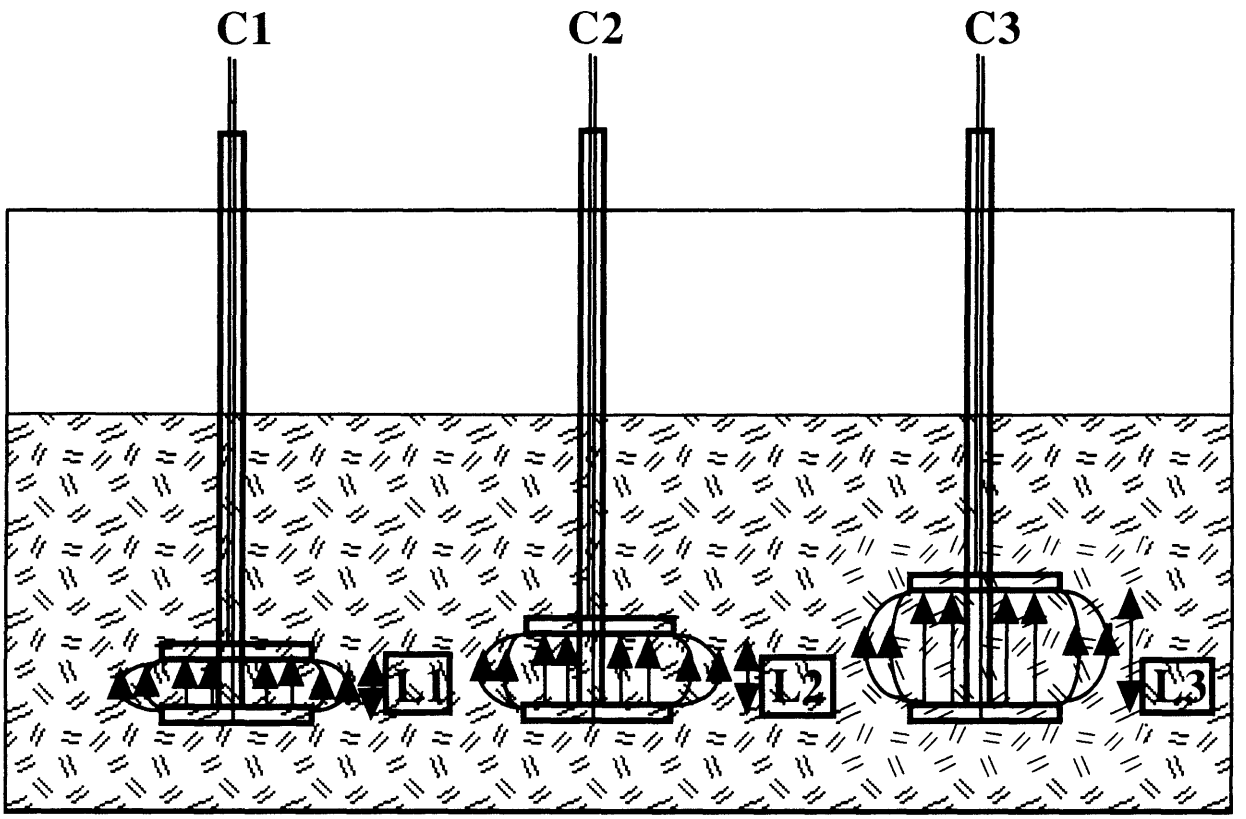

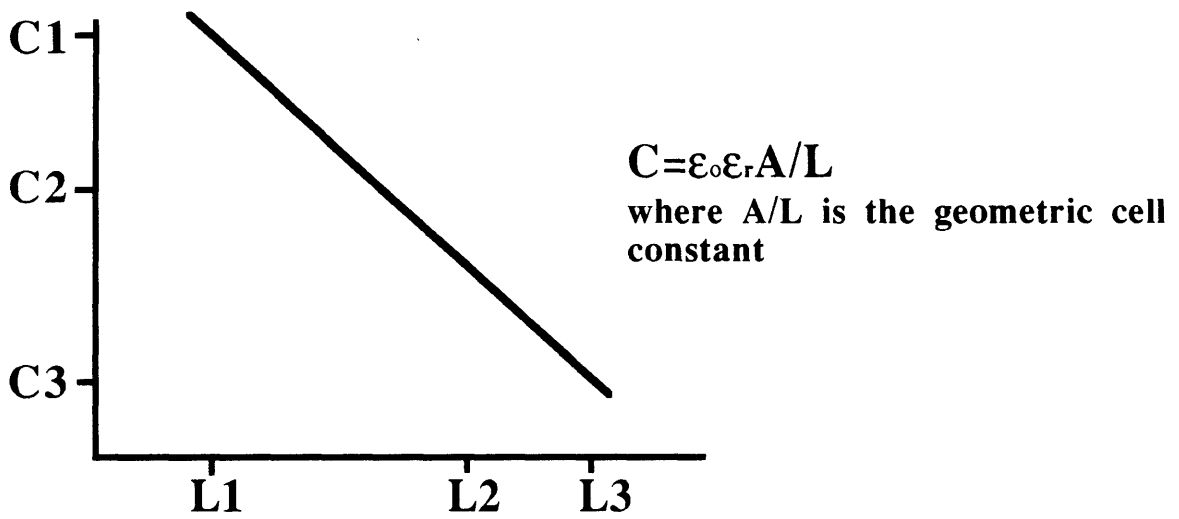

Figure 3.2.7b. *Moveable Parallel Plate Electrodes*. By varying the depth of immersion of the electrodes, the interelectrode separation is changed. Calibration is conducted as a function of depth of immersion to give a differential cell constant. As long as the electrodes are far enough from the bottom of the cell, the fringing fields are constant and therefore are eliminated from the differential cell constant.

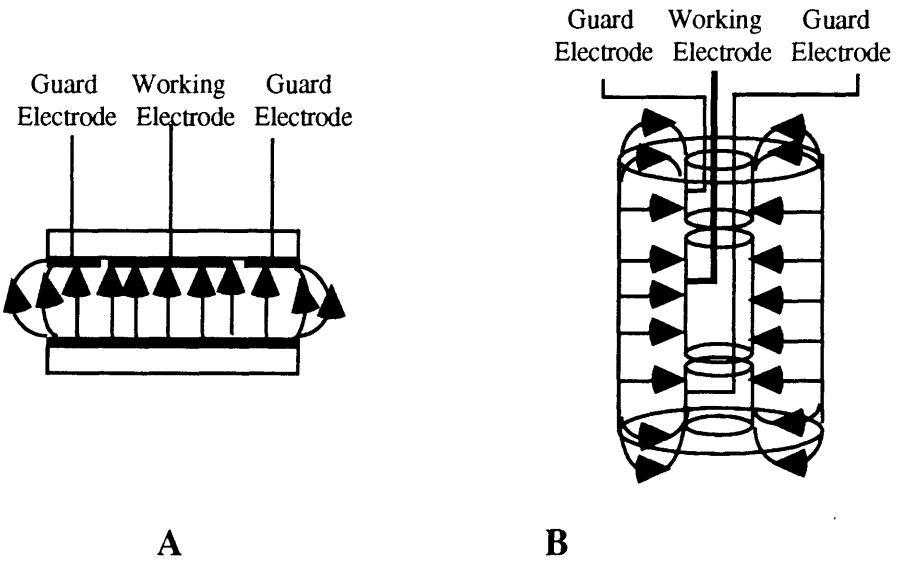

Figure 3.2.8 *Guarded Electrodes.* With the guarded configuration, the guard and working electrodes are at the same potential. If these electrodes are in close proximity the field configuration closely approximates that of a single electrode. The measurement is taken only on the working surface where the field is well behaved. **A.** Parallel plate configuration. **B.** Cylindrical configuration.

A second method is to measure the cell constant using liquids of known values of relative dielectric constants. When the calibration liquids have relative dielectric constants of comparable value to the unknown solvents, the fringing fields are expected to remain the same. The calibrated cell constant is then the same for the calibrating liquid and the unknown liquids. For butyronitrile and chloroethane, literature values reported relative dielectric constants within a range of 15 to 25 at temperatures higher than those to be measured in this work. Since the relative dielectric constant is expected to increase as the temperature decreases, methanol was selected as a calibration medium. The relative dielectric constant as a function of temperature for methanol ranges from 32 to 70 between room temperature and -80°C.

The last factor to be considered in designing electrodes is their size. Instrumentation limits the magnitude of the resistance and capacitance that can be reliably measured. For liquids with high resistivity and low relative dielectric constants, large cell constants are desired. This reduces the measured resistance ($R=\rho/G$) and raises the measured capacitance ($C=\varepsilon_o\varepsilon_r G$). In particular, it is desirable to have the capacitance of the sample as large as possible so that stray capacitances, which unfortunately cannot be reduced to zero, are a small percentage of the total capacitance measured.

In considering these factors, an interdigitated electrode design was chosen for its large cell constant and ease of fitting into the rest of the electrochemical impedance cell. A variable air capacitor [Hammarlund model #MAPC-75] was found to meet the necessary requirements. It was made of nickel-plated brass. The soldered connections did not corrode in either the calibration or unknown solutions. The capacitance in vacuum and the corresponding cell constant were nearly constant as a function of temperature and is shown in Table 3.2.2 below.

Table 3.2.2 Capacitance of Interdigited Electrodes as a Function of Temperature

Temperature (°C)	Capacitance (pF)	Cell Constant (m)
-35	80.34	9.08
-50	80.14	9.06
-65	80.10	9.05
-80	80.13	9.05
-95	80.14	9.06
-105	80.37	9.08
average ± std dev.	80.20± 0.11	9.06± 0.01

3.2.2.2. Electrochemical Impedance Cell

The electrodes as described above are the main feature of the electrochemical cell. There are other aspects that need also be considered. The first is the outer housing of the cell. It must be inert to the solvents considered. It also is necessary that the entire cell be sealed from the atmosphere. This is necessary to maintain the vacuum during cell constant measurements and also to maintain the purity of the solvents from moisture in the atmosphere. A variety of polymer materials were tested (Fiberglas®, PVC®) for their light weight and ease of sealing. However, the low temperatures and the vacuum conditions caused them to fail. A quartz cell was found to be acceptable with a cap made of stainless steel. A compression fitting with o-rings as part of the cap was used to isolate the cell from the environment.

As mentioned in the preceding section, stray capacitances cannot be eliminated, but they can be reduced. For these measurements, it was found that the lead wires were the main contributor of stray capacitance. To reduce its impact, these leads, from the instrument to the variable capacitor electrodes, were made as short as possible. To reduce the communication between the remaining length (Parker Effect) [Shedlovsky, Spiro], the lead wires were kept as far apart as the interior of the cell would allow. To further reduce the capacitance of the lead wires, magnetic reed switches were placed between the variable capacitor electrodes and the lead wires. When activated, the switches electrically disconnected the wires from the variable capacitor electrodes allowing a "null" measurement to be taken. This allowed the measurement of the wire capacitance prior to any measurement. [The value

of the "null" changes as the relative dielectric constant of the medium between the wires changes. By nulling before each measurement, the changes in stray capacitance due to relative dielectric constant differences that arise due to composition and/or temperature changes can be taken into account.]

The electrochemical impedance cell used for these measurements is shown in figure 3.2.9. The air variable capacitor electrodes were supported with a Teflon® rod (not shown) that screwed into the cap. Alnico magnets slide up and down glass tubes that were heat sealed at the bottom. These glass tubes were fit into the cap with compression fittings to give a vacuum tight seal. [Due to the difficulty of machining Alnico, a hole was drilled in a small iron rod and attached with string. The magnet, attracted to the iron, was raised and lowered in this manner.] The lead wires were feed through glass tubes and sealed with epoxy. The ends of the wires had a grooved copper fitting. These grooves allowed for a good attachment of the alligator clips at the ends of the leads from the instrumentation. The glass tubes, through which the lead wires were fed, also were fit to the cap with compression fittings for a good seal. A fifth compression fitting with a Teflon® plug is found on the cap. Because of the limits to dexterity that accompany the use of a glovebag during the charging of the cell, the Teflon® plug is removed and replaced with a funnel to fill the cell. The plug is replaced to seal the opening and thus the inert atmosphere of the glovebag is maintain within the cell. Thus, during charging only one part needed to be manipulated easing the filling of the cell and prevented damage to the parts within the cell. Two tubes with shut-off valves extending out of the sides of the cap allowed a vacuum to be drawn and also allowed pressure release during charging of the cell within the glovebag.

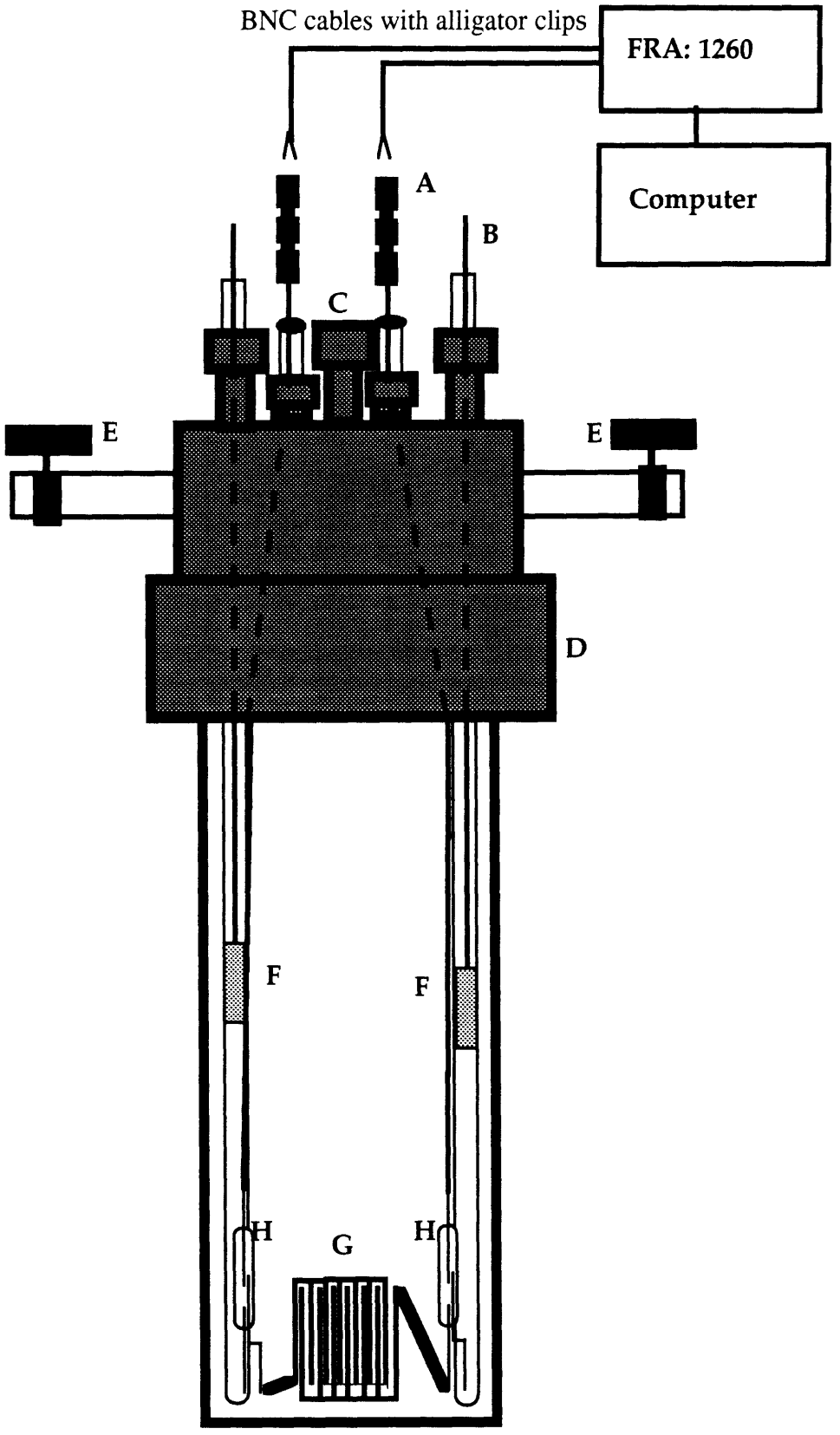

Figure 3.2.9. *Dielectric Measurement Cell.* A. Lead wire from capacitor/magnetic reed switch with notched copper fitting; B. Glass tube sealed at the bottom contains magnet to activate reed switch. **C**. Feed through, capped during measurement, holds funnel during charging of cell. **D**. Stainless steel cap, seals with o-ring to glass of cell. **E**. Tubes with shut-off valve **F**. Alnico magnet with string attached to raise and lower it. **G**. Air variable capacitor. **H**. Magnetic reed switch.

3.3 Procedure

3.3.1 Experimental

Prior to use the cell was cleaned with distilled water and kept under vacuum a minimum of twelve hours. Just prior to filling the cell, the cryostat, to be described later, was set for -35°C. This allowed the experimental cell to be kept at a low temperature before and during measurements so that the solutions do not alter their concentration due to the boiling of chloroethane (gas at room temperature). The cell and the sample to be tested were placed in a glovebag filled with nitrogen gas dried with 3A molecular sieve and Drierite® that were part of the gas train.

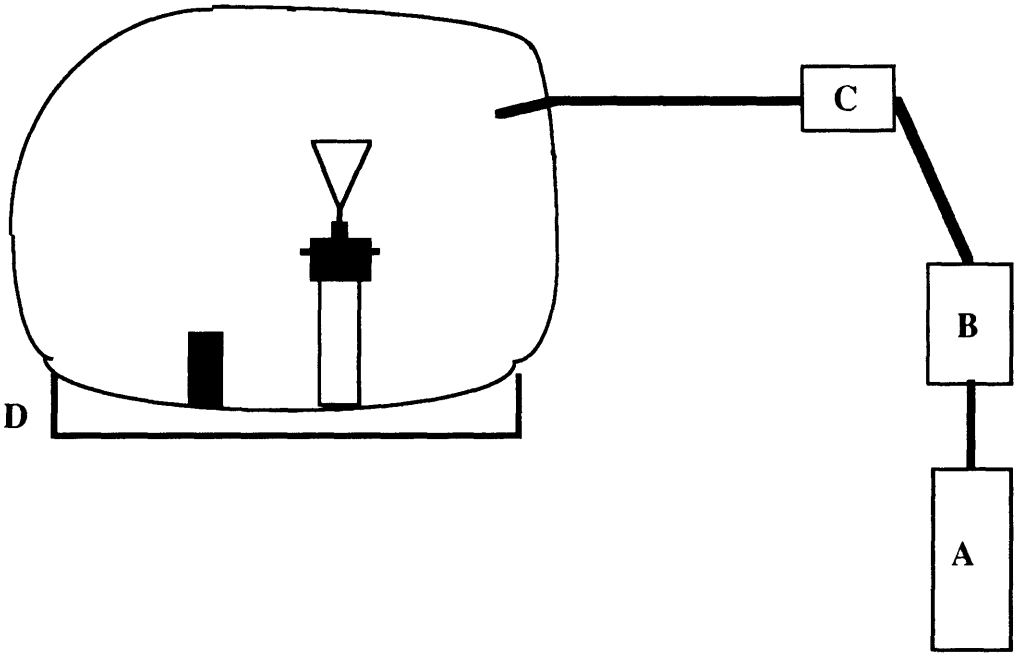

Figure 3.3.1 *Glove bag Schematic.* Electrochemical cell was charged in inert gas (**A**) filled glove bag. The gas flowed through drying agents (**B, C**) of 3A molecular sieve and drierite. The cell and the samples were cooled in an external liquid nitrogen pool (**D**).

The samples were measured by weight which was later converted to mole fraction and kept in a freezer at -30°C prior to measurement. With the

exception of the pure butyronitrile sample (liquid at room temperature), all samples while within the glovebag were kept in an external liquid nitrogen pool to prevent the boiling of chloroethane. With these solutions as well, the cell and funnel were also cooled in the liquid nitrogen for the same reason. One of the shut-off valves was then opened and the Teflon® plug on the cap was removed and replaced with the funnel. The sample was then poured into the cell and the cap replaced. The valve was then shut. The cell was now sealed with the nitrogen atmosphere of the glovebag maintained within the cell [figure 3.3.1]. The experiment was now placed within the cryostat and the measurement begun.

The cryostat used was a liquid-state cryostat where a liquid was simultaneously cooled and warmed to achieve the desired temperature (figure 3.3.2). The liquid medium used was methylcyclohexane (ε_r=2.024) [Landolt-Bornstein]. Liquid nitrogen flowed through a copper coil as a coolant. The nitrogen was then released into the atmosphere and/or rerouted to a gas-dispersion tube within the bath for stirring. Strong bubbling aided in thermal transport, maintaining a broad isothermal region within the bath [$\pm$0.03°C], and also acted as a warming element in conjunction with the heater. A resistor-heating element was controlled by a Lakeshore temperature controller [Model 330] with a silicon diode used as a temperature sensor. The sensor was calibrated by the manufacturer [two point SOFTCAL™] with an absolute accuracy of 0.15°C. The temperature within the bath can be maintained for over thirty minutes to $\pm$0.03°C and often to within $\pm$0.01°C. For more details of the cryostat design refer to H. Shapiro.

There was a thermal lag between the bath and the sample within the cell. It was found that within seven minutes of achieving bath temperature, the sample reached the setpoint temperature. To account for this lag, a

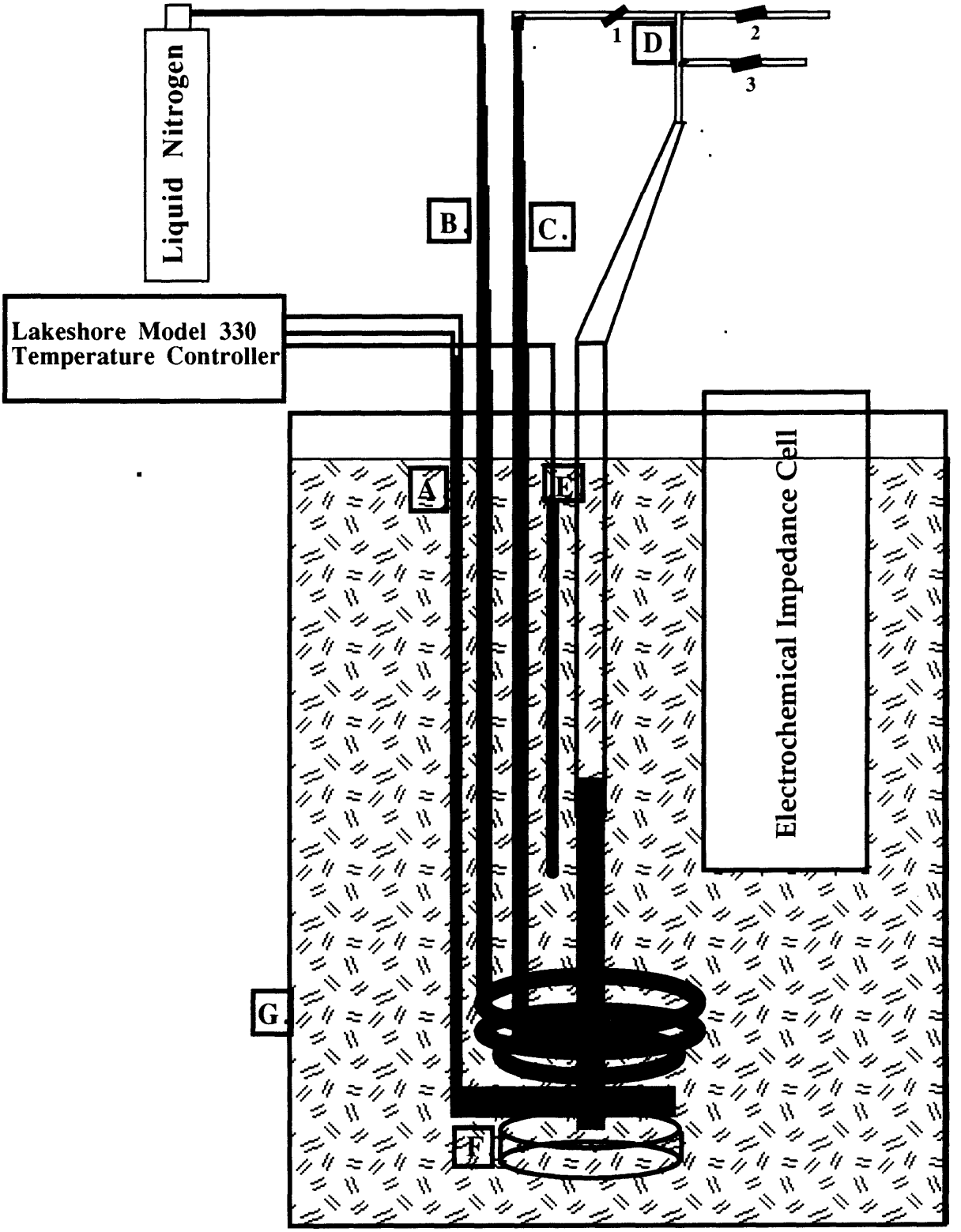

Figure 3.3.2 *Cryostat.* Liquid based cryostat using methylcyclohexane as cryogen. May be used for long term experiments from +40°C to -105°C and for short time to -110°C. **A**. Resistive heater controlled by Lakeshore temperature controller. **B**. Coil input for liquid nitrogen coolant. C. Output of liquid nitrogen coil. **D**. Manifold. By controlling the opening of the valve 1 the liquid nitrogen flow rate into the coil is controlled. With valves 2 and 3 the flow to the atmosphere is controlled (the higher the flow the faster is the cooling rate). The nitrogen gas not vented to the atmosphere returns to the bath through the gas dispersion tube, F. Vigourous bubbling ensures thermal uniformity in the cryostat. **E**. Silicon diode temperature sensor for Lakeshore temperature controller. **F**. Gas dispersion tube. **G**. Nalgene dewar.

measurement was begun a minimum of fifteen minutes after the cryostat reached the setpoint temperature to assure thermal equilibrium within the experimental cell. Temperatures used in these measurements were -35°C (238.16K), -50°C (223.16K), -65°C (208.16K), -80°C (193.16K), -95°C (178.16K), -105°C (168.16K). Below -105°C, the setpoint temperature was difficult to maintain within the cryostat.

The measurements were taken using a frequency response analyzer [Schlumberger Model 1260]. Commercial software [Z60] was used to set the analyzer parameters and to gather the data. The setup parameters used for the unknown samples and for the methanol calibration were as follows:

instrument output:
frequency varies logarithmically
descends from 1MHz to 500Hz
10 points per decade
zero bias voltage
generator amplitude of 300mV

for the instrumentation's analysis:
integration time of 5 seconds with a 3 cycle delay
input voltages sense of 300mV
input current sense of 600μA

For the vacuum condition, the parameters were

instrument output:
frequency varies logarithmically
descends from 1MHz to 500Hz
10 points per decade
zero bias voltage
generator amplitude of 2.8V

for the instrumentation's analysis:
integration time of 5 seconds with a 3 cycle delay
input voltages sense of 3V
input current sense of 600μA

Once thermal equilibrium was achieved within the cell, the two Alnico magnets were lowered to open the reed switches. This allowed the capacitance measurement of the lead wires, from the reed switch to the 1260 unit, to be measured. This accounted for the majority of the stray capacitance of the measurement. By measuring this value with the sample within the cell, the contribution of the sample to this capacitance is also taken into account. Once this measurement is completed (approximately five minutes), the magnets were raised so that the air variable capacitor electrodes are now part of the circuit. The total capacitance of the sample between the electrodes and the wires is now measured. Once completed, the temperature setpoint of the cryostat is changed and the procedure repeated at each temperature. After all the temperatures are measured the cell is cleaned with distilled water and kept under vacuum until its next use.

The first sample tested was vacuum. From this measurement a cell constant was determined [$C = \varepsilon_o \varepsilon_r G$, eq. 3.2.1, where ε_r =1 for vacuum]. Then reagent grade methanol was measured from 25°C (298.16K) to -50°C (193.16K). Comparison of these values with those found in the literature confirm the validity of the measured cell constant. Next pure chloroethane and pure butyronitrile were measured. The consistency of these values with those reported in the literature further confirmed the measured cell constants. Lastly, solutions of nominally 20, 40, 60, 80 mole percent butyronitrile were measured as a function of temperature.

3.3.2 Data Analysis

Using an in-house null program [K. Rhoads], the experimental data are treated to subtract the wire capacitance from the total measured capacitance still as a function of frequency. The remainder is the capacitance of the air

variable capacitor with the sample dielectric between the plates measured as a function of frequency. A sample of this data is seen in figure 3.2.5. As can be seen the data forms a semi-circle which is expected for a capacitor and resistor in parallel, the equivalent circuit (figure 3.2.4).

A commercial software least-squared fitting package [ZSIM, a framework about LEVM] was used to fit the data to determine the values for the capacitance and resistance. A sample of the measured and fit data is shown in figure 3.3.3. From the values of capacitance, the relative dielectric constants were computed by division with the capacitance in vacuum.

$$C_{sample}[F] = \varepsilon_o[F/m]\varepsilon_{r,\,sample}G[m]$$
$$C_{vacuum}[F] = \varepsilon_o[F/m](1)G[m] \qquad \text{eq. 3.3.1}$$
$$\frac{C_{sample}[F]}{C_{vacuum}[F]} = \frac{\varepsilon_{r,\,sample}}{1}$$

These relative dielectric constant measurements along with literature values, where appropriate, of methanol, butyronitrile, chloroethane, and a sample solution are found in figures 3.3.4 a-d A compilation of the relative dielectric constant variation with composition and temperature is shown in figure 3.3.5.

Using the cell constant, the electrical conductivity can be determined from the resistance.

$$R[\Omega] = \frac{1}{\kappa[S/cm]G[cm]} \qquad \text{eq. 3.3.2}$$

Figures 3.3.6 shows a compilation of the conductivity data as a function of temperature. For the actual numerical values for both the relative dielectric constants and the conductivities refer to Appendix B.

3.3.3 Error Analysis

The dielectric constant is determined through the measurement of the sample capacitance divided by the capacitance as measured in a vacuum. The

Experimental and Fitted Data

Pure Butyronitrile at T=238.16K

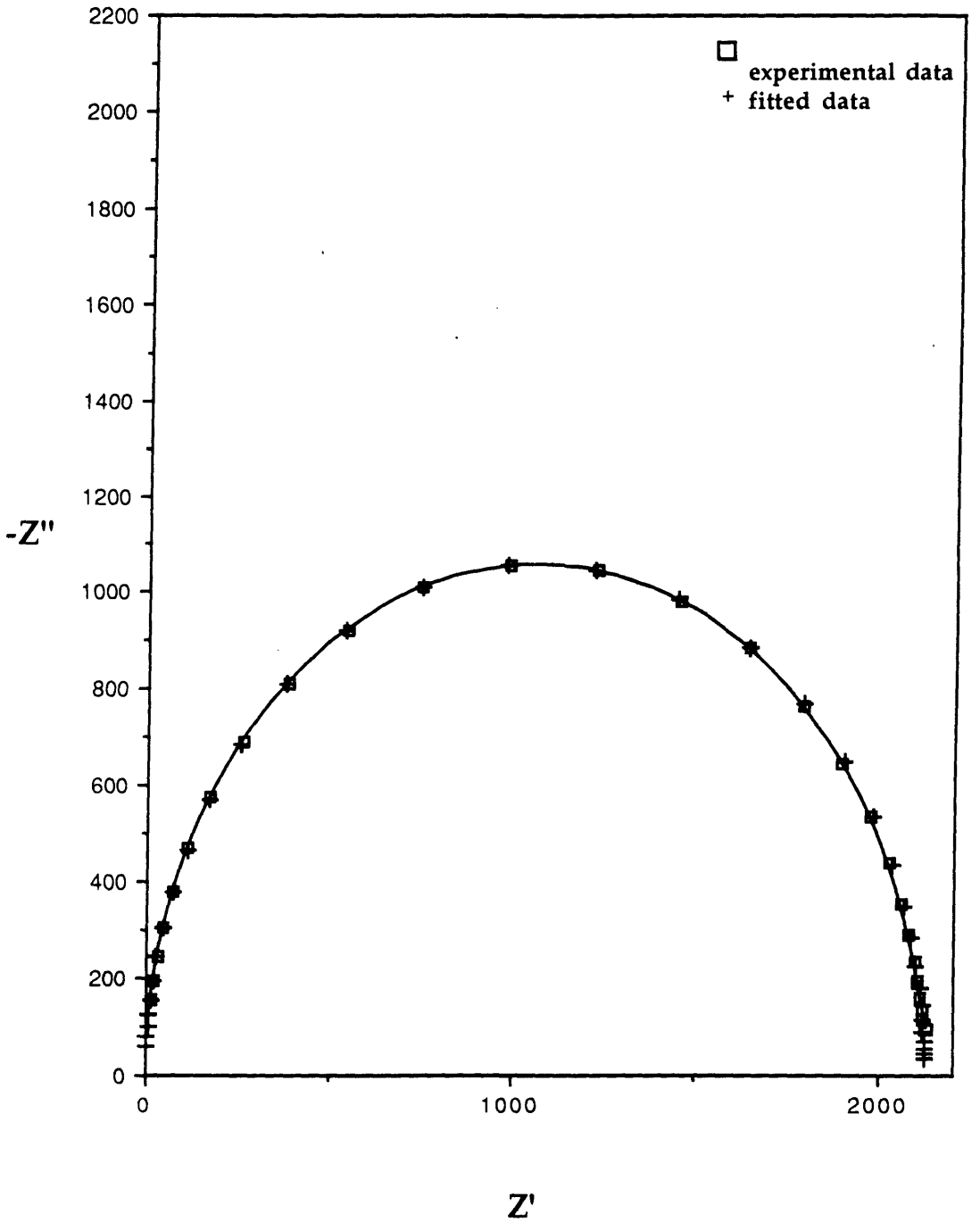

figure 3.3.3 Sample of Measured Data. The measured data forms a semi-circle which is well modeled by a capacitor and resistor in parallel.

lack of true vacuum during the vacuum measurements and the presence of stray capacitances contributes to the error in the vacuum measurement. This error was determined to be 0.11×10^{-12} F from both the curve fitting of the impedance data and the scatter of the 18 vacuum measurements by root mean square analysis. The error of the sample capacitance from the curve fitting and experimental noise was determined by root mean square analysis of three points to be 15×10^{-12} F. The total error in the relative dielectric constant as determined from these errors is no more than 0.26. This was computed from the relationship $\delta\varepsilon_r = \frac{\delta C_s}{C_v} + \frac{C_s}{C_v^2}\delta C_v$ where C_S and C_V are the average values of the capacitance of the sample and vacuum respectively.

The error in the correlation factor are attributed to errors in temperature, mole fraction, relative dielectric constant, the use extrapolated values for the index of refraction, assumptions related to the dielectric constant at infinite frequency and zero excess volumes, and errors in the literature values of the dipole moment of the components. The correlation factor was determined through interpretation of the linear relationship of these factors as will be discussed in section 3.4. The error in the compution of the correlation factor is no greater than 0.065.

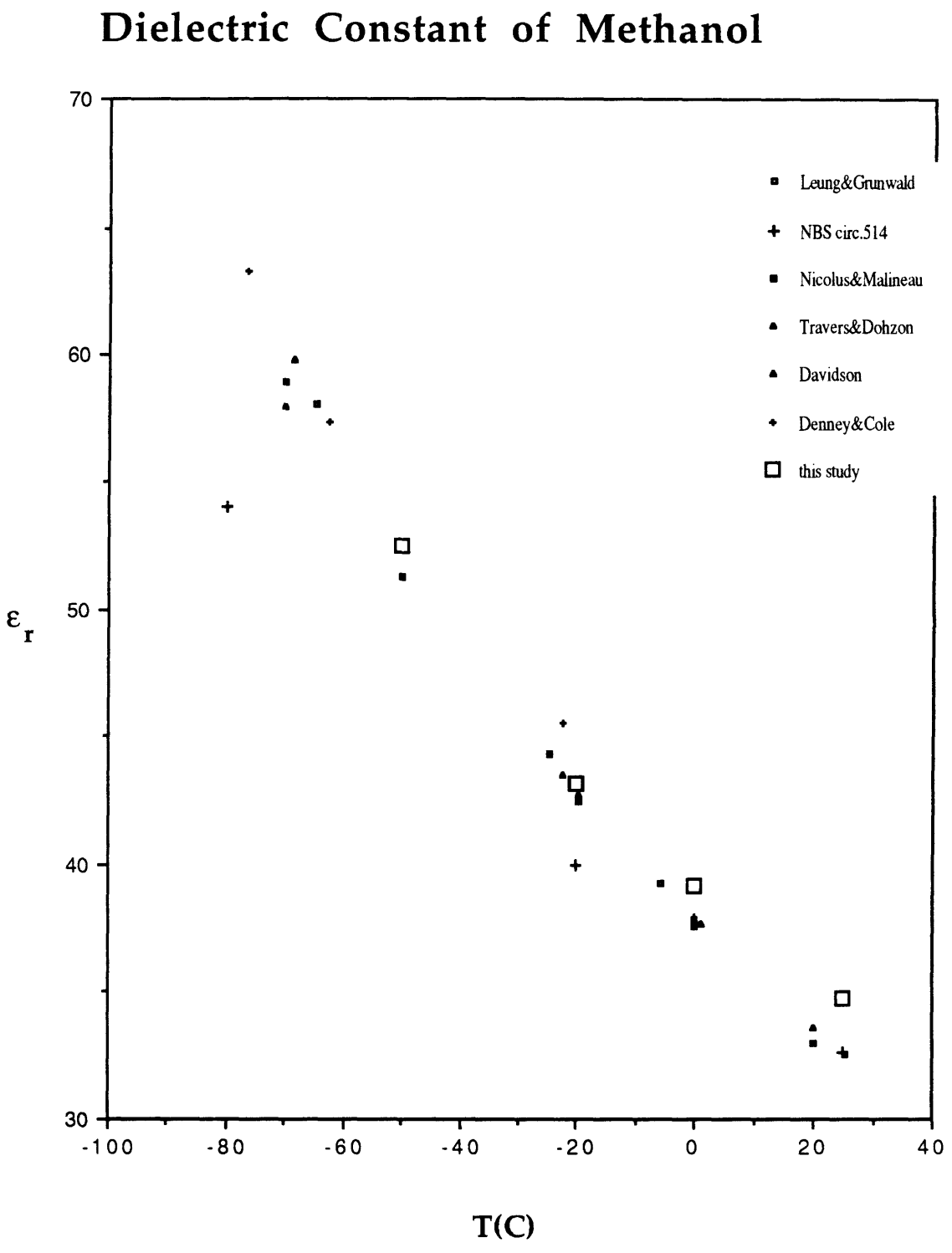

figure 3.3.4a Relative Dielectric Constant of Methanol. Comparison of measured and literature values of the relative dielectric constant of methanol as a function of temperature.

The NBS circ.514 values are those cited in the CRC. These values were measured at the turn of the century.

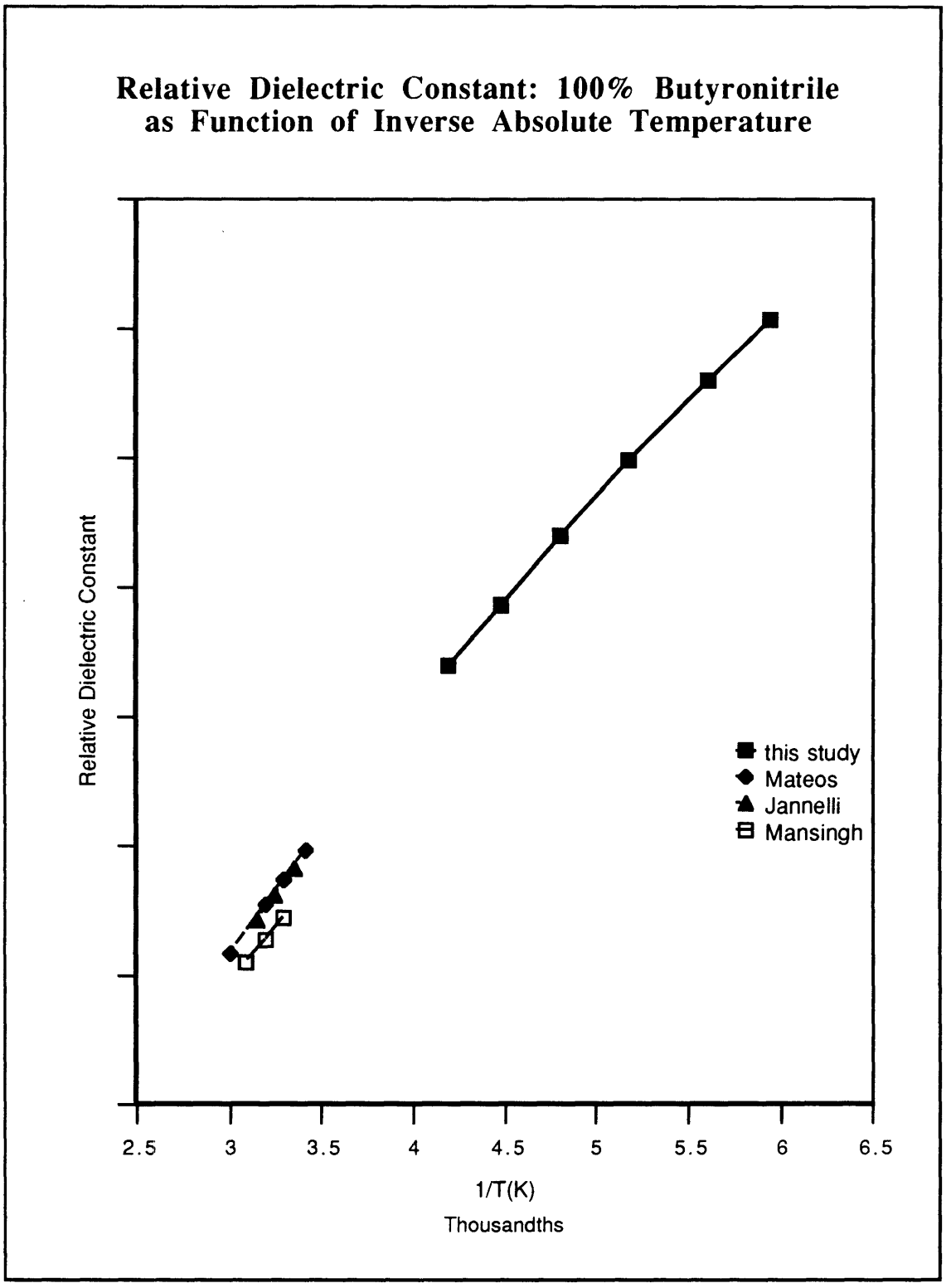

Figure 3.3.4b. *Pure Butyronitrile.* Relative dielectric constant of pure butyronitrile plotted as a function of inverse temperature. Both measured and literature values are plotted.

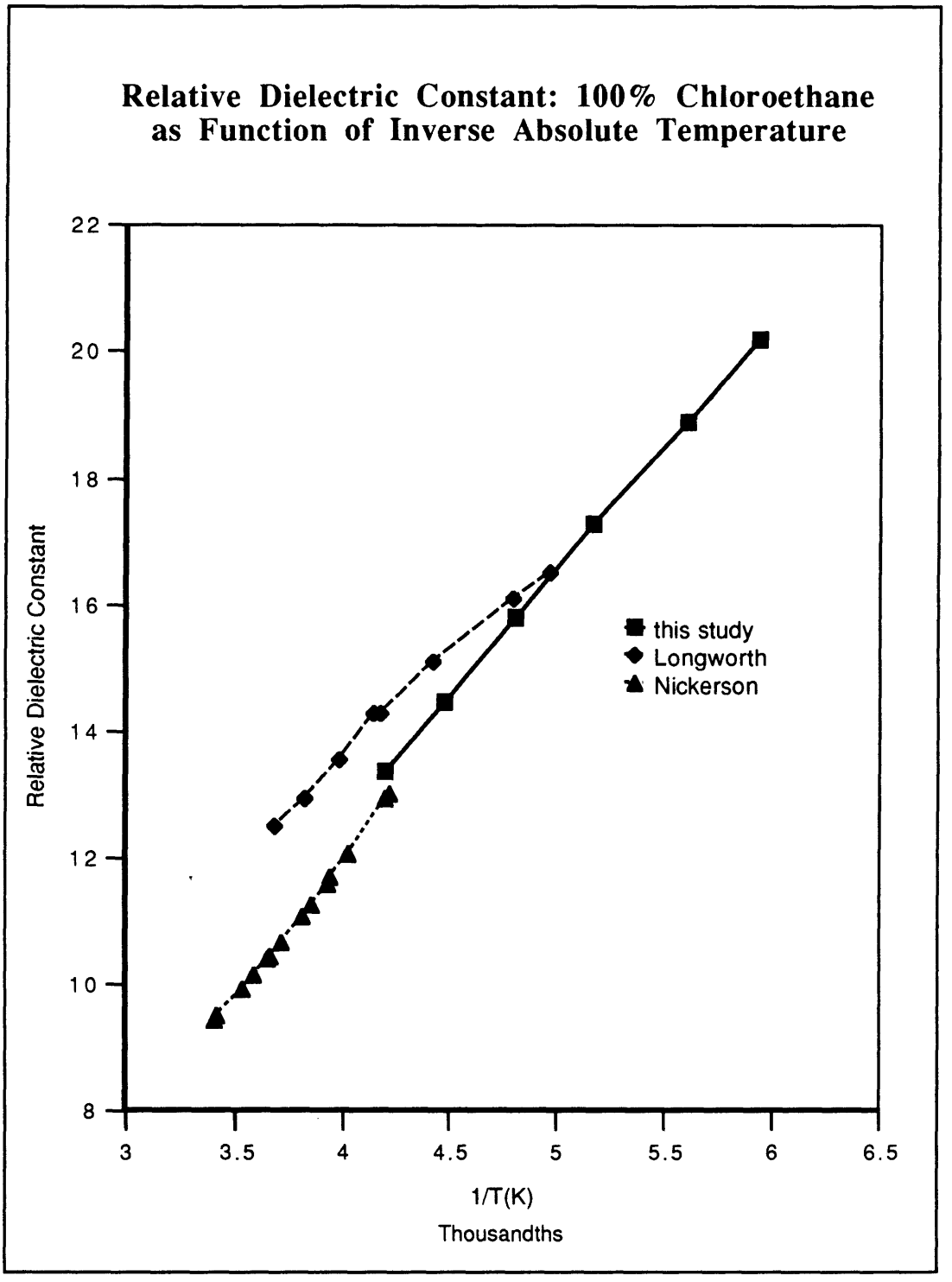

Figure 3.3.4.c. *Pure Chloroethane.* Relative dielectric constant of pure chloroethane plotted as a function of inverse temperature. Both measured and literature values are plotted.

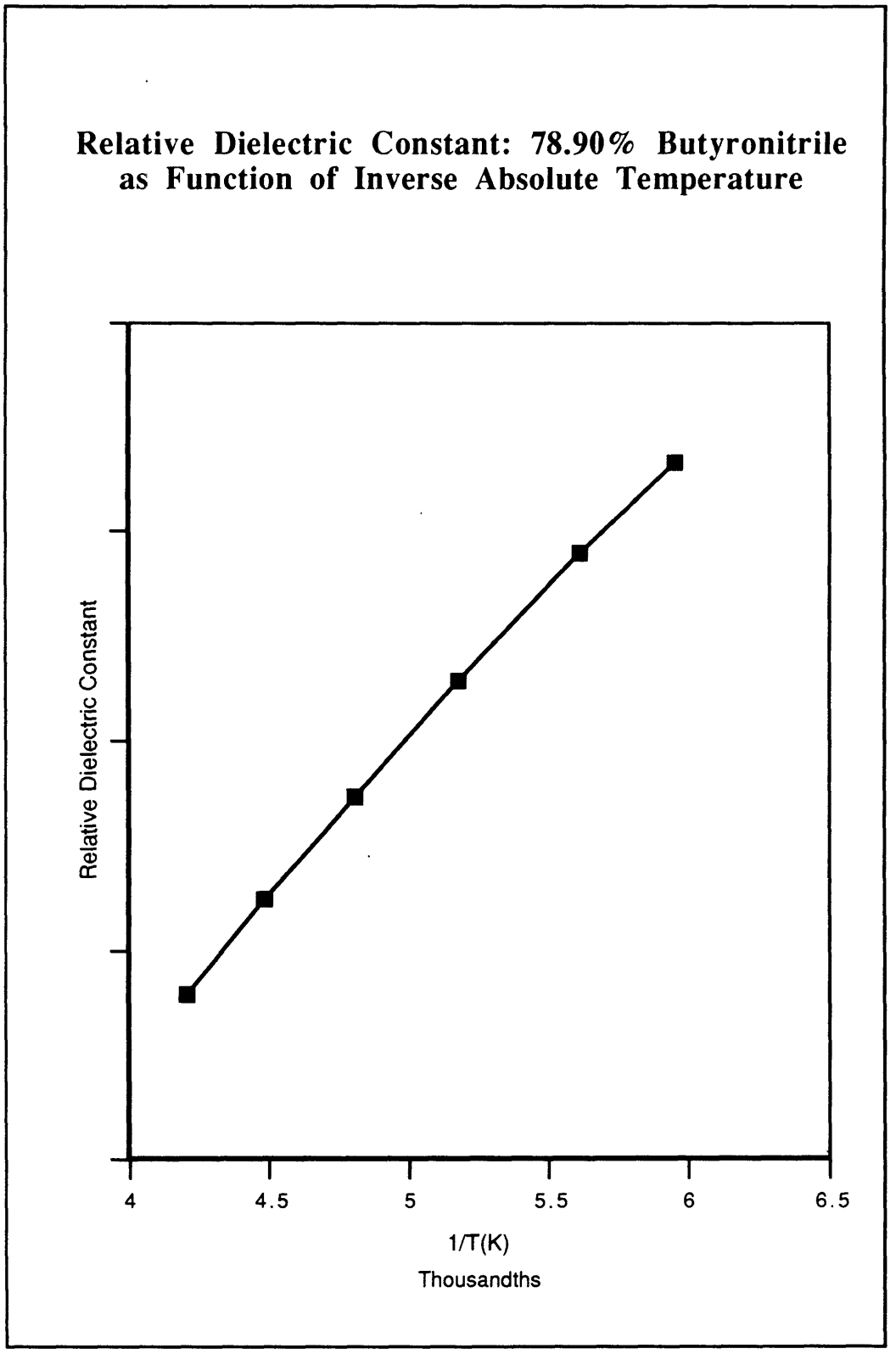

Figure 3.3.4d. *78.90m/o Butyronitrile*. Relative dielectric constant of 78.90m/o butyronitrile in chloroethane plotted as a function of inverse temperature.

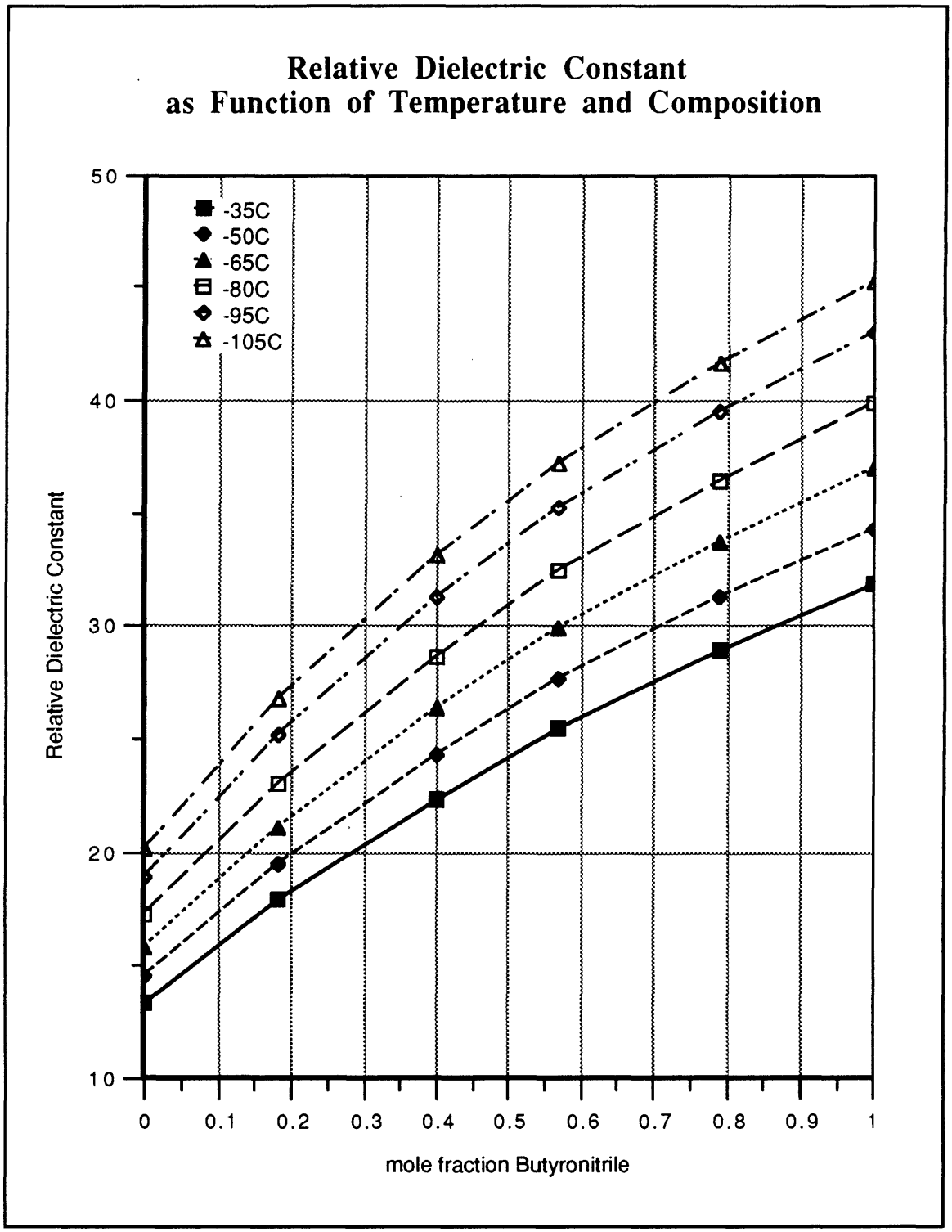

Figure 3.3.5 *Relative Dielectric Constants.* Plot of variation of the measured relative dielectric constant as a function of temperature and composition.

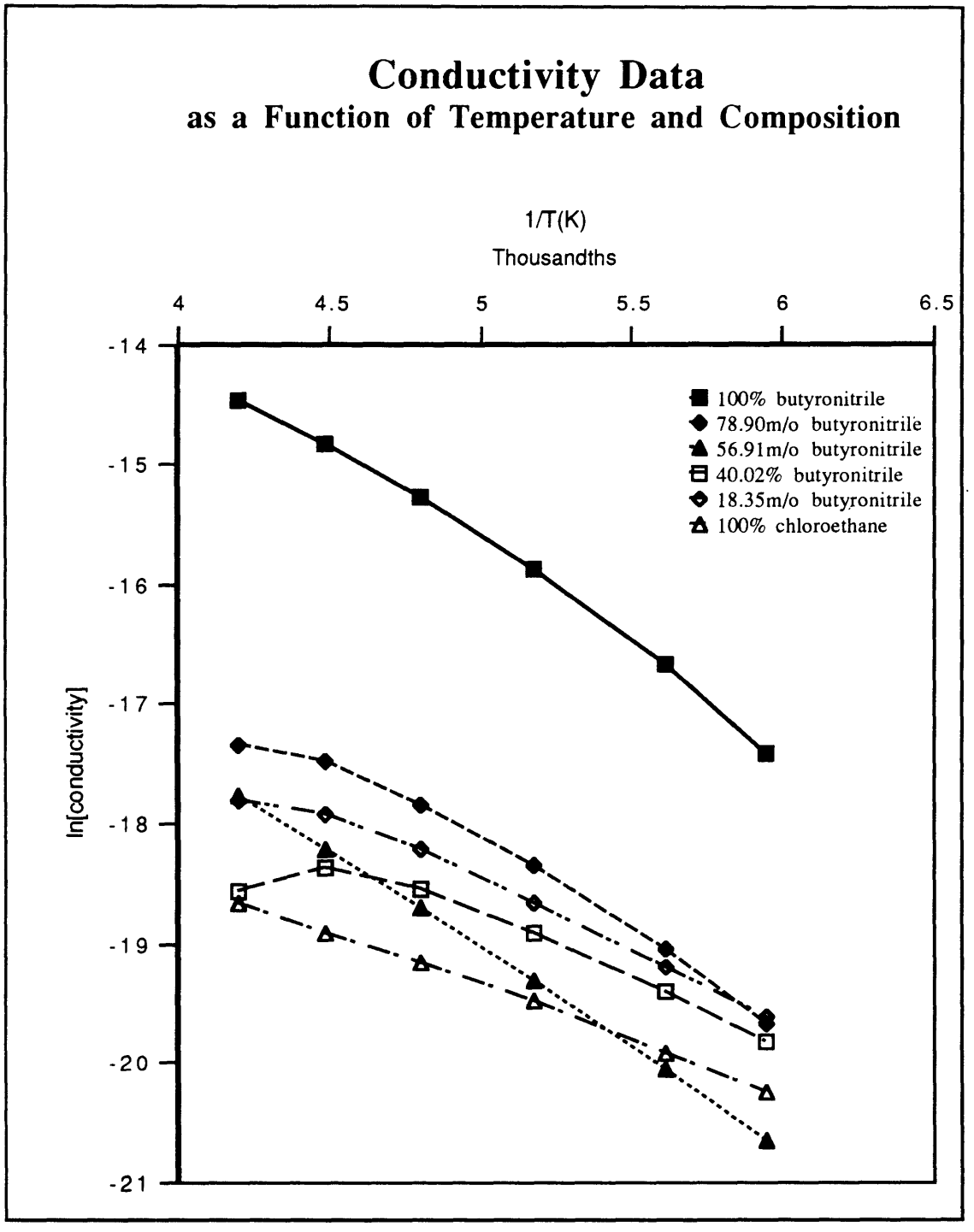

Figure 3.3.6 *Conductivity*. Plot of the variation of the natural logarhithm of the measured conductivity as a function of inverse absolute temperature and composition.

3.4 Discussion

3.4.1 Qualitative

3.4.1.1 Cell Constant Calibration and Confirmation

As mentioned in the experimental section, the cell constant was determined by measuring the capacitance of the air variable capacitor in a vacuum. From this value, the cell constant was computed. The values determined were found to be essentially invariant with temperature (Table 3.2.1). As the relative dielectric constant of vacuum is invariant, the only source for change of the measured capacitance is the thermal contraction of the electrodes which causes changes in the cell constant. If there were no constraints on the electrodes, linear expansion would at most change the cell constant by less than 0.2%. The variations of the values in table 3.2.1 can most likely be attributed to stray capacitances that were not accounted for by the "nulling" of the data. The unknown liquids have capacitances two orders of magnitude greater than those measured in vacuum. As a result, the stray capacitances are a much smaller percent of the total measured capacitance, becoming insignificant.

To confirm the values of the cell constant derived from vacuum capacitance, reagent grade methanol was measured as a function of temperature and the relative dielectric constant computed. These values and those found in the literature are shown in figure 3.3.4a. As can be seen the values determined in this study are in conformity with a majority of the reported values. If values from the literature are compared, they have a standard deviation on average of 0.5 when significantly different values are

excluded. When the values of the relative dielectric constant measured with the apparatus described herein are included in this computation, the standard deviation remains on average 0.5. This conformity over a number of temperatures (i.e. relative dielectric constants) validates the experimental cell for use in the measurement of the unknown solutions.

3.4.1.2 Relative Dielectric Constants Measurements

For the pure butyronitrile sample (figure 3.3.4b), the relative dielectric constant was found linear with the inverse temperature. In the figure, the literature values were plotted. As can be seen, the measured values are linear as well with two sets of data reported in the literature. This gives further evidence of the reliability of the measuring apparatus. The relative dielectric constant for the chloroethane was also found to be linear with the inverse temperature (figure 3.3.4c). The literature values also agree reasonably well with the measured values.

For the solutions of butyronitrile and chloroethane the relative dielectric constants vary linearly with the inverse temperature (as an example, figure 3.3.4d). The compilation of all of the relative dielectric constants measured as a function of composition and temperature fall on a smooth curve (figure 3.3.5). The variation of the dielectric constant with composition is nearly linear. There have been no values reported in the literature for the relative dielectric constant of butyronitrile-chloroethane binaries. A comparison of systems of similar molecules validates the shape of the curves as a function of composition of the measured relative dielectric constants. In figure 3.4.1a, the variation of the relative dielectric constant of butyronitrile and 1-butanol measured at 25°C is shown based upon literature values [Mateos]. In figure 3.4.1b, a similar relative dielectric phase diagram

Compositional Variation of Relative Dielectric Constant Butyronitrile-1-Butanol

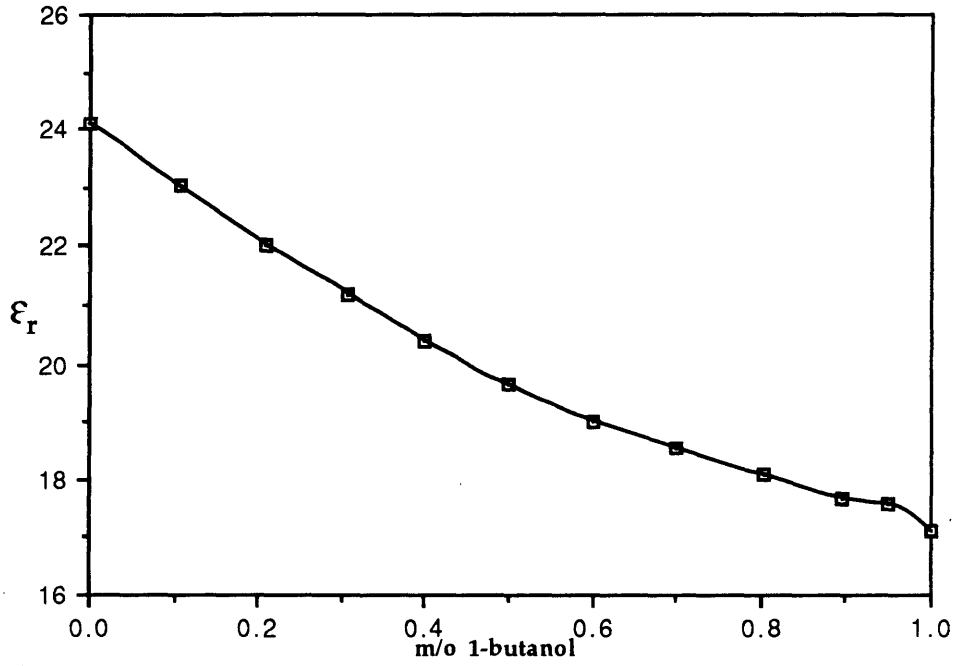

Figure 3.4.1a. Relative dielectric constant reported in literature. Similar shape to measured relative dielectric phase diagram [Decroocq]. T=25 C.

Compositional Variation of Relative Dielectric Constant Bromoethane-Acetonitrile

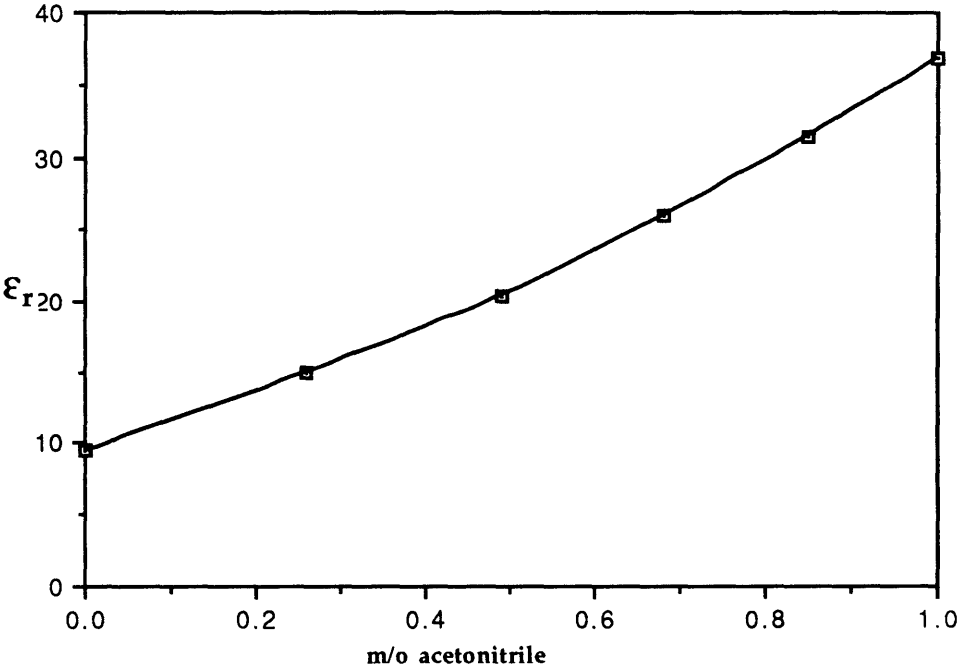

Figure 3.4.1b. Relative dielectric constant reported in literature. Similar shape to measured relative dielectric phase diagram. [Mateos] T=20 C.

for bromoethane and acetonitrile is plotted based upon literature values [Decroocq] measured at 20°C. In the measured relative dielectric phase diagram and the two that were reproduced from the literature, the changes in the relative dielectric constant are smooth as a function of composition. The deviations from strictly weighted additivity (i.e. $\varepsilon_m = x_1\varepsilon_1 + x_2\varepsilon_2$) are comparable among the three systems. While the measured system is concave down the reported curves are concave up. This in part is attributed to the difference in size of the molecules. The different molecular interactions also play a role. For figure 3.4.1a, the hydrogen bonding associated with the -OH group of 1-butanol changes the nature of the intra- and intermolecular interactions. For figure 3.4.1b, the difference in the chain length of acetonitrile as compared to butyronitrile changes the effects of the nitrile group on the intra- and intermolecular interactions.

In figure 3.4.2 the deviation of the measured relative dielectric constant from ideal mixing is plotted where

$$\delta\varepsilon = \varepsilon_{measured} - x_{BN}\varepsilon_{BN} - x_{CE}\varepsilon_{CE} \qquad \text{eq. 3.4.1}$$

where $\varepsilon_{BN\ or\ CE}$ is the measured value in the pure liquid

The curves have similar shapes as a function of temperature. The curves are concave down with values greater than zero. At a given temperature, this indicates that the dipoles in solution align to give a greater net moment than predicted by ideal mixing [Marcheselli, Nath, Papanatasiou]. Both the increase in density and the reduction in thermal energy contributes to the increase in $\delta\varepsilon$ as the temperature is lowered. The maximum of all the curves lies between 40 and 50 mole percent butyronitrile. Though a broad range, this indicates the possible tendency to form 1:1 type complexes. The one

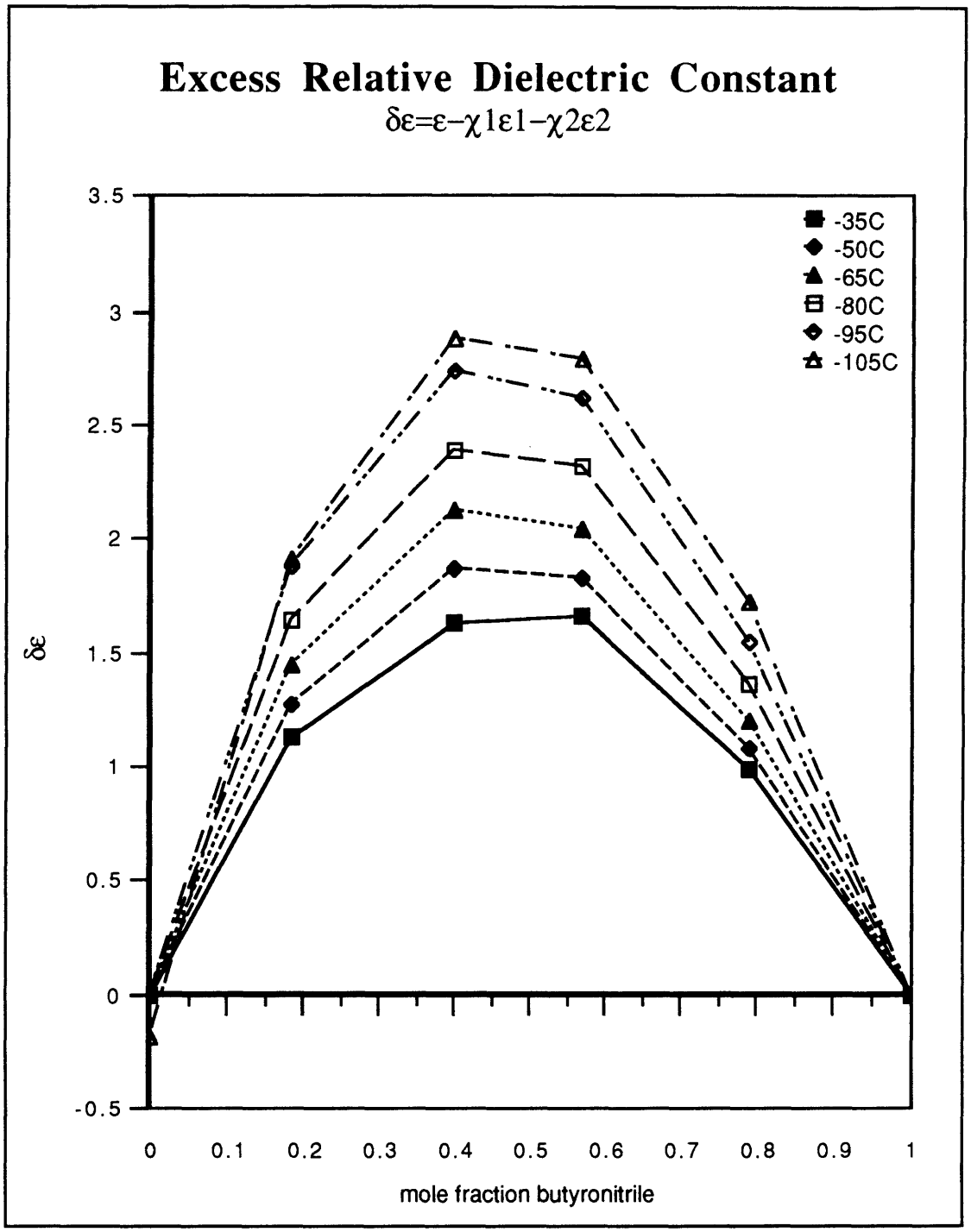

Figure 3.4.2 *Excess Relative Dielectric Constant.* Measure of the deviation of the relative dielectric constant from ideal mixing.

difference among the curves is the shifting of the maximum from close to 50 mole percent butyronitrile to closer to 40 mole percent as the temperature is reduced. This may be due to the change in density of the solution. At lower temperatures the density is increased meaning the molecules are in closer proximity (i.e. a reduction in the free volume). This may serve to amplify the dipole interactions of the smaller chloroethane with the butyronitrile slightly changing the molecular interactions. An alternative is that at reduced temperature, the likelihood for self-association increases. Self-association in nitrile compounds is well documented [Dannhauser, 1963, 1964, Murray, Mansingh]. In butyronitrile-sulfolane the increase in the magnitude of the excess dielectric constant and the shifting of the maximum is attributed to an increase in self-association of the nitrile [Jannelli]. In the measured system, a slight increase in like-molecules associating would shift the maximum towards the chloroethane rich end where parallel dipole alignment (refer to section 3.1) gives a larger relative dielectric constant than values attributed to the dipole moment alone.

3.4.1.3 Conductivity Measurements

The electrical conductivity is a function of the number of charge carriers and their mobility. The sources of charge carriers include water impurities, other organic impurities, and self-dissociation of the molecules and, in the case of an electrolyte, intentionally added ions. Mobility is related to the complexing of the ionic species, the temperature, and viscosity of the solvent [Bard]. It is expected that conductivity follows an Arrhenius equation $\kappa = Ae^{-E_a/kT}$. The magnitudes of the conductivity for butyronitrile indicate water impurities of less than 100 ppm by Karl-Fisher titration. For the chloroethane the magnitude is on the order reported in the literature

[Riddick]. In figure 3.3.6 the natural logarhithm of the conductivity versus the inverse of the absolute temperature is approximately linear. There is a slight curvature which may be attributed to the combined effects of increased relative dielectric constant and reduced mobility as the temperature is reduced. Based upon the work of Fuoss *et al* [Fuoss], the higher relative dielectric constant reduces the likelihood of the ions complexing with each other. The result would be a larger number of charge carriers as the temperature is reduced all else being equal. As the temperature is reduced, however, the mobility is reduced due to a reduction in density which favors the interaction of the solvent with the ions. The integrity of complexes of the solvent with the solute is also favored as the thermal energy is lowered. Quantitative interpretation of this data is limited by the lack of information concerning concentration of carriers and mobility of these species.

3.4.2 Quantitative

The measured relative dielectric constants were fit to the Kirkwood equation (eq. 3.1.4) and values for the correlation factor and the dispersive polarizability determined. In order to use this equation, molar volume data and refractive indices are required. The molar volumes for the pure butyronitrile and chloroethane were determined from a correlation found in the literature (eq. 2.4.3.6) [Daubert]. For the binary solutions, a weighted molar volume was used (i.e. zero excess volume assumed). For the refractive index, only ambient values were reported in the literature [Riddick] These values were found to be linear with temperature and were extrapolated to the reduced temperatures studied within this document. As with the molar

volume, a weighted average was used for the binary solutions. [*N.B.*, The values of the refractive index squared are then multiplied by 1.1 to account for the atomic polarization. See section 3.1.] Values for the dipole moment in the gas phase for both butyronitrile and chloroethane were found in the literature [Daubert]. For the solutions a weighted average was again used. In figures 3.4.3, $\frac{(\varepsilon-1)(2\varepsilon+1)}{3\varepsilon}$ was plotted versus $\frac{N_A}{V\varepsilon_o}\left[\frac{(2\varepsilon_r+1)^2(n^2+2)^2}{27(2\varepsilon_r+n^2)^2}\frac{\mu_g^2}{k\mathrm{T}}\right]$ where the terms were described in section 3.1 of this document and where the dipole moment conversion to the value in the gas phase (eq. 3.1.5) has been incorporated into Kirkwood equation.

The correlation factor, g, is a measure of the average molecular configuration of the liquid at a particular temperature. In general, it is expected to be a function of temperature. In butyronitrile-chloroethane over the temperature range studied, the correlation factor was found to be approximately temperature independent based upon the linearity of figures 3.4.3. The correlation factor is the slope of this line. Had the correlation factor been temperature dependent figures 3.4.3 would have shown curves not straight lines.

The distortion polarization, α, is based upon the distortion of the electron cloud and the interatomic positions. In the model, these distortions add additional effects to the total polarization of the molecule under investigation. The distortion polarization, a function of the electronic cloud motion and to a lesser extent interatomic motion, is not expected to be a function of temperature [Hill] and shows as the intercepts of the curves found in figure 3.4.3. This value should be small and is related to the refractive index measured. It is not, as some of the measured curves suggest, supposed to be less than zero. The cause of the negative distortion polarizations is due

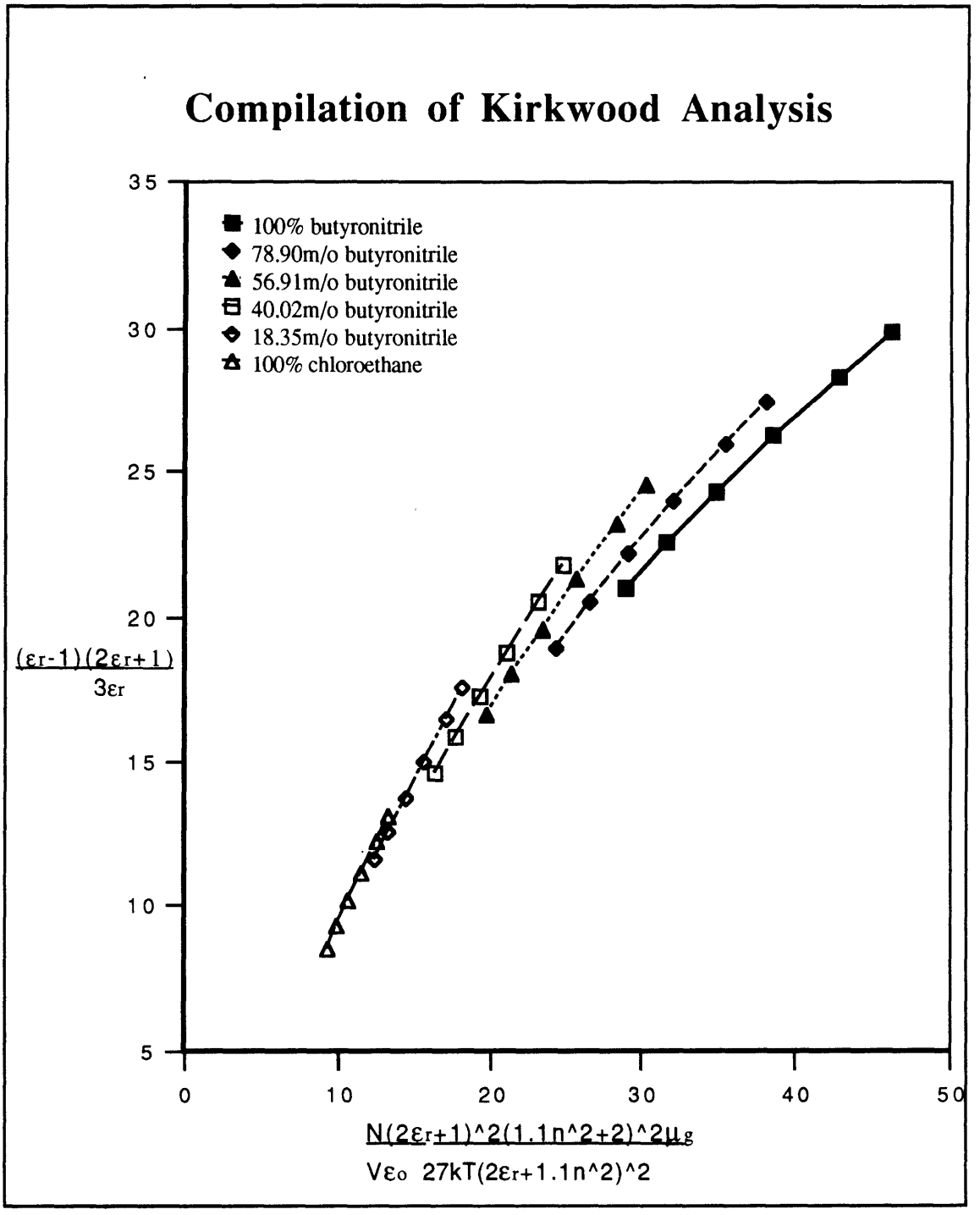

Figure 3.4.3 *Kirkwood Equation*. The measured solutions were plotted using the Kirkwood equation. The slope is the correlation factor; the intercept is the polarizability.

in part to the assumptions made in the Kirkwood equation (i.e., spherical molecules [Kirkwood], value of the dielectric constant at infinite frequency equalling $1.1n^2$ [D'Aprano]). Also, because this value is small and equal to the intercept, errors in the measurements that cause a change in the slope can shift the value from positive to negative. The variation of the correlation factor and the distortion polarization with composition is shown in figure 3.4.4.

3.4.2.1 Liquid Structure

As mentioned in section 3.1, the correlation factor reflects the effects of neighboring dipoles on the effective magnitude of the dipole moment in question. This effect is averaged over all the dipoles and is defined mathematically in the Kirkwood model as [Kirkwood]

$$\mu \cdot \bar{\mu} = \mu^2 \left[1 + \frac{N}{v} \int^{v} \cos\gamma e^{-W/kT} d\omega dv \right] \qquad \text{eq. 3.4.2}$$

$$\int^{v} e^{-W/kT} d\omega dv = 1$$

where γ is the angle between the dipole moment of an arbitrary pair of molecules

v_o is a sphere outside of which the liquid has bulk dielectric properties

W is the potential of average force and torque acting on the arbitrary pair of molecules.

The relationship in the brackets is the correlation factor. As seen it is the change in the moment of the dipole under question by the addition of the averaged effects of the neighboring molecules. The integral is the average of the correlated moments in the direction of the applied field ($\cos\gamma$) on the central dipole. This is a function of thermal energy and the energy required

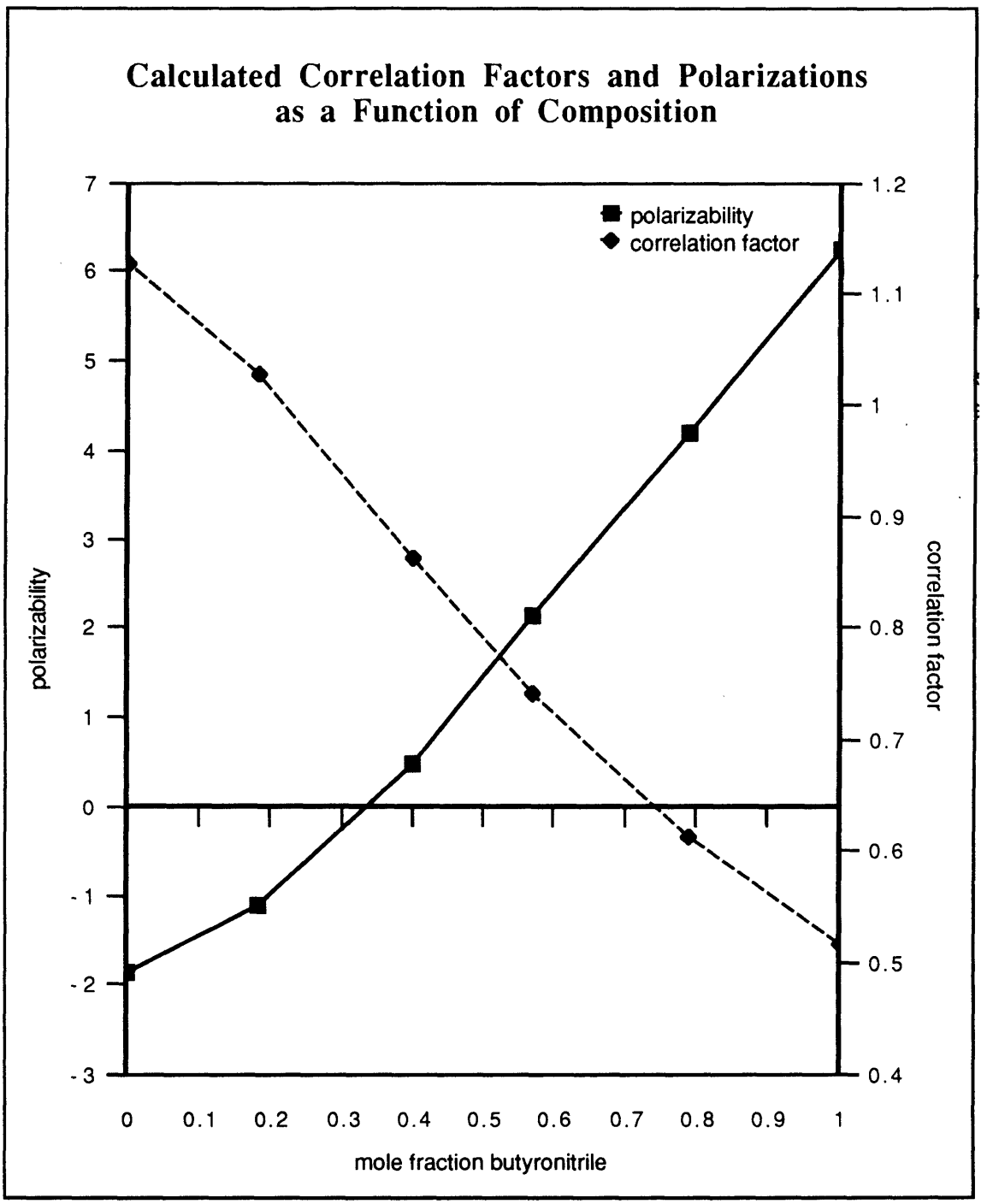

Figure 3.4.4 *Correlation Factors and Distortional Polarization.* The slope of the Kirkwood equation fit of the measured data (figures 3.4.3a-f),is the correlation factor. Since the fit is linear, the correlation factor has no discernable temperature dependence. The intercept is equal to the distortion polarization. These factors are plotted here as a function of composition.

for the neighboring dipoles to align which Kirkwood defined as the hindering to rotation [Kirkwood].

The measured value of the correlation factor may be broken up into two factors. The first is due to the dipole itself, the second to its neighbors.

$$g_{measured} = 1 + g_{surroundings} \qquad \text{eq. 3.4.3}$$

where $g_{surroundings}$ is the average correlation of the neighbors to the central dipole.

Barring additional information, the relationship of the liquid structure to the magnitude of $g_{surroundings}$ is open to a variety of interpretations. For example in figure 3.4.5, two different molecular arrangements are depicted which result in the same magnitude of the component in the direction of the field.

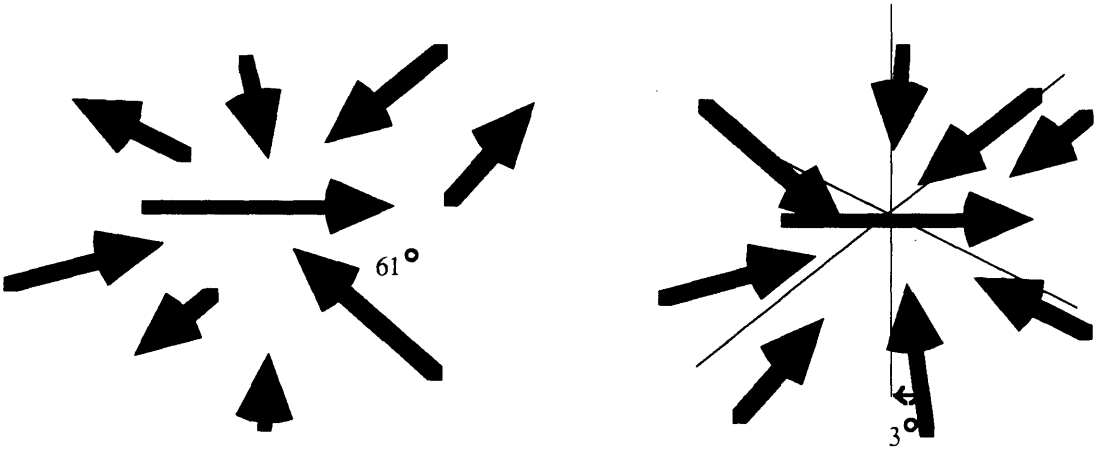

Figure 3.4.5 *Possible Molecular Arrangements.* The correlation factor alone can only be interpreted as a net arrangement. There are many possible molecular orientations that can form to give the same value for the correlation factor. Most likely more than one arrangement exists in the liquid with constant changes occurring among the different structures due to thermal motion. Two possible correlations are seen in the figure. **A.** At a given time all of the molecules are randomly arranged except one which is formally "associated" with the central dipole at an anti-parallel angle of 61° for example. **B.** All of the molecules are correlated to the central dipole at an angle of 3.5° off the perpendicular in an anti-parallel direction. Each neighbor then contributes equally to the excess dipole moment of the central molecule in the direction of the field.

The measured correlation factors can only be used to generalize about the liquid as a whole.

The correlations in the liquid are expected to increase as the temperature is reduced. This is because thermal energy tends to disrupt the dipole interactions. Thermal energy also causes a variation in the angles of dipole interactions. If **A**, in the figure above, were the only type of arrangement in the liquid (all neighbors random save one), the angle between the two dipoles may still vary about an average angle of 61° due to thermal motion. Thus, for these two reasons the liquid tends to be less correlated as the temperature rises. For all of the measured liquids over the tested temperatures, the correlation factor was found to be independent of temperature. This apparent contradiction and generalizations about the liquid structure of the pure liquids and their solutions will be discussed in more detail in the following sections.

3.4.2.1.1 Pure Butyronitrile

The value of the correlation factor measured in pure butyronitrile is 0.5152. This value, being less than unity, suggests on average an antiparallel alignment of the molecules. Utilizing eq. 3.4.3, $g_{surroundings}$ =-0.4848. On average, the molecules in the neighborhood of a given dipole may be summed into a single dipole with the same magnitude of the dipole moment as the fixed dipole set at an angle of 61° from true anti-parallel as shown in figure 3.4.6.

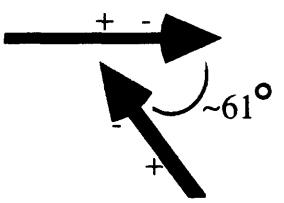

Figure 3.4.6 *Schematic of Dipole Orientation of Butyronitrile* . If the effects of all the neighboring dipoles are summed,vectorially, the resultant dipole would need be at an angle of 61° to the dipole in question to generate the measured correlation factor.

This is a lumped sum of all the neighboring effects. (*N.B.* , No assumptions have been made about the size of the neighborhood.) The effects of some neighbors may cancel the effects of others. Regardless, the net sum of all the neighbors on the central dipole is -0.4848.

For liquid nitriles, there is a general tendency to form dimers [Janelli, Danhauser, 1964a]. A monomer-dimer equilibrium was found to exist in the gas phase for acetonitrile. For the variety of liquid nitriles studied, the correlation parameters are attributed to the formation of dimer anti-parallel associates [Danhauser, 1964a]. Whether these dimers are strictly anti-parallel is unknown. (If strictly anti-parallel, the correlation factor is zero. If not, there is a finite addition to the dipole moment of the central dipole due to its neighbor.) Considering this, it is possible to consider liquid butyronitrile as being a random solution where on average one neighbor is correlated at an average angle of 61° from direct anti-parallel alignment. As the energy difference between the random and associated molecule is expected to be small, on the order of 1kcal/mole [Danhauser, 1964a], changes in thermal energy induce only small changes in the number of dimers that form.

An alternative method for interpreting the correlation factor for pure butyronitrile is to assume that strictly antiparallel associates form. If it is assumed that these associates mix ideally with unassociated molecules, than 48m/o of the solution is associated in this manner.

The butyronitrile molecule, shown in figure 2.4.1.3, is drawn as a linear molecule composed of four carbons atoms linked by sp^3 hybrid orbitals. These bonds tend towards tetragonal symmetry (the nitrogen disrupts this somewhat [Murray]) and rotations may occur along the bond axis. Though the molecules are unlikely to entangle, as with polymers, the length and twisted shape of the molecules will tend to hinder molecular motion. This is

related to the W energy in eq. 3.4.2 which defined the correlation factor. As the temperature is reduced, the free volume between molecules is also reduced. Thus, molecular motion is further hindered with temperature. This effect combined with the low energy changes in the formation of an associated species counterbalances the expected increase in net interactions as the temperature is reduced. The result is the independence of the correlation factor with temperature in butyronitrile.

Because of the average nature of the correlation factor, a definitive statement about the molecular structure of the liquid cannot be made based only on relative dielectric constant measurements. From these measurements, the only complete statement is that there is a general trend toward anti-parallel alignment of the molecules. This may be caused by slightly off-random arrangements of molecules or due to one of a few single neighbors. The latter is more likely as it does not require coordinated motion of the neighboring molecules. Also, the dipole moment is concentrated at the nitrile group [Murray]. Due to geometric considerations, this would encompass only a few molecules.

3.4.2.1.2 Pure Chloroethane

The Kirkwood model proposes a simple approximation to eq. 3.4.2 where [Kirkwood]

$$\mu \cdot \bar{\mu} = \mu^2 \left[1 + z \langle \cos \gamma \rangle_{AV} \right] \qquad \text{eq. 3.4.4}$$

$$\left\{ \langle \cos \gamma \rangle_{AV} = \iint \cos \gamma e^{-W_o / kT} d\omega_1 d\omega_2 \right\}$$

where W_o is the potential of average torque acting on a pair of nearest neighbors.

γ is the angle between dipole pairs

z is the number of nearest neighbors

When there is free rotation of the bonds

$\langle \cos \gamma \rangle_{AV} = \cos^2 \gamma$.

The value for the correlation parameter following this model is then

$$g = 1 + z\cos^2\gamma. \qquad \text{eq. 3.4.5}$$

As seen, this model is only appropriate when g is greater than 1.

For chloroethane, the correlation factor was measured as 1.1281. This value is similar to 1.0690 a value found in the literature [Nickerson]. Because the correlation factor is greater than unity, parallel alignment of the dipoles is suggested. To use the Kirkwood approximation, a value of the number of nearest neighbors, z, is assumed. Table 3.4.1 lists the average angle between the molecules as a function of z.

Table 3.4.1 Analysis of Correlation Factor of Chloroethane

Z	$\cos^2\gamma$	γ
6	0.02135	81.598
7	0.01830	82.225
8	0.01601	82.730
9	0.01423	83.148
10	0.01281	83.501
11	0.01165	83.805
12	0.01067	84.070

At present, there is no information regarding the number of nearest neighbors found in liquid chloroethane. For liquids an average number of nearest neighbors of 8 is often used [Marcus]. Under such considerations, the expected liquid structure is a skewed "head to tail" arrangement of the dipoles.

If a net sum of the neighboring molecules is used instead of defining a particular number of nearest neighbors, a lumped dipole of the same magnitude as the central dipole would be at an angle of approximately 83° from a parallel arrangement (figure 3.4.7). This angle is of the same order as the model with an average of eight nearest neighbors.

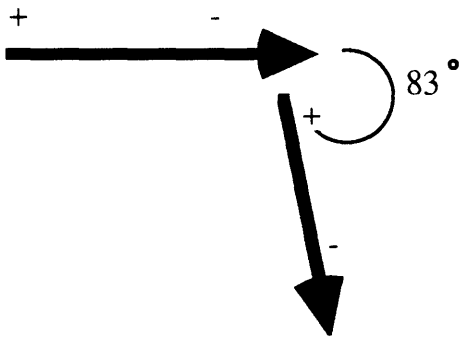

Figure 3.4.7 *Schematic of Dipole Orientation of Chloroethane.* If the effects of all the neighboring dipoles are summed,vectorially, the resultant dipole would need be at an angle of 83° to the dipole in question to generate the measured correlation factor.

Similar to butyronitrile, the molecular arrangement about the central molecule has a number of possible interpretations. For chloroethane the interpretation must consider the following. No reports have been located that suggest dimer or other complex formation in the literature for chloroethane. If a associated species were to form in a strictly parallel arrangement and if these species mix ideally with unassociated chloroethane molecules, then approximately 13m/o of the solution would be associated in this manner.

Hydrogen bond formation is unlikely as this type of bonding is found when hydrogen interacts with oxygen, nitrogen, or fluorine, not chlorine. Further for hydrogen bonded liquids such as hydrogen cyanide, methanol, and water [Dannhauser, 1963 and 1964, Kirkwood respectively], long polymer

like chains result with large correlation factors as a consequence (4.02, 3.12 at 280K and 3.55 at 298K respectively). For pure chloroethane the correlation factor is not far from unity (1.1281). These factors suggest that the majority of the neighbors are arranged randomly at the temperatures measured with a small tendancy to favor a parallel alignment. This overrules the more ordered configuration of the eight nearest neighbor model.

For chloroethane the deviation from random orientation is small suggesting very little dipole interaction in general over the temperatures measured. In other words, the interdipole energy is lower than thermal energy and so most of the ordering is disrupted. The lowest temperature measured was approximately 30°C warmer than the melting point of chloroethane. With the low interaction energy it seems likely that the measuring temperature would need to be closer to the melting point for variation of the correlation parameter with temperature to be measurable.

Unlike pure butyronitrile, chloroethane appears to be randomly arranged in the liquid phase. There is a small tendency of the molecules to orient causing slightly greater than unity multiplicative factor to the dipole moment of the central molecule.

3.4.2.1.3 Solutions of Butyronitrile-Chloroethane

For the solutions of butyronitrile-chloroethane, the correlation factors are nearly linear with mole fraction as seen in figure 3.4.4. Figure 3.4.8 is a plot of the deviation of the observed correlation factor from the ideal mixing law as expressed by eq. 3.1.6. This is tabulated in table 3.4.2. The deviation is small never exceeding 5.3% of the observed value and is less than the error of the measurement.

Table 3.4.2 Deviation of Correlation Factor From Ideal Mixing				
x_{BN}	g_{obs}	x_1g_1	x_2g_2	Δg
1	0.5152	0.5152	0	0
0.7890	0.6130	0.4065	0.2380	-0.0315
0.5691	0.7419	0.2932	0.4861	-0.0374
0.4002	0.8639	0.2062	0.6766	-0.0189
0.1835	1.0277	0.0945	0.9211	+0.0121
0	1.1281	0	1.1281	0

The observed correlation factor was determined based upon the weighted average of the dipole moments of the two components. The formation of a complex or an unlike molecular associated pair, postulated from figure 3.4.2 the deviation of the relative dielectric constant from ideal mixing, cannot be considered to be represented by a strong alignment of two (or more) weighted averaged dipoles. Therefore, the correlation factor computed by weighted values cannot be used, as is often done, to interpret the coordination of the complex or the complex within its environment in the same manner as the interpretation of a pure liquid. Only when the difference in the magnitudes of the moments is neglible, may the observed correlation factor be used to determined structural features as was done in the previous sections for the pure liquids. For the measured system, the dipole moment of butyronitrile is approximately twice that of chloroethane. Therefore, the correlation factors cannot be used alone to infer detailed orientational configurations to the molecules.

The environment about a species influences the dipole moment of a species resulting in the effective dipole moment. This moment is related to

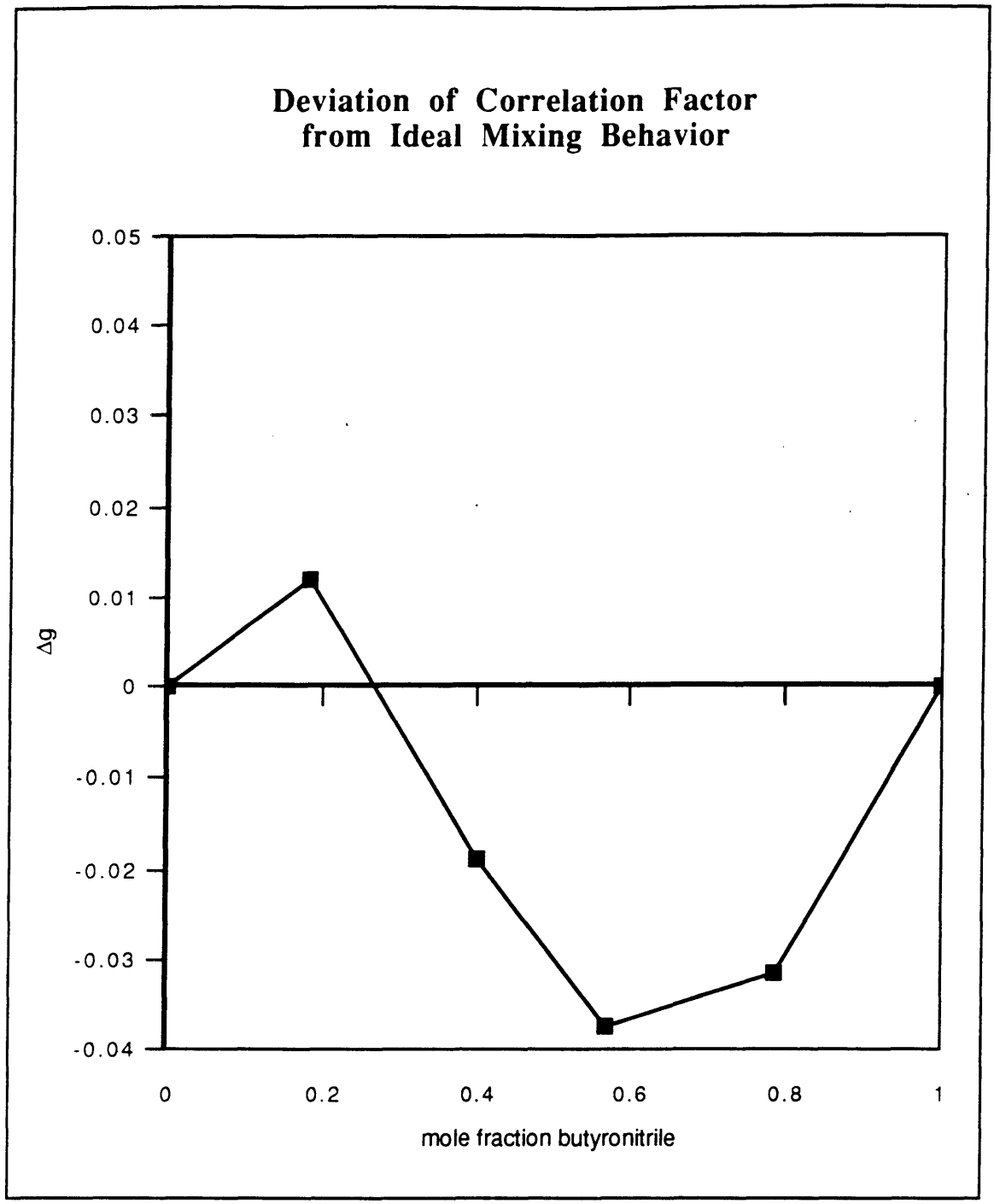

Figure 3.4.8 *Excess Correlation Factor.* Compute the excess based upon ideal mixing law (g(id)=x(1)g(1)+x(2)g(2)).

the value without the influence of the neighbors through the correlation factor (section 3.1). Thus,

$$g = \frac{\bar{\mu}_{effective}}{\mu} \qquad \text{eq. 3.4.6}$$

where $\bar{\mu}_{effective}$ is the magnitude of the dipole moment including the effects of the neighbors
μ is the dipole moment without the influence of the neighbors.

If the weighing factors used in computing the correlation factors of the solutions is taken into account, it is possible to compute an effective dipole moment. Barring additional information, the following must be assumed. First, all possible complexes that can form do form, composed of one chloroethane to one butyronitrile. Second, molecules that are not part of the complex are assumed to behave in the same manner as in its pure state. Lastly, ideal mixing is assumed between the complexed and uncomplexed species. Under these circumstance the effective dipole moment of the complex is computed by relationship 3.4.7

$$\bar{\mu}_{observed} = x_{complex}\,\bar{\mu}_{complex} + \left(1 - x_{complex}\right)\bar{\mu}_{uncomplexed} \qquad \text{eq. 3.4.7}$$

$$g_{observed}\left[x_{BN}\mu_{BN,g} + x_{CE}\mu_{CE,g}\right] = x_{complex}\,\bar{\mu}_{complex} + \left(1 - x_{complex}\right)g_{pure,uncomplexed}\,\mu_{uncomplexed}$$

The following is an example of the use of this relationship for the 78.90m/o butyronitrile solution.

$$0.6130\left[0.789\times1.3576\times10^{-29} + 0.211\times6.8381\times10^{-30}\right] = \frac{0.211}{0.211+\left(0.789-0.211\right)}\,\bar{\mu}_{complex} + \left(1-\frac{0.211}{0.789}\right)0.5151\times1.3576\times10^{-29}$$

$$\bar{\mu}_{complex} = 8.704\times10^{-30}\ \text{C - m}$$

For the remaining solutions the effective dipole moment is 1.401×10^{-30}, 6.754×10^{-30}, and 6.04×10^{-30} C-m for the 56.91, 40.02, and 18.35m/o solutions respectively.

The value of the effective dipole moment is related to both the intramolecular effects of the complex (in particular their relative orientations) and the effects of the environment on the complex. [Based upon the assumptions of ideal mixing in eq. 3.4.7, all of the non-ideal effects, e.g. the complex-"pure" interactions, are computed as part of the effective dipole moment of the complex.] The complexes are expected to have the same intramolecular effects and so the differences in the magnitudes of the effective moments of the complexes indicates the different effects of the environment. The solution with the greatest amount of "free" butyronitrile has the largest effect on the complex. The pure butryonitrile has a strong tendency to self-associate. It also has the larger dipole moment of the two components. This combines to give the greatest net effect on the complex.

The 56.91m/o and 40.02m/o solutions have nearly the same number of complexes if all possible complexes form. The effective moment of the latter, though, is nearly five times that of the former. There is also a shift from a "free" butyronitrile to a "free chloroethane" environment. The difference in the effective moment may be attributed to any of the following factors. With much fewer "free" butyronitrile molecules, the 56.91m/o solution most likely has few self-associates. On a species scale, both of these solutions have uncomplexed and complexes only. The butyronitrile, with its larger moment, would be expected to have a greater effect. Since the effective moment is lower in the 56.91m/o solution, this may be interpreted as the butyronitrile molecule interacting in a net anti-parallel arrangement to give a lower effective moment.

Comparing the effective moments of 40.02m/o to 18.35m/o butyronitrile, the effective moment is lower by approximately 10% for the latter. There are fewer complexes, assuming all possible complex form, in the

latter. The lower effective moment of the 18.35m/o solution by only 10% indicates that there is some interaction between the complexes as well.

The 1:1 complex formation, where the nitrogen of the nitrile group is associated with the hydrogen of the chloroethane, is supported by the freezing point diagrams of butyronitrile with chloroform and hydrogen chloride reported in the literature [Murray]. Under the configuration suggested by Murray, the lone pair electrons on the nitrogen act as donor electrons for a hydrogen on the chloroethane. From spectroscopic evidence it has been reported that nitriles are excellent proton acceptors [Danhauser, 1964a]. This further supports the molecules configuration as a linear head-to-tail complex.

If the complex is assumed to be in a strictly parallel arrangement, it has a dipole moment of 2.04141×10^{-29} C-m. Using eq. 3.4.6, a correlation factor for the effects of the environment about the complex may be computed for each solution measured. The correlation factors are 0.426, 0.0686, 0.3309, and 0.2960 for the 78.90, 56.91, 40.02, and 18.35 m/o solutions respectively. As with the pure liquids, this value includes the magnitude of the complex as well (eq. 3.4.3). All of the values are less than unity. The environment may be lumped into a single dipole of the same magnitude as the complex at an angle of 55.0°, 21.4°, 48.0°, and 45.25° from a strictly anti-parallel alignment. Information about the number of complexes is required to interpret these values reliably since the neighborhood may be composed of uncomplexed, self-associated, and/or complexed molecules.

Some general trends are prevalent from the computed values. The low value for the 56.91m/o butyronitrile solution indicates that on the whole the complexes and butyronitrile interacts in an anti-parallel fashion with other complexes.

The 78.90m/o solution has on average the most randomness of the four solutions measured. This is in conformity with the thermodynamic interpretation of the phase diagram which requires greater entropy in butyronitrile rich solutions. The term increased randomness may be misleading, however, because this solution most likely has the greatest number of butyronitrile self-associates. So while the solution on the whole is more random, it is composed of more oriented species.

The 40.02m/o solution is slightly more random than the 18.35m/o solution. There are a larger number of complexes in the former solution. These complexes are expected to interact based upon the magnitudes of the effective moments. Given the size difference of the complex to the chloroethane molecule, the 40.02m/o solution is expected to have less interactions of the chloroethane with the complexes and with other chloroethane molecules. This results in more randomness on the part of the chloroethane. This is offset to some degree by the increased interactions of the complexes. Measurements of the volume on mixing would be required to better interprete these effects.

As with the pure butyronitrile and chloroethane solutions, the correlation factor is not dependent on temperature a fact attributable to the same counterbalancing phenomenon of thermal effects (volume changes versus less thermal energy). For these solutions, the measurements were conducted above the two phase region. As a result the molecules are free to move and no molecules precipitate out into the solid phase. This allows the various thermal effects to counterbalance. At lower temperatures, particularly within the two phase region, the correlation factor is expected to change due to changes in the liquid composition as well as to thermal effects.

In the preceding analysis, it was assumed that the complex forms. The correlation factors measured may instead suggest a net orientation of the neighborhood without a complex forming. This interpretation is similar to that of the pure liquids. Under such circumstances, the central dipole may be interpreted as having the weighted average of the molecular dipole moments and is in an environment that is lumped into a single dipole of the same moment at an angle to it. Using eq. 3.4.3 the angles for the different solutions measured are 112.21°, 104.96°, 97.82°, and 88.41° for the 0.7890, 0.5691, 0.4002, and 0.1835 mole fraction butyronitrile solutions respectively.

Without the formation of the complexes, the liquid must become more random as chloroethane is added to the solution. This is in contradiction to the phase diagram where the excess entropy increases dramatically between 30 and 60m/o butyronitrile. Also, the strong deviation of the butyronitrile correlation factor from unity leads to the expectation that complexing of some nature should exist in the solutions. Lastly, the literature strongly suggests that butyronitrile and chloroethane should complex together based upon the complexes butyronitrile forms with hydrogen chloride [Murray] and chloroethane with boron trichloride [Martin].

In the determination of the correlation factor, an assumption of zero excess volume was made. Given the difference in the molar volumes of the two molecules (Table 2.4.3), the tendency towards association of some form, and the ability of the molecules to rotate, the assumption of ideal volumetric mixing is no doubt poor. Future measurements of this system should include volumetric measurements. These results would replace the volume term that was computed by ideal mixing of the components which when incorporated into the Kirkwood equation would give a more accurate

correlation factor. This would allow a better interpretation of the molecular arrangement in the solutions.

3.4.2.2 Summary of Liquid Structure

Beginning at the pure butyronitrile end, the molecules of butyronitrile tend towards an anti-parallel arrangement. This arrangement may be a net average of the neighborhood about the central molecule or a single neighboring molecule where the effective dipole moment of the central molecule is lower than it would be if the liquid was completely random. The large deviation of the correlation factor from unity suggests the formation of weak dimer associates. From both the low energy difference between the dimer and monomer structure and the charge density attributed to the nitrile group by Murray, it seems likely that the correlation factor is attributed to a single molecule in the neighborhood of the central dipole, but that the duration of a particular dimer is of short length. This residence time is likely to increase as thermal energy decreases. If the dimer forms as a strictly antiparallel associate, approximately 48m/o of the solution at any given time would be associated pairs. As chloroethane is added to the liquid, the average molecular arrangement of the pure butyronitrile is broken up with complexes of chloroethane-butyronitrile forming. These complexes are expected to be in a parallel arrangement. The neighborhood about these complexes is, on average, anti-parallel. As chloroethane is added the number of complexes is expected to increase and so the solution is more ordered. [As to the entropy, this ordering does not distiguish between self-associated pairs, complexes, or "free" molecules. The ordering here reflects a change in the ratio of the mole fraction of each of these species. The entropy of mixing may still increase as chloroethane is added even as the solution from a local standpoint is more

ordered!] Greater than 50m/o chloroethane, the solution would have a decreasing number of complexes forming. This should lead to less order by analogy to the approach to 50m/o through the addition of chloroethane to the butyronitrile. This is not the case as the solution seems to have a small increase in order as more chloroethane is added. This may be attributed to volume effects. The pure chloroethane is more random than the pure butyronitrile with no indication of stable self-associates forming. If these associates do form in a strictly parallel alignment, approximately 13m/o of the solution would be associated pairs. There is a small tendency towards a parallel arrangement which slightly augments the effective dipole moment.

The invariance of the correlations with temperature may be attributed to several factors. The first is the shape of the molecules. The molecules are singly bonded between the carbon atoms with tetragonal sp^3 hybrid orbitals. The molecules can therefore rotate easily and tend not to be simply linear as depicted in the various molecular structures drawn in this document. This molecular configuration combined with the reduction in free volume as the temperature is reduced hampers molecular motion. As the temperature is reduced, the thermal disruption of the molecules lessens, this favors an increase in the dipole interactions. This may result in more complexes and dimers forming and/or a reduction in the variation in the angles between the "lumped" environment and the central dipole. The former should increase the degree of correlation. But, the hampered motion of the molecules counterbalances the increase in ordering within the ability of these measurements to detect changes in the correlation factors. The net result is the measured invariance of the correlation factor over the temperatures measured.

Overall, based upon the values of the computed correlation factors, the butyronitrile-chloroethane system shifts from a molecular configuration where the effective dipole moment is lower than would be expected based on the value of the dipole moment as measured in the gas phase to a value that is higher. As a result the measured dielectric constant under predicts the ionizability of the liquid from pure butyronitrile to approximately 20 mole percent butyronitrile and over predicts is from 20 mole percent butyronitrile to the pure chloroethane. (Refer to section 3.0 of this document.)

As mentioned, a major assumption is ideal volume of mixing. This is in general a poor assumption for alkyl nitriles [Jannelli]. The addition of x-ray experiments would also augment the analysis of the liquid structure.

4.0 Conclusions

4.1 Contributions of the Dissertation Measurements

1. Expressly for the purposes of this investigation, a DTA apparatus capable of operating near liquid nitrogen temperatures was designed and constructed.

2. An EIS experimental cell was designed and constructed with the capability of measuring solutions of high resistivity and low dielectric constant.

3. A simplified procedure for drying organic reagents was developed. By sequential use of drying agents, distillations were avoided. This procedure also produced butyronitrile with lower water impurities than reported for the distillation methods.

4. From the determination of the phase diagram, the enthalpies of fusion of the pure components were found to agree with values found in the literature.

5. For the first time, the phase diagram of the butyronitrile-chloroethane system has been measured. The butyronitrile-chloroethane phase diagram is a simple eutectic, the eutectic point being -185°C and 48 mole percent butyronitrile.

6. The thermodynamic interpretation of the liquidus led to the conclusion that the liquid is an associated solution comprised of (1) free chloroethane, (2) free butyronitrile, (3) dimolecular complexes composed of one butyronitrile and one chloroethane, and (4) dimolecular self-associates of butyronitrile. Dimolecular self-associates of chloroethane may also form.

7. An equilibrium among butyronitrile, chloroethane, and other species in the liquid was defined. The values of the equilibrium constant conformed to Gibbs-Helmholtz behavior while reproducing the measured liquidus. The enthalpy of association was calculated to be -5.35 kJ/mole. Over the temperature interval spanning 160K to the eutectic, the value of the equilibrium constant indicates that the number of associated species [BN-CE and BN-BN] far exceeds the number of free species [BN and CE].

8. The relative dielectric constant at subambient temperatures was measured for butyronitrile, chloroethane, and their solutions for the first time. These values were modeled with the Kirkwood equation. This resulted in the calculation of the polarizabilities and the correlation factors of these solutions. Both of these factors were found to be temperature independent and approximated ideal mixing.

9. Through correlation factors computed from the Kirkwood equation, butyronitrile is found to self-associate in an anti-parallel manner. This reduces the effective moment of the solution, and therefore, the

measured relative dielectric constant under predicts the ionizing ability of the liquid butyronitrile when viewed in light of the Nernst-Thompson Law.

10. Liquid chloroethane, as determined from the correlation factor, does not tend to form complexes. There is a small trend towards parallel ordering in the liquid. This results in an effective dipole moment that is greater than the actual value. This causes the relative dielectric constant, when viewed in the light of the Nernst-Thompson Law, to over predict the ionizing ability of the liquid chloroethane.

11. A new method for interpreting the correlation factors of solutions is presented. When the dipole moments of the binary components differ and complexing of unlike species is considered, interpretation of the solutions as if they were composed of molecules with a dipole moment equal to the weighted average of the components is not realistic. This document overcomes this limitation by converting the observed correlation factor into an effective dipole moment. Interpretation of the effective dipole moment can be made using the dipole moments of the species in solution if assumptions are made about the nature of their coordination. Based on the location of the lone pair of electrons on the nitrile group, a strictly parallel complex of one butyronitrile and one chloroethane is assumed. The analysis of the effective dipole moment with this assumption suggests that the complexes interact with one another, self-associates of butyronitrile still form in the solutions, and "free" chloroethane has a low tendency to interact with itself or with a complex.

4.2 Determination of Molecular Arrangements in the Liquid Phase

From the thermodynamic model of the butyronitrile-chloroethane phase diagram (section 2 of this document), the best model considered the liquid as composed of butyronitrile, chloroethane and a 1-1 butyronitrile-chloroethane complex and at least one other complex. This results in a much larger entropy of mixing as compared to an unassociated view of the liquid. The value of the interaction energy to form the complex, as determined by the variation of the equilibrium constant with temperature, is on the order of the energy between two dipoles. In this model, the molar volumes were not considered. From theoretical considerations and from the goodness of the fit, the neglect of the molar volumes was not significant.

The view of the liquid as being composed of "free" butyronitrile and/or chloroethane molecules, butyronitrile self-associates as the "other" complex, and a complex of the two is supported by the relative dielectric constant measurements. Though these measurements were conducted in liquids at temperatures higher than the liquidus temperature, the linearity of the relative dielectric constant with temperature suggest that the trends at higher temperature hold to a first approximation at lower temperatures. The formation of a 1-1 butyronitrile-chloroethane complex is suggested by the sign of deviation of the correlation factors from ideal mixing. As the correlation factor is an average molecular arrangement factor, the data may be interpreted in a variety of ways. The correlation factor determined by the relative dielectric constant is somewhat limited because of the assumption of ideal mixing in terms of the volume behavior.

While neither experiment completely defines the liquid structure, the combination of these experimental results gives a good picture of the

molecular arrangement in the liquid phase. The liquid appears to be composed of a complexes of one butyronitrile to one chloroethane and time averaged butyronitrile self-associates. The complex is expected to be a parallel alignment of butyronitrile-chloroethane. The butyronitrile self-associated complex is aligned with the molecules in an antiparallel arrangement with no definite angle between the molecules. The neighboring molecules to the unlike complex (butyronitrile-chlroethane) tend to have an average association with the complex. These molecules may be represented as "lumped" dipoles which are aligned anti-parallel to the complex. The magnitude of this lumped dipole may vary as does the angle between it and the complex. How random the molecules that make up the "lumped" dipole cannot be determined through the measurements conducted. In light of the measurements the total number of species in solution increases for increases in the amount of butyronitrile because the butyronitrile that is not complexed to chloroethane may be complexed with itself or uncomplexed. As a result, the entropy of mixing for the butyronitrile rich end, the configuration of three or four species, is somewhat greater than for the chloroethane rich end, the configuration of two or three species. This may explain the shift of the eutectic composition by approximately twenty mole percent butyronitrile and a lowering of the eutectic temperature by over thirty five degrees celsius in the measured phase diagram as compared to the ideal phase diagram (figure 2.4.2.2). Because butyronitrile rich liquids have a higher entropy of mixing, the liquid has a lower free energy than expected based upon ideal mixing.

4.3 Solvent Selection

The variety of electrochemical experiments that can be conduction at very low temperatures in butyronitrile-chloroethane based electrolytes is

broad. The choice of the solution composition for the solvent depends upon the experimental goals. For example, based upon the present measurements for electrolytes where the highest electrical conductivity is required, solvents richer in butyronitrile are preferred. This is not only because the relative dielectric constant as measured is higher than for the chloroethane rich solutions. The correlation factor, being less than unity, for these solutions tends to indicate that the ionizing ability will be greater than the relative dielectric constant predicts. However, using very butyronitrile-rich solutions as a solvent may not proof judicial as at low temperatures the solution will be deeper in the two phased region. Though values for the viscosity have not be determined, it is likely that very butyronitrile rich solutions would be more viscous. As a result, with the given information solutions only somewhat richer in butyronitrile than chloroethane would be optimum for electrolytes with the highest attainable conductivity.

4.4 Recommendations for a More Detailed Determination of the Liquid Structure and Thermodynamics

1. Butyronitrile is known to self-associate. This was found in this study and has been reported in the literature [Danhauser, Janelli]. The determination of the excess volume on mixing of butyronitrile and chloroethane would result in a better determination of the correlation factors. These values would also enhance the interpretation of thermodynamic models.

2. As stated throughout section 3.4.2, the correlation factors are average values. No definitive molecular structure may be determined by these values alone. Likewise, the degree of self-association of butyronitrile and of unlike complexes forming cannot be distinguished by the phase diagram alone. Even together these measurements only point to a tendencies in the molecular orientations. X-ray diffraction is a common method for determining structural features in both solids and liquids. The extent of ordering may be determined from these measurements. This will aid in the differentiation of contributions to the correlation factor from like and unlike complex formation and will augment the interpretation of the molecular arrangements in the liquid.

Appendix A

Derivation of Van't Hoff Equation

$\mu_a = \mu_a^\circ + RT \ln a_a$ — chemical potential (μ_a) of "a" in solution is related to its standard state chemical potential and its activity

$\gamma_a = 1$ — assume the activity coefficient is equal to one; implies $a_a = x_a$, the mole fraction

$\mu_a = \mu_a^\circ + RT \ln x_a$

$x_a = 1 - x_b$ — for a two component system this is true by definition let "a" be the solvent, and "b" the solute

$\mu_a = \mu_a^\circ + RT \ln (1-x_b)$

$\mu_a - \mu_a^\circ = -RT\, x_b$ — for small x_b, $\ln (1-x_b) \sim -x_b$

at melting

$\mu_a - \mu_a^\circ = -\Delta G_{fusion} = -\Delta H_{fusion} + T\Delta S_{fusion}$

$-\Delta H_{fusion} + T\Delta S_{fusion} = -RT\, x_b$

$-\Delta H_{fusion} + T_m \Delta S_{fusion} = 0$ for pure solvent at its melting point

$$\Delta S_{fusion} = \frac{\Delta H_{fusion}}{T_m}$$

$$-\Delta H_{fusion} + \frac{\Delta H_{fusion}}{T_m} = -RT\, x_b$$

$$\Delta H_{fusion} - \frac{\Delta H_{fusion}}{T_m} = RT\, x_b$$

$$\frac{\Delta H_{fusion}}{RT}\left[1 - \frac{T}{T_m}\right] = x_b$$

where T refers to the actual melting point
T_m to the melting point of the pure solvent

from. Liquids and Solids, Classic Researches in General Chemistry Service, H. Hart, ed. Houghton Mifflin Co., Boston, 1966. (QD541.D771)

Appendix B: Compilation of Experimental Electrochemical Impedance Spectroscopy Data.

Compilation of Relative Dielectric Constant Data as a Function of Temperature and Composition

	mole fraction	mole fraction	mole fraction	mole fraction	mole fraction	mole fraction
	BN:= 0	BN= 0.1835	B=: 0.4002	BN= 0.5691	BN= 0.7890	BN= 1
T(K)|						
238.16	13.33	17.86	22.38	25.54	28.94	31.87
223.16	14.51	19.42	24.30	27.61	31.23	34.33
208.16	15.80	21.13	26.39	29.89	33.71	36.98
193.16	17.25	23.03	28.68	32.42	36.44	39.85
178.16	18.91	25.21	31.30	35.25	39.48	43.02
168.16	20.13	26.77	33.14	37.25	41.64	45.17

Compilation of Conductivity Data as a Function of Temperature and Composition

	0m/o Butyronitrile		18.35m/o Butyronitrile		40.02m/o Butyronitrile	
T(K)|	Cond-S/cm-N	ln(cond)	Cond-S/cm	lnCond	Cond-S/cm	lnCond
238.16	7.93E-09	-18.6523	1.83E-08	-17.8162	8.70E-09	-18.5597
223.16	6.21E-09	-18.8973	1.64E-08	-17.9249	1.07E-08	-18.3568
208.16	4.81E-09	-19.1529	1.24E-08	-18.2046	8.91E-09	-18.5362
193.16	3.49E-09	-19.4746	7.87E-09	-18.6603	6.12E-09	-18.9122
178.16	2.23E-09	-19.9195	4.62E-09	-19.1927	3.75E-09	-19.4021
168.16	1.60E-09	-20.2558	3.04E-09	-19.6113	2.47E-09	-19.8208

	56.91m/o Butyronitrile		78.90m/o Butyronitrile		100m/o Butyronitrile	
T(K)|	Cond-S/cm	lnCond	Cond-S/cm	lnCond	Cond-S/cm-N	ln(conduct)
238.16	1.92E-08	-17.7664	2.94E-08	-17.3415	5.20E-07	-14.4696
223.16	1.24E-08	-18.2020	2.54E-08	-17.4882	3.63E-07	-14.8276
208.16	7.56E-09	-18.7010	1.79E-08	-17.8393	2.33E-07	-15.2743
193.16	4.15E-09	-19.2993	1.07E-08	-18.3524	1.29E-07	-15.8603
178.16	1.95E-09	-20.0534	5.35E-09	-19.0455	5.72E-08	-16.6770
168.16	1.06E-09	-20.6625	2.87E-09	-19.6689	2.70E-08	-17.4262

Appendix C: Purification of Solvents

The literature recommends a variety of different distillation techniques to remove water from butyronitrile and chloroethane. Water impurities contribute to errors in conductivity measurements of the pure solvents. The effects on the relative dielectric measurements is neglible as long is the concentration is low. Therefore, very careful control of water content was not critical for this research.

Butyronitrile:

The procedure adopted in this work consisted of drying the reagent with successive treatments with drying agents. The procedure is as follows:

- 3A molecular sieve is reactivated by heating in a furnace to 400°C for 20 hours (overnight essentially) in an inert atmosphere. It is important that this atmosphere is maintained during the furnace cool down.
- Approximately 200ml of reagent is mixed with 20ml of sieve. This is capped and left overnight.
- Decant the butyronitrile over fresh sieve.
- Alumina pellets are reactivated by heating in a furnace to 700°C for at least 20 hours in an inert atmosphere.
- Butyronitrile that has been on the molecular sieve is now decanted over the alumina.
- Repeat the last step with fresh alumina.

With this technique the conductivity of butyronitrile at 25°C can be reduced to approximately 1×10^{-8} S/cm. [The lowest value reported in the literature is 5×10^{-8} S/cm. This reference claimed the water content was below 3ppm. D'Aprano]

Chloroethane:

Chloroethane was dried by condensing the gas over reactivated 3A molecular sieve.

Appendix D: Conversion From Rationalized MKS Units to Gaussian CGS Units

Symbol	Quantity	MKS units	CGS units	
		The MKS unit below	*is equal to the following number of CGS* electromagnetic *units:*	*and is also equal to the following number of CGS* electrostatic *units:*
q	Charge	1 coulomb	10^{-1}	3×10^{9} (stat-coulombs)
I	Current	1 ampere	10^{-1} (ab-amperes)	3×10^{9}
V	Electromotive force	1 volt	10^{8} (ab-volts)	$\frac{1}{3} \times 10^{-2}$
R	Resistance	1 ohm	10^{9}	$\frac{1}{9} \times 10^{-11}$
C	Capacitance	1 farad	10^{-9}	9×10^{11} (stat-farads or centimeters)
L	Inductance	1 henry	10^{9}	$\frac{1}{9} \times 10^{-11}$
$\mathbf{F}$	Force	1 newton	10^{5} (dynes)	10^{5} (dynes)
U	Energy	1 joule	10^{7} (ergs)	10^{7} (ergs)
W	Power	1 watt	10^{7} (ergs/sec)	10^{7} (ergs/sec)
σ	Conductivity	1 mho/meter	10^{-11}	9×10^{9}
Φ	Magnetic flux	1 weber	10^{8} (maxwells)	$\frac{1}{3} \times 10^{-2}$
$\mathbf{B}$	Magnetic flux density	1 tesla	10^{4} (gauss)	$\frac{1}{3} \times 10^{-6}$
$\mathfrak{F}$	Magnetomotive force*	1 ampere (-turn)	$4\pi \times 10^{-1}$ (gilberts)	$12\pi \times 10^{9}$
$\mathbf{H}$	Magnetic field strength*	1 ampere/meter	$4\pi \times 10^{-3}$ (oersteds)	$12\pi \times 10^{7}$

*The starred quantities are affected by rationalization. For these quantities the conversion factors are shown for converting from *rationalized* MKS units to *unrationalized* CGS units.

Reproduced from:
E. C. Jordon, K. G. Balmain, Electromagnetic Waves and Radiating Systems, Prentice-Hall, Inc., Englewood Cliffs, NJ, 1968.

Appendix E: Estimated Vapor Pressure

Literature values for the pure component were scaled to the required temperatures [Daubert].

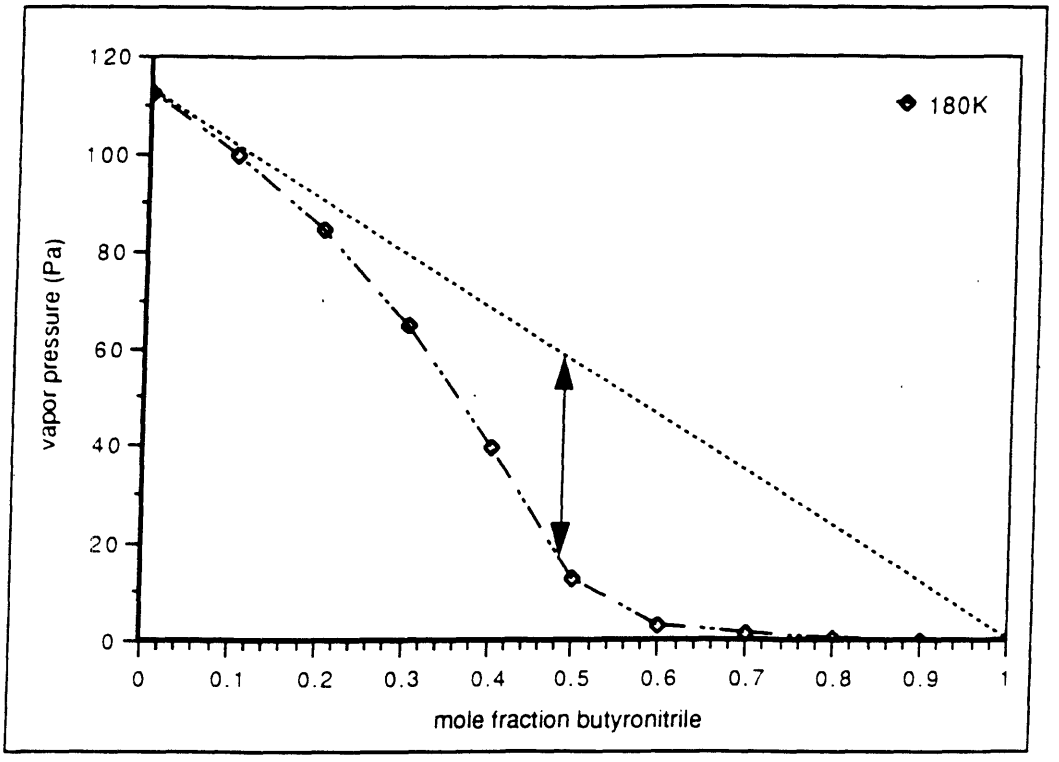

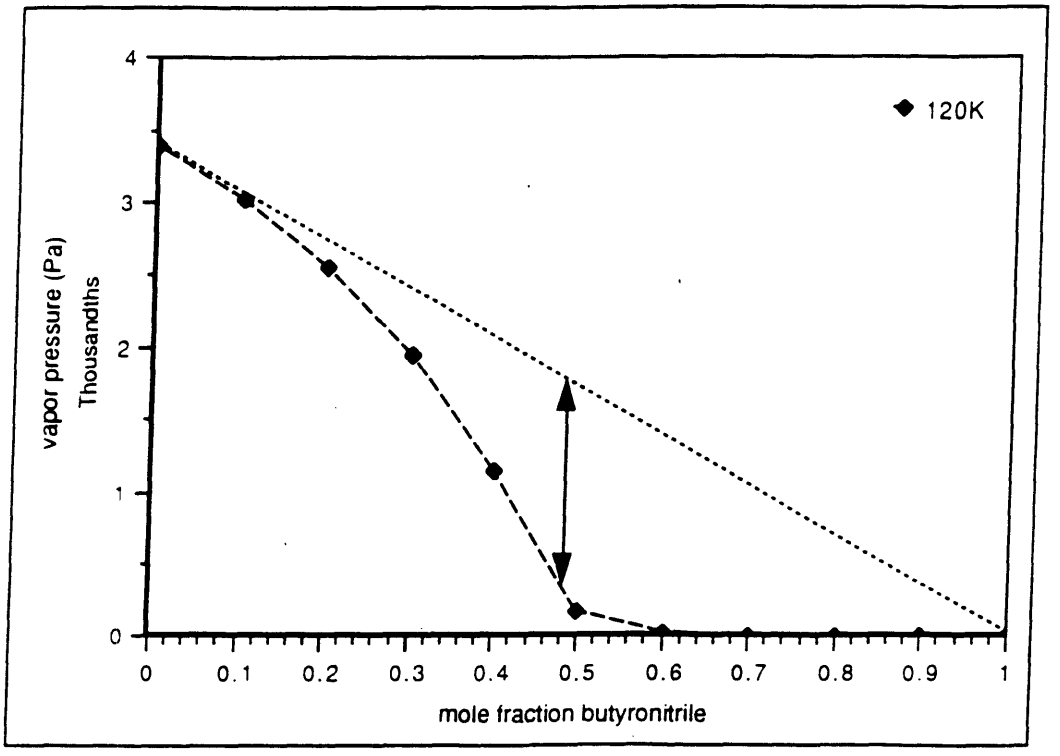

6.0 References

for introduction

A. J. Bard, L. R. Faulkner, Electrochemical Methods, Wiley & Sons, New York, 1980.

M. W. Breiter, W. J. Lorenz, G. Saemann-Ischenko, Surf. Sci., 230, 1990, 213-221.

L.J. Cava, B . Batlogg, et al., Phys. Rev. B., 36(10), 1989, 5719-5721.

L. S. Curtin, S. R. Peck, *et al.*, Anal. Chem., 65, 1993, 386-392.

M. Gauthier, A. Beanger, et al., "Solid State Potentiometric Gauges for Gaseous Species, " Solid Electrolytes, P. Hagenmuller, V. Van Gool, ed., Acad. Press, New York, 1978, 501.

S. J. Green, D. R. Rosseinsky, M. J. Toohey, J. Am. Chem. Soc., 114, 1992, 9702-9704.

A. A. Maryott, E. R. Smith, Table of Dielectric Constant of Pure Liquids, NBS Circ. 514, 1951.

J.McDevitt, S. Ching, et al., J. Am. Chem. Soc., 111, 1989, 4528-4529.

E.J. O'Sullivan and B.P. Chang, Appl. Phys. Lett., 52(17), 1988, 1441-1443.

S. R. Peck, L. S. Curtin, *et al.*, J. Am. Chem. Soc., 114, 1992, 6771-6775.

B. D. Razumovskii, G. E. Zaikov, Ozone and Its Reactions with Organic Compounds, Elsevier, Amsterdam, 1984.

M. Schwartz, D. Cahen, et al., Solid State Ionics, 32/33, 1989, 1137-1142.

Texacar®Ethylene and Propylene Carbonate, Texaco Chemical Company,

J. Timmermans, Bull. Soc. Chim, Bel., 27, 1913, 334-343.

J. Timmermans, Bull. Soc. Chim, Bel., 36, 1927, 502-516.

R. C. Weast, M. J. Astle, ed., CRC Handbook of Chemistry and Physics, CRC Press, Inc., Boca Raton, FL, 1983.

H. Yugami, T. Watanabe, et al., Jpn. J. Appl. Phys., 28(8), 1989, L1411-L1414.

for phase diagram

S. Ching, J. T. McDevitt, S. R. Peck, R. W. Murray, J. Electrochem. Soc., 138(8), 1991, 2308-2315.

T. E. Daubert, R. P. Danver, Physical and Thermodynamic Properties of Pure Chemicals, Hemisphere Publishing Corp., NY, 1989.

P. J. Flory, J. Chem. Phys., 10, 1942, 51-61.

J. B. Gill, D. C. Goodall, B. Jeffreys, J. Chem. Soc. Dalton Trans., 1986, 2603-2605.

D. K. Gosser, Q. Huang, J. Electroanal. Chem., 267, 1989, 333-338.

J. H. Hildebrand, S. E. Wood, J. Chem, Phys., 1 (12), 1933, 817-822.

J. H. Hildebrand, J. Chem. Phys., 15(5), 1947, 225-228.

J. H. Hildebrand, J. M. Prausnitz, R. L. Scott, Regular and Related Solutions: The Solubility of Gases, Liquids, and Solids, Van Nostrand Reinhold Co., NY, 1970.

H.V. Kehiaian, ed. International Data Service Selected Data on Mixtures, Thermodynamics Research Center, College Station, TX, 1979.

R. C. Mackenzie, Differential Thermal Analysis, Academic Press, London, 1970.

S. Malanowski, A. Anderko, Modelling Phase Equilibria: Thermodynamic Background and Practical Tools, John Wiley & Sons, NY, 1992.

Y. Marcus, Introduction to Liquid State Chemistry, John Wiley & Sons, London, 1977.

D. R. Martin, W. B. Hicks, J. Phys. Chem., 50, 1946, 422-427.

F. E. Murray, W. G. Schneider, Can. J. Chem., 33, 1955, 797-803.

I. Prigogine, R. Defay, Chemical Thermodynamics, John Wiley and Sons, N Y, 1954.

S. R. Rafikov, S. A. Pavlova, I. I. Tverdokhlebova, Molecular Weights and Polydispersity of Polyers, J. Eliassat, transl., J. Schmorak, ed., Israel Program for Scientific Translation Ltd., 1964.

Y. K. Rao, "Thermodynamics of Phase Diagrams", Phase Diagrams, Materials and Technology, A. M. Alper, ed., Academic Press, NY, 1970.

O. Redlich, Thermodynamics: Fundamentals, Applications, Elsevier Scientific Publishing Co., Amsterdam, 1976.

O. Redlich, A.T. Kister, Ind. & Eng. Chem., 40, 1948, 345-348.

K. G. Rhoads, *private communication.*

G. Scatchard, W. J. Hamer, J. Am. Chem. Soc., 57, 1935a, 1805-1809.

G. Scatchard, W. J. Hamer, J. Am. Chem. Soc., 57, 1935b, 1809-1811.

L. Sarolea-Mathot, Trans. Faraday Soc., 49, 1953, 8-21.

G. R. Taylor, G. E. Dunn, W. B. Easterbrook, Anal. Chim. Acta, 53, 1971, 452-453.

J. Timmermans, Bull. Soc. Chim, Belg., 44, 1935, 17-40.

D. A. Vassallo, J. C. Harden, Anal. Chem., 34(1), 1962, 132-135.

B. Wunderlich, Thermal Analysis, Academic Press, Inc., SanDiego, CA, 1990.

for relative dielectric constant

Y. Y. Akhadov, Dielectric Properties of Binary Solutions: A Data Handbook, Pergamon Press, Oxford, 1980.

W. Dannhauser, A. F. Flueckinger, J. Chem. Phys., 38(1), 1963, 69-72.

W. Dannhauser, A. F. Flueckinger, J. Phys. Chem., 68 (7), 1964a, 1814-1819.

W. Dannhauser, L. W. Bahe, J. Chem. Phys., 40(10), 1964b, 3058-3066.

A. D'Aprano, I. D. Donato, J. Soln. Chem., 19(9), 1990, 883-892.

T. E. Daubert, R. P. Danver, Physical and Thermodynamic Properties of Pure Chemicals, Hemisphere Publishing Corp., NY, 1989.

D. Decroocq, Bull. Soc. Chim. Fr., 1964, 127-136.

R. M. Fuoss, C. A. Kraus, J. Am. Chem. Soc., 55, 1933, 21-36.

W. Gerhartz, Ullmann's Encyclopedia of Industrial Chemistry, VCH, Weinheim, 1985.

T. E. Hawes, R. L. Kay, J. Phys. Chem., 69(7), 1965, 2420-2431.

L. Janelli, et al, J. Chem. Eng. Data, 28, 1983, 166.

G. Jones, S. M. Christian, J. Am. Chem. Soc., 57, 1935, 272.

J. G. Kirkwood, J. Chem. Phys., 7, 1939, 911.

O. Madelung, ed., Landolt-Börnstein Numerical Data and Functional Relationships in Science and Technology, Vol.6, Springer-Verlag, NY, 1991.

W. R. Longworth, J. Chem. Soc., 1959, 1618.

K. Mansingh, et al, J. Chem. Phys., 41, 1964, 827.

L. Marcheselli, G. Pistoni, et. al., J. Chem. Eng. Data, 38, 1993, 204-206.

Y. Marcus, Introduction to Liquid State Chemistry, John Wiley & Sons, London, 1977.

D. R. Martin, W. B. Hicks, J. Phys. Chem., 50, 1946, 422-427.

M. C. Mateos, P. Perez, R. M. Roy, et al, Rev. Acad. Cienc., Exactas Fis. Quim. Nat. Zaragoza, 41, 1986, 73.

E. F. Meyer, T. A. Penner, K. S. Stec, J. Phys. Chem. 75 (5), 1971, 640-648.

T. E. Morris, W. D. Tasto, Kirk-Othmer Concise Encyclopedia of Chemical Technology, M. Grayson, ed., Interscience Publ. John Wiley and Sons, Inc. , NY, 1978.

F. E. Murray, W. G. Schneider, Can. J. Chem., 33, 1955, 797-803.

J. Nath, M. Tevari, J. Chem. Soc. Faraday Trans., 88 (15), 1992, 2197-2202.

J. D. Nickerson, R. McIntosh, Can. J. Chem., 35, 1957, 1325-1331.

L. Onsager, J. Am. Chem. Soc., 58, 1936, 1486-1493.

G. E. Papanastasiou, I. I. Ziogas, J. Chem. Eng. Data, 37, 1992, 167-172.

K. Rhoads, *private communication.*

J. A. Riddick, W. B. Bunger, T. K. Sakano, Organic Solvents, 4th edition, 1986.

H. Schlundt, J. Phys. Chem., 5, 1901, 503-526.

H. Shapiro, *Ph D. thesis,* Department of Materials Science and Engineering, MIT, 1993.

T. Shedlovsky, L. Shedlovsky, "Conductometry,"Physical Methods of Chemistry, A. Weissberger, B. W. Rossiter, ed., Wiley-Interscience Publ., John Wiley and Sons, Inc., NY, 1971.

M. Spiro, "Conductance and Transference Determinations," Physical Methods of Chemistry: Electrochemical Methods Vol. 2, Rossiter, Hamilton ed., Wiley-Interscience Publ., John Wiley and Sons, Inc., NY, 1986.

Z60, Scribner Associated Inc., Charlottesville, VA.

ZSIM/CNLS, Scribner Associated Inc., Charlottesville, VA.

Appendix C

A. D'Aprano, R. M. Fuoss, J. Soln. Chem., 3(1), 1974, 45-55.